Influence of stress factors and fluid dynamics on lysozyme conformation and enzymatic activity

Ariane de Espindola

Université de Haute-Alsace

Ecole doctorale : Physique et Chimie-Physique (ED 182)

Thesis

Influence of stress factors and fluid dynamics on lysozyme conformation and enzymatic activity

By

Ariane DE ESPINDOLA

September 2023

Under supervision of Dr. Arnaud PONCHE and Pr. Patrick DUTOURNIÉ.

Jury:

Pr. Murielle RABILLER-BAUDRY, Université de Rennes (Rapporteur)

Dr. Marianne WEIDENHAUPT, Grenoble-INP Phelma (Rapporteur)

Pr. Valérie SAUTOU, Université Clermont-Auvergne (Examinateur)

Dr. Arnaud PONCHE, Université de Haute-Alsace (Examinateur)

Pr. Patrick DUTOURNIÉ, Université de Haute-Alsace (Examinateur)

Acknowledgements

Firstly, I would like to thank and express my admiration to my supervisors Dr. Arnaud Ponche and Pr. Patrick Dutournié. Thank you for trusting my work from the beginning when I was still in Brazil. Thank you also for your patience, support and all the scientific guidance. You always encouraged me to think critically, valued my curiosity and I believe this was part of the good thesis we obtained. Finally, thank you for always showing me professional career possibilities clearly. I will always remember your advice and support.

Thank you for the thesis jury composed of Pr. Murielle Rabiller-Baudry, Dr. Marianne Weidenhaupt and Pr. Valérie Sautou for their willingness to evaluate my manuscript. Thank you also for our rich discussion during the defense of the thesis and for all the suggestions given as well as the questions asked. Having a doctoral degree after your evaluation as a jury is an immense pleasure.

I would also like to thank my colleagues from the TRM2P and Biointerfaces-Biomaterials groups and my office friends Gabriel Trierweiler, Mohamed Zbair and Amir Astafan. Thank you for the fun moments, scientific discussion, exchange of opinions and not least our coffee breaks and good laughs.

None of this would have been possible without the support of my family. Thank you to my parents Lourdes Rosa de Espindola and Francisco Dorval de Espindola, first for giving me life but also for showing me how to follow my dreams. Thank you for your love, support, and education. A special thank you to my sister Araceli de Espindola Cardoso for giving me the opportunity (staying at her house) to study in São Paulo before coming to France. This stage of my life was essential to acquire knowledge from a great university.

Finally, thank you to my boyfriend, partner for 8 years now, for agreeing to embark on this adventure with me. Thank you for always believing in me and for showing me how to make the best of difficult situations. Thank you for your love, patience and for the scientific discussions along the way.

Table of contents

List of Tables

List of Figures

Chapter I – Introduction

Résumé Chapitre I.

Introduction

Ce chapitre présente une introduction générale, les objectifs de la thèse et un état de l'art sur le domaine étudié. Il est divisé en deux parties, la première présente les différentes applications des protéines dans l'industrie et les conditions requises pour disposer d'un produit de qualité (efficacité et stabilité). Pour cela, les différents étapes et problématiques (facteurs de stress) de fabrication, préparation, stockage, transport et administration sont présentées. La seconde partie de ce chapitre présente un état de l'art décrivant les structures primaires secondaires et tertiaires des protéines avec un focus sur la protéine utilisée dans ce travail : le lysozyme. Les principaux résultats de la littérature concernant l'impact des facteurs dénaturants étudiés sont présentés et discutés ainsi que les connaissances actuelles en matière de phénomènes d'adsorption et d'interactions entre protéines et surfaces. Ce chapitre se termine par une présentation des différentes techniques utilisées pour caractériser les différentes propriétés des protéines.

1. General introduction

1.1. Application of proteins in industry

Proteins are examples of macromolecules present in living systems from bacteria to human beings. Human, animal, vegetal or microorganism cells are composed, in their dry weight, by 50% of proteins. In human bodies, proteins are present in muscles, hair, nails, organs and skin, playing functions as hormones, enzymes, oxygen carriers, antibodies, muscle messenger, among others[1,2]. These macromolecules are initially formed by the bonding between amino acids residues and the final structure has a 4-level organization. This complex structure is one of the reasons that explain the versatility and importance of protein roles.

Proteins are well known for industry applications mainly as biocatalysts due to their enzymatic function. Enzymes have been used since ancient times for baking, cheese making, brewing and spontaneously microorganism growing. Some enzymes derived from animal sources as α-amylases, papain, pepsin and lysozyme are used in the food sector to increase the volume of the dough, meat tenderization, cheese production and prevent of final blowing defects in cheeses by spore-forming bacteria, respectively[3,4]. Other examples of enzyme applications are the cellulases in detergent production, xylase in paper or animal feed sectors and lipase in fat and oil industry.

In addition to its application as biocatalysts, proteins have been widely studied as therapeutic active ingredients in the biomedical industry. Human diseases can be caused by high or low protein concentration, mutation, or some abnormally. That is the reason why proteins can be used as therapeutic drugs to treat some specific illness. Besides that, comparing with small molecule drugs, proteins present advantages such as specificity and complex functions that sometimes cannot be replaced by a synthetized drug. Due to this specificity, proteins are less likely to interfere with natural biological processes causing side effects. Linked on this last advantage, the approval of therapeutic proteins is one year faster than a common drug, making them more financially interesting for the pharmaceutical industry[5].

The first protein used in this field was the insulin in the treatment of diabetes mellitus types I and II. This disease is a result of insulin lack, which is a hormone that signals functions related to intermediary metabolism and glucose homeostasis. When insulin is present in the body at low concentration and the signaling does not happen, the consequences are severe weight loss and can lead to death[6].

One promising protein that has been studied since the 90s as an active pharmaceutical ingredient is the lysozyme (LSZ) due to its antibacterial, antiviral and immunostimulant activities[7]. *Okamoto et al.* synthetized gold nanoclusters containing lysozyme and they observed the increase of antibacterial activity of the material in photodynamic therapy due to the presence of this protein[8]. LSZ can also be used in wound healing as demonstrated *in vivo* and *in vitro* by *Yang et al.*[9]. In addition, *Ragland et al.* presented in their review that LSZ has antibacterial mechanisms both for gram-positive and gram-negative bacteria and beyond that, they illustrated the relationship between this antibacterial activity and immunomodulatory functions of lysozyme in infection context[10].

As previously mentioned, proteins play a major role in all living being systems and, to ensure the proper functioning of the body, it is important to consume proteins from external sources. The daily and simplest source is food, being the more common from the animal as milk, meat, fish and egg. There are also vegetable protein sources as soybeans, chickpeas, beans, lentils, nuts, among others[4].

While some proteins can be used directly from its source, others must be engineered, isolated, processed, among others unitary steps before commercialization. These steps are necessary to achieve industrial or pharmaceutical requirements. In the case of pharmaceutical area, the protein drugs have to reach good stability and efficiency. These factors are aligned and depend on protein conformation and the native state is in general required for high efficiency[11].

1.2. Problem statement and thesis objectives

As stated before, two factors are crucial for treatment based on protein: efficiency and stability. Stability is the ability of the interest molecule to keep its physicochemical properties over a period and administration. Efficiency is when the compound maintains its biological function with an expected result. In the case of proteins, these two parameters have a mutual influence. If protein change its native structure as a consequence of low stability, it can also lose its function.

The most stable conformation, the native state can unfold into an inactive form under stress conditions such as temperature and pH changes, shearing, surface contact, etc. These

conditions can be part of protein processing from extraction, filtration, purification, lyophilization, storage and transport to drug application (as shown in figure I-1).

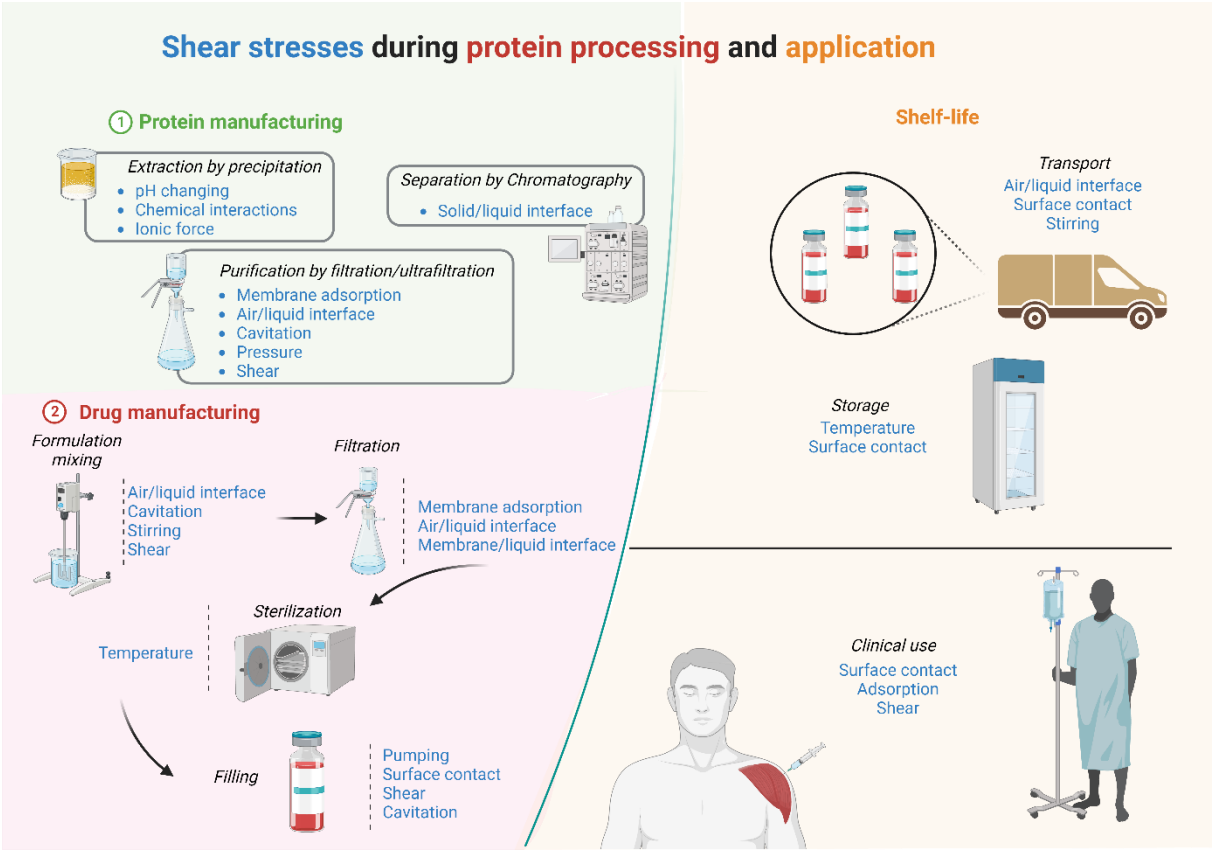

Figure I-1: Examples of shear stresses that protein faces from processing to application. Created with BioRender.com.

Structural or conformational changes in protein without alteration in the amino acid sequence and peptide bonds is called denaturation. For the most part of the proteins, the denatured state induces, in addition to being inactive for the disease, the formation of insoluble aggregates that is unacceptable in drug intravenous release[12].

In this context, to maintain the physicochemical stability of the protein as well as guarantee its efficiency, the boundary conditions of each stress factor must be known. Consequently, this thesis was separated into three parts:

- The first one aimed to build a denaturation scale based on the antibacterial activity of lysozyme (model protein). For this scale, lysozyme was treated in solution varying the applied stress factor. Thermal, chemical and mechanical treatments were used and the enzymatic activity was measured through an optimized turbidity assay.

- The second part was the study of protein-surface interactions. In this purpose, the adsorption kinetics and structure evolution of lysozyme on different surfaces were obtained. Common surfaces such as polydimethylsiloxane (PDMS) and glass were used as, hydrophobic and hydrophilic surfaces, respectively, and surfaces with intermediate surface energy were created using Self-Assembled Monolayer (SAM) method.
- The last part aims to study the protein-surface interactions in a tangential fluid flow, reflecting conditions during industrial applications.

2. State of the art

2.1. Protein's structure

Protein structure is organized in four levels. The first level is the primary structure: it represents the sequence of amino-acids (20 residues possible) along the polypeptide chain formed by the bond between amino acids. The amino acids present hydrogen atom, side organic chain R, carboxyl, and amino groups linked to an asymmetric central carbon (figure I-2). Among 20 different amino acids, two contains sulfur atoms. These formation blocks are connected by peptide bonds where, by a condensation reaction, the amino group of one molecule reacts with the carboxyl from the other, resulting in water and dipeptide formation. The resulting molecule is called polypeptide and the sequence of amino acids along the chain forms the primary structure level of the proteins. Possibility of different residue sequences is one of the reasons why each protein has its own function and properties[1].

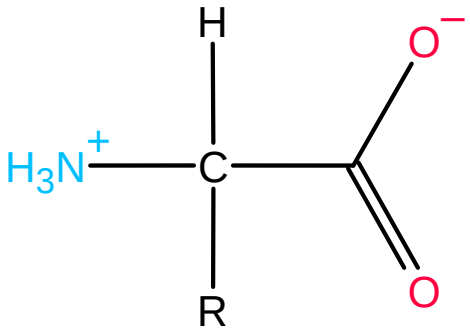

Figure I-2: Amino acid general structure.

Each protein is defined by a unique amino acid sequence followed by secondary, tertiary and quaternary structure. Covalent bonds of the polypeptide chain allow the polypeptide to turn and assume different conformational shapes due to interactions, mainly hydrogen bonds, and these different conformations are called secondary structure[1]. The most common secondary arrangements are alpha-helix and beta-sheets. The α-helix, as showed in figure I-3, is a right-handed helix with its side chains extending outward forming a helical array. It is stabilized by hydrogen bonds between C-O and N-H where each turn has 3.6 amino acid residues at a distance of 0.15 nm from each other. β-sheet is also represented in figure I-3 and when compared to α-helix, it is a stretched-out and a more extended structure where the residues are at 0.35 nm of distance. This type of secondary design is formed by beta strands (amino acid residues interacting by hydrogen bond and following a zig-zag organization)[13,14].

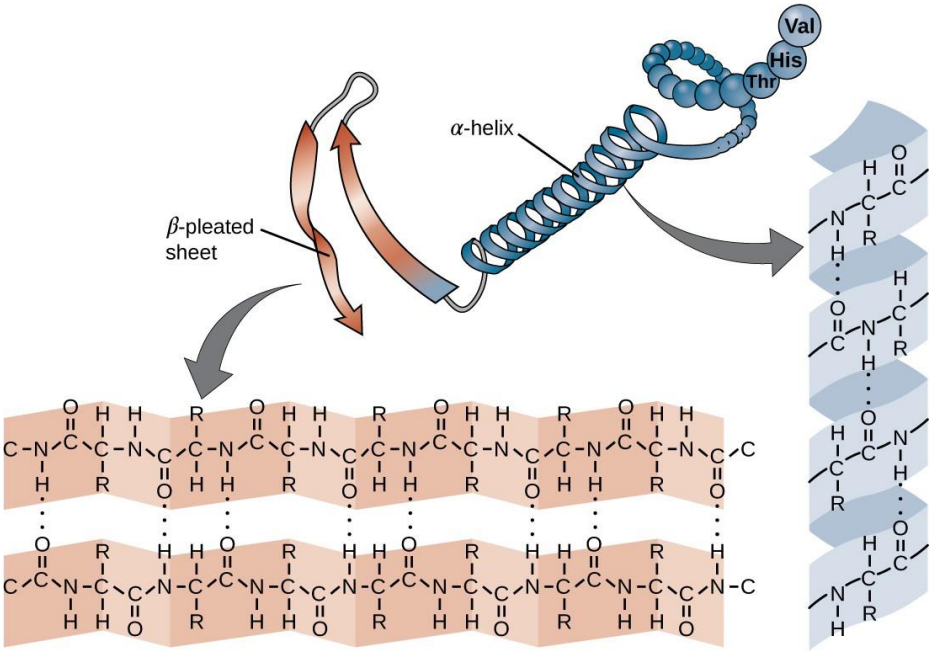

Figure I-3: Secondary protein structure scheme[15].

The tertiary structure is the 3D folded polypeptide chain. For example, considering globular small proteins (approximately 150 amino acid residues), the 3D arrangement is a spherical compact molecule that in aqueous solution have a hydrophobic core and the hydrophilic residues exposed on the surface. Thus, this structure level is formed by the interaction of secondary elements that can involve covalent disulfide bridges, hydrogen bonds, electrostatic and van der Waals interactions and hydrophobic contact. In addition to the tertiary

structure, many proteins are composed of more than one polypeptide chain and the interaction between them characterize the quaternary structure (mostly dimers or tetramers). The interactions responsible for this structural level are the same as for tertiary one[1,2,13,14]. The more energetically stable conformation giving a biological activity to the protein is known as the native state[16].

2.2. Lysozyme (LSZ)

Lysozyme (LSZ), as presented in figure I-4a, is a monomeric small protein with its structure stabilized by four disulfide bonds between eight cysteine residues. LSZ can be isolated from organs and secretions of vertebrates, invertebrates, bacteria and plants, that is the reason why lysozymes can be divided mainly into three groups: chicken type, goose-type and invertebrate-type. hen egg-white lysozyme (HEWL) has attracted a great attention due to its abundance and properties as antibacterial action. HEWL was the first enzyme to have a 3D structure determined by X-ray crystallography. The protein is composed of a single polypeptide chain made of 129 amino acids and presents mainly α-helix conformations (figure I-4b)[17,18].

(a) **(b)**

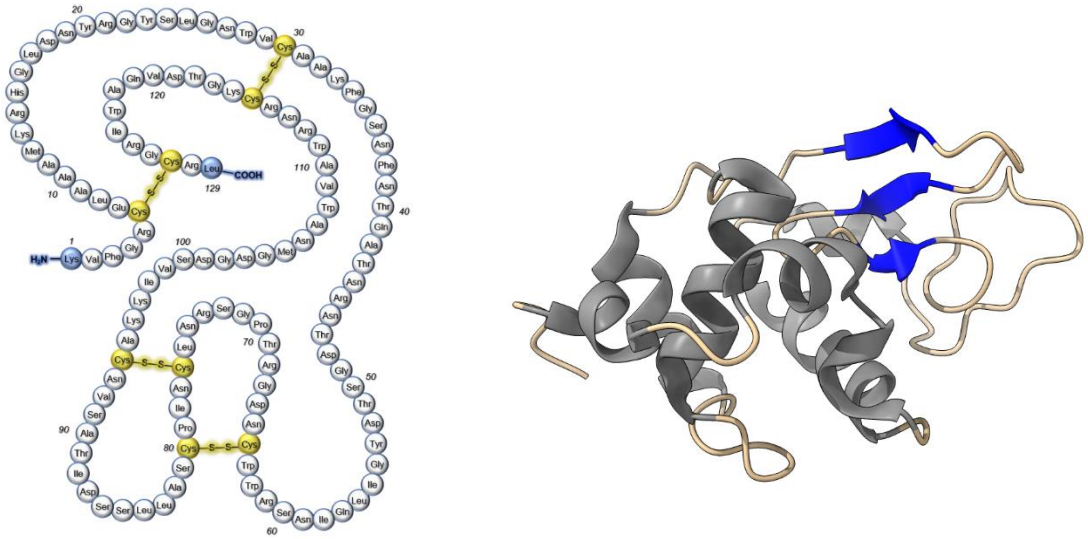

Figure I-4: Lysozyme primary (a)[19] and tertiary (b) structures.

HEWL has a molar mass of 14.3 kDa and isoelectric point (pI) of 11, it means that in neutral pH it is globally positively charged. It presents an antibacterial action due to the ability to catalyze the hydrolysis of the β-(1-4)-glycosidic bond between N-acetylmuramic acid and N-acetylglucosamine residues of gram-positive bacteria wall. This hydrolysis results in cell lysis and death. This mechanism is mostly enzymatic occurring in the active site of lysozyme (Glu 35 and Asp 52) where it can accommodate six sugars of the polysaccharide chain at the same moment, cleaving one of the bonds and releasing the fragments. The detailed mechanism is showed in figure I-5[19–22].

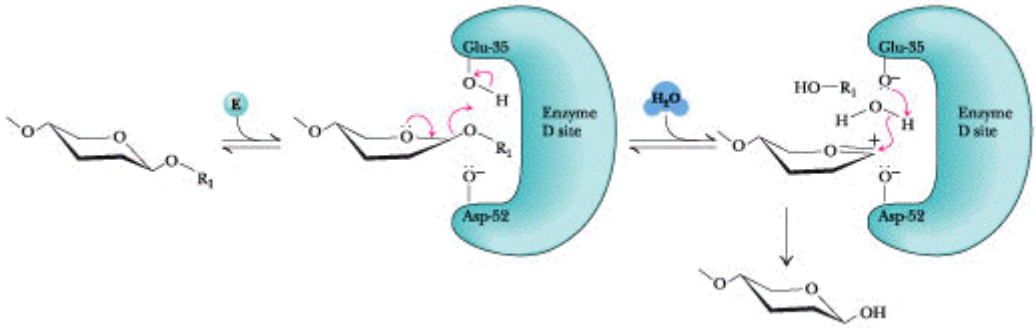

Figure I-5: The catalytic mechanism of lysozyme[23].

The mechanism starts with the substrate binding to the enzyme and changing its conformation to a strained one. The glutamic acid Glu35transfers a proton to the polar oxygen atom of the glycosidic bond, cleaving the C-O bond of the substrate. The enzyme stabilizes the formed oxonium ion with the negative charge in Asp 52 that interacts with the intermediate state and does not react with it because of the distance between the reactive groups (around 3 Å). At the end, the oxonium ion reacts with water molecule from the solvent, extracting a hydroxyl group and re-protonating Glu 35. The enzyme releases the substrate and the reaction is complete[23]. The mechanism is completely dependent of the residues position that could change due to a conformational modification (LSZ activity is structure dependent).

Lysozyme is mainly used in two industrial sectors: pharmacy and food. Pharmaceutical development faces the increase of bacteria resistance to already commercialized antibiotics (use of drug with lysozyme for laryngitis and pharyngitis). It leads the development of new

molecules and comparing therapeutic proteins with small chemical drugs, proteins are more selective, less toxic and normally present high activity even in low concentration. Lysozyme has been used for treatment of fistulas, cleaning wounds from necrotized tissues, skin grafting and other infections[24]. *Staphylococcus aureus* is a bacterium responsible for post-operative skin infections and it has been resistant against antibiotics such as methicillin. *Karachi et al.* proved the use of lysozyme against *Staphylococcus aureus* in mice skin infections and that it is a potential candidate to replace commercial antibiotics[25]. In the same area of skin infections, it was found that a concentration 5% of lysozyme-shelled microbubbles in therapeutic skin creams and ointments for local treatment produces high therapeutic effect[26]. In addition to the use in skin infections, lysozyme has been studied for the treatment of gastrointestinal diseases. Some patients need to take drugs to reduce the stomach pH. This reduction allows the bacteria *E. coli* to pass through the gastric barrier. For this, in 2014 a patent was published proposing the use of N-acetyl cysteine and microencapsulated gastro-protected lysozymes with probiotic bacteria to restore the barrier and avoid infections[27].

Enzyme use in food is associated to food preservation by adding it to the product or using it as a protective matrix during food processing. Food safety is a public health problem that is challenged by the presence of spoilage microorganisms. These microorganisms can change physically and chemically the product rendering the food unacceptable and besides can cause food-borne illnesses[28]. Natural antimicrobial agents, such as lysozyme, are being applied as food preservative to avoid the use of synthetic additives [27]. Sometimes, lysozyme has to be associated with some thermal techniques as pasteurization to reduce the required temperature to achieve spore inactivation. This protein has been used to control the two major food pathogens: *Listeria monocytogens* and *Clostridium botulinum*[29].

To the market of refrigerated meat products, lysozyme is efficient against *Listeria monocytogens* that is the responsible bacteria of pork sausage, beef and turkey meat degradation[30,31]. In the dairy industry LSZ has been used to inhibit *Clostridium botulinum*, the pathogen responsible to undesired taste and texture on cheese[29].

Independently of the application, lysozyme must undergo some industrial processes like separation and purification before application in food preservation or as an active ingredient in medical formulations. Moreover, it can be submitted to additional stress factors during its application, for example in the process of microencapsulation (pharmacology) or pasteurization (food preservative). As reported above, activity of lysozyme is dependent on its structural conformation that can change due to stress factors as heating, stirring, surface contact, among

others. It is then important to know the effect of each stress factors to guarantee the efficiency of this protein and limit the loss of bioactive molecules during the process.

Lysozyme activity is measured through a turbidity assay also called muramidase activity assay. The test consists of mixing the lysozyme solution with a solution of the bacteria *Micrococcus Lysodeikticus*. After this, turbidity is measured using UV-Vis spectroscopy at 450 nm as a function of time. The absorbance decay means that bacteria are lysed by the action of lysozyme. The higher the slope of the curve, the faster this lysis happen and the bigger the activity of lysozyme. One unit of activity is defined as an absorbance decay of 0.001 min^{-1} [10,32–35].

In the present work, lysozyme was used as a model protein to evaluate its antibacterial activity and aggregate formation after different denaturation methods as thermal, chemical and mechanical treatment. The loss or the release in the antibacterial activity as well as the formation of soluble and insoluble aggregates, can be used as an indication of denaturation. Adsorption of lysozyme on different surface substrates was also evaluated following the amount of protein adsorbed and conformational changing by FTIR-ATR.

2.3. Protein processing and denaturing agents

The native structure of a protein is the state of global minimum free energy. This structure is folded and maintained by weak interactions as hydrophobic, electrostatic, hydrogen bonds and van der Waals. These interactions are considered weak when they are taken into account individually, however, in the case of the protein structure, there is a high number of them making this molecule stable[1,36]. Denaturation is the modification of protein native structure by these interactions' breakage. It means that quaternary, tertiary and secondary structures can be modified without modification of the primary one.

When in solution, hydrophobic effect is the dominant force of stability. The non-polar side chains stay in the protein core limiting the water access to the interior of the molecule. This native state is not infinitely stable, there is an equilibrium between the folded and unfolded (denatured) protein and this equilibrium can be disturbed by some stress factors[36].

After the modification of proteins caused by denaturing agents, soluble and insoluble aggregates can be formed, protein-protein interactions are then favored compared to protein-solvent interactions. Protein aggregate are obtained by interaction between protein monomers and presents a high molecular weight as dimers, trimers, oligomers, etc. Aggregate formation

can follow different pathways as it can be constituted by native, unfolded or partially unfolded structures. Noncovalent aggregates are formed normally by van der Waals, hydrogen bonds and hydrophobic interactions while covalent ones can be the result of disulfide bonds or crosslink pathways as dityrosine formation. Therefore, reversible or irreversible aggregates are present in the solution. Irreversible aggregates can be permanently eliminated by separation techniques like filtration for example[37,38].

In literature, stress factors as temperature, pressure, shear stress and surface contact are directly correlated to the denaturation and loss in biological function of proteins. *Raškovic et al.* studied the cold storage of papain in cycles of 1 hour at -20°C. They observed an increase of 40% of intermolecular β-sheet content followed by 75% of loss in papain enzymatic activity[39]. For this particular protein, cold storage can provoke denaturation and as consequence, loss in biological activity. *Iqbal et al.* applied an ultrasonic treatment in polyphenol oxidase and observed that intensity of 400 W during 20 minutes can lead to structure changes, loss of α-helix content (secondary structure reorganization) and enzymatic activity reduced by 35%[40]. *Frachon et al.* used a microfluid setup to analyze in real time the effect of a triple interface on the insulin aggregation using a hydrophobic surface. They concluded that the insulin aggregation occurs in a triple interface (air, liquid and surface) and not only due to hydrodynamic shear stress only. A combination of shear stress, surface contact and liquid-air interface exposition[41] is necessary to induce aggregation. *Nault et al.* also studied the formation of insulin aggregates on a model hydrophobic surface (Gold-coated prism functionalized with hexadecane thiol) and they demonstrated a two-phase adsorption changes the protein conformation and allows further insulin amyloid formation in solution[42]. It indicates that sometimes more than one stress factor can act simultaneously leading to structural changes and biological activity loss due to denaturation and/or aggregation.

More details about each denaturing agent will be given on the following items considering the lysozyme as a protein of interest.

2.3.1. Thermal denaturation

Thermal stress is considered a physical factor that can break weak interactions. As the temperature rises, the kinetic energy of the medium increases, causing the protein atoms to vibrate. When the polypeptide chain atoms vibrate faster, they can disrupt hydrogen bonds, hydrophobic and van der Waals interactions. Even if the thermal denaturation of proteins is

something of everyday life like cooking eggs and meat, for the industry that sells proteins, temperature is a parameter to be controlled to guarantee the physical, chemical and biological properties of the protein.

Pasteurization and sterilization are two examples of thermal treatment used in food industry. The main goal is to eliminate microorganisms of the product. However, when proteins are present in the treated formulation aggregation or loss of biological activity can happen. These effects change the physical-chemical of product and can also reduce final efficiency[43].

Zhao and Yang 2008[44] did a comparative between the use of pulsed electric fields (PEF) and thermal treatment of lysozyme as methods to eliminate microorganisms of liquid foods. They observed, by circular dichroism and enzymatic assay, that both heating at 100°C and PEF at 35 $kV.cm^{-1}$ induced conformational and activity changes on lysozyme. While similar results of biological activity were found, structural modification mechanisms were different for these two stresses. Unfolding of the secondary and tertiary structures of lysozyme occurs concurrently to the PEF treatment. On the other side, there is a molten-globule state (mainly tertiary structure changes) during thermal unfolding of lysozyme. *Xing et al. 2016*[45] used Raman spectroscopy to analyze the molecular skeletons and side groups during the thermal modification of lysozyme. They observed that thermal denaturation follows a three-step mechanism that starts from 74°C changing the microenvironment of side groups. *Vilcacundo et al. 2018*[46] studied the antibacterial activity of lysozyme against Gram-positive and Gram-negative bacteria, after modification using heat from 80 to 120°C. They observed that heating at 120°C induced oligomer formation. These new molecules had a positive effect against Gram-negative bacteria and an activity loss against gram-positive after treatment at 80°C.

In this work, an optimized method using a 96-well microplate was used to determine antibacterial activity of lysozyme, after thermal treatment at 70 and 90°C, against *Micrococcus Lysodeikticus*. It was a first step to combine thermal treatment with ultrafiltration process as it has a potential application to avoid extreme conditions of pasteurization (temperatures from 60 to 100°C during some minutes). For example, as presented by *Subramanian 2014,* pasteurization (at mild conditions) could be used with ultrafiltration to complete product purification[47]. It is a good alternative to eliminate microorganisms without using extreme heat conditions: combining pasteurization and ultrafiltration.

2.3.2. Chemical denaturation

Chemical denaturation is a method commonly used to determine protein conformational stability[48,49]. The chemical denaturant is used to disturb protein's folded state by three possible ways: direct interaction with the protein atoms making the interactions with the denaturant more important than native ones, solvent environment modification that forces the solvation of hydrophobic core groups or a combination of both[50]. The disturbance caused on protein native state is monitored by some spectroscopic techniques like ultraviolet absorbance, circular dichroism, fluorescence and infrared. Guanidine hydrochloride (GdHCl) and urea are the most known chemical denaturants as they are very potent and also highly soluble in water [51].

Hédoux et al. 2010[52], investigated the effect of GdHCl and urea on lysozyme chemical and biological stability. They used measures of activity, microcalorimetry and Raman spectroscopy to show that both denaturants presented a direct bond with the polypeptide chain, modifying the lysozyme native structure. While 10M of guanidine hydrochloride solution induced a 40% activity loss to the lysozyme, urea decreased the activity only by 15%. They associated these decreases to the conformational changes. GdHCl impacts the secondary structure with α-helix reduction and urea modifies only the tertiary structure (molten globule state). A detailed mechanism was elucidated by *Xing et al. 2016*[45] through Raman spectroscopy. They used guanidine hydrochloride to promote the chemical denaturation of lysozyme and they followed the modifications by Raman measures. It was observed that GdHCl denatures LSZ by a multi-state and outside-in mechanism. They suggested that before changes the secondary structure, the denaturant induce modifications on the microenvironment around CH groups (with Arg, Lys and Asn residues) on the protein surface. Then, with the increase of GdHCl concentration, the microenvironment around all the side groups changes. These first two steps are characterized by a tertiary structure modification. Thirdly, the disulfide skeleton groups (closer to the surface) changes and as final step the amino skeleton groups are modified.

Siddaramaiah et al. 2017[53] used GdHCl and urea in different concentrations to denature bovine serum albumin (BSA), lysozyme, trypsin and ribonuclease A. They studied secondary structure modifications by laser induced autofluorescence and circular dichroism. They clearly demonstrated that GdHCl disrupt preferably helices as compared to β-sheets and, on the other hand, urea was more effective disrupting β-sheets.

Considering the information found in literature, chemical denaturation of LSZ with urea and guanidine hydrochloride (varying the concentration) was analyzed using the final

antibacterial activity. The results were used to compose a denaturation scale with different stress factors and also to evaluate if our optimized assay was able to detect different mechanisms of denaturation, in that case, urea *versus* GdHCl.

2.3.3. Ultrasound denaturation

Ultrasound (US) is based on cavitation generated when sound waves transit through a liquid medium. This wave transmission generates energy that can be felt in the liquid as a vibration. Vibration makes the pressure increase fast, it means, the higher the ultrasonic energy, the higher the pressure. Ultrasonic waves induce cycles of compression and expansion (formation and collapse of bubbles) in the solution, resulting on cavitation. Cavitation is the phenomena responsible to breakdown of microstructures, cell destruction and production of free radicals in the solution[54]. These properties of ultrasound can be attributed to chemical (free radical formation) or physical (cavitation, mechanical or thermal effects) principles[55].

The formed bubbles (cavities) can reach critical sizes before collapse creating strong shear stress, high pressure and temperature. These phenomena promote the protein denaturation in the called hot spots (solution region where they are combined) breaking hydrogen bonds and van der Waals interactions[35].

Ultrasound has been used as an alternative method to pasteurization in the food industry. Literature shows that pasteurization, despite eliminating unwanted microorganisms from foods, can cause the denaturation of food proteins. Degradation of these proteins changes chemically and physically the food leading to undesired effects on sensorial characteristics (taste and flavor) and nutritional value. Due to the presence of more than one type of protein, for example in dairy foods, the control of the temperature used in thermal treatments to avoid denaturation becomes complex. Ultrasound comes as a non-thermal treatment when used at low-frequencies (20-100 kHz), that is simple and low-cost[56].

Ultrasonication can be also applied in pharmaceutical sector during microencapsulation steps for enhanced drug delivery. Controlled release of proteins encapsulated in microspheres made of polymers is important to maintain the drug within the desired therapeutic range[57]. The process of microencapsulation starts with the production of a primary emulsion dispersing the protein aqueous solution into an organic solution of polymer. To promote this emulsion, ultrasound is used to generate a more homogeneous dispersion and as consequence, a higher

encapsulation quality[58]. Other pharmaceutical application that is related to the proteins is the formation of protein-coated microspheres. Ultrasonication has been used to prepare protein microspheres that present potential biomedical applications as drug delivery systems and as echo contrast for sonography and magnetic resonance imaging[57].

Taking into account that lysozyme can be used in biomedical and food sectors as antibacterial agent, it is important to know the boundary conditions of ultrasound application to avoid activity loss by denaturation. *Krishnamurthy et al. 2000*[58] dissolved LSZ in aqueous solution in the presence of methylene chloride to mimic the first step of microencapsulation. They measured the enzymatic activity of lysozyme before and after ultrasonication. They also measured the amount of precipitates formed. It was observed that ultrasonication of lysozyme with or without methylene chloride decreased the activity of LSZ using a sonic dismembrator set to deliver 50W at 20kHz during 15s. Activity loss was associated to chemical modification of lysozyme active site by free radicals. *Marchioni et al.*[59] studied the US modification during 10, 20, 30, 40, 50 and 60 minutes for lysozyme and other proteins. A change in the secondary structure can be detected after 20 minutes. They observed a decrease in α-helix content.

Ultrasound was chosen because it is a common industrial treatment. Different treatment times were studied, since several works in the literature showed its importance. Ultrasound was performed for 3, 15, 30 and 45 minutes. The final solution was analyzed in terms of biological activity and aggregate formation.

2.3.4. Ultrafiltration process

Conventional filtration is the separation of insoluble solids from a liquid or gaseous streams. Membrane filtration processes increased the separation possibility for soluble components according to their size. The membrane acts as a selective barrier that allows the passage of some components retaining the ones bigger than its pores. Membranes can be porous or nonporous and they are classified by their nature, structure, application and action mechanism.

Ultrafiltration (UF) is a pressure driven force filtration. Hydraulic pressure in this case is used to speed up the separation process and in the UF, molecules bigger than 10-200 Å are retained while the smaller ones pass through the pores. This filtration process is used in purification, concentration, desalting and fractionation[60]. UF can be operated in a dead-end or

cross-flow mode. The second one is more common, the fluid flows is tangential to the membrane surface and the permeation occurs by pressure difference. This configuration reduces membrane fouling and filter cake formation[61]. Cross-flow ultrafiltration is used for molecules concentration and separation, buffer removal, or bacteria removal in protein industry because this separation process does not require chemical reagents or heating.

To evaluate the selectivity and hydraulic membrane performances, rejection rate and hydraulic permeability are studied. The rejection rate is the percentage of molecules rejected (equation 1).

$$R_{obs} = \left(1 - (A_{perm}/A_{ret})\right) \qquad \text{Eq. 1}$$

Where: R_{obs} is the observed rejection rate, A_{perm} is the absorbance for the permeate and A_{ret} is the absorbance of the permeate.

The hydraulic performance is investigated by pure water filtration. The permeation flux (J_v) is the flow rate which passes through the membrane per m^2 of surface. It is measured at different transmembrane pressures (ΔP) and gives the hydraulic permeability (L_p) by using equation 2 (slope of the linear curve).

$$L_P = \frac{\mu . J_v}{\Delta P} \qquad \text{Eq.2}$$

Where μ is the dynamic viscosity of water at room temperature (25°C).

These two parameters, when calculated before and after molecule filtration, can give information about molecule-membrane interaction and adsorption phenomena. These parameters inform us about the condition of the membrane. For example, fouling is a problem in an industrial process because it increases the operational costs due to bigger energy consumption, cleaning, maintenance and decreases the membrane lifetime.

In the case of proteins, some studies showed a long-term fouling due to protein denaturation in the pores. *Meireles et al.* [62] observed that increasing the operational temperature induces the denaturation of bovine serum albumin. Appearance of aggregates in solution

increased the fouling of the membrane that can be detected by rejection rate increase and hydraulic permeability decrease. In the case of lysozyme, ultrafiltration is mainly used to separate it from the other proteins (ovalbumin, ovotransferrin, ovomucoid and ovomucin) in hen-egg white. However, this fractionation process is complex because shear rate and transmembrane pressure can differently influence the characteristics of each protein. In ultrafiltration at low cut-off, sieving is not the only separation mechanism separation; other parameters like electrostatic charge, pH, ionic strength and protein/protein/solvent/surface interactions are critical for protein transmission into the pores[63].

Lesnierowski et al. 2009[21], used the ultrafiltration as a preparation method of LSZ polymeric form. There are works in literature that prove the efficiency of lysozyme oligomers against Gram-negative bacteria. They studied the influence of hydrodynamic parameters of ultrafiltration on the final antibacterial activity of the polymers formed. The optimal condition to obtain a polymer formation was determined changing pressure, pH, temperature and time of ultrafiltration. Highest activity against gram-negative bacteria was observed to the lysozyme prepared after 2 hours of ultrafiltration at 50°C, 20 bar and pH 7.0. With these conditions, 53.3% of polymeric forms were obtained (33.2% of dimers and 20.1% of trimers).

A previous study showed the passage of lysozyme through the pores of ceramic (TiO_2) membranes with low cut-off (1kDa)[64]. In this study, the average pore radius was estimated around 1.6 nm (via vitamin B12 filtration) while the hydrodynamic radius of lysozyme is around 1.9 nm. It means that in its native state, LSZ could not go into the pore. However, the increase of LSZ amount in the permeate with the increase of transmembrane pressure showed that this protein could pass through the pores. They also observed hydrodynamic size changes of permeated molecules by SEC-HPLC. The passage of LSZ through the pores was associated to protein unfolding. In this work, lysozyme was ultrafiltrated using different membranes and protein sources. In that case, ultrafiltration can be considered as a denaturation method combining pressure, surface contact and shear stress.

2.4. Protein adsorption

2.4.1 Interaction protein-surface

Assuming that proteins have an amphiphilic property, they can interact with hydrophilic or/and hydrophobic surfaces. The adsorption phenomena play an important role during protein processing independently of surface material. Adsorption is caused by interactions as

electrostatic, hydrophobic and hydrogen bonding. Hydrophobicity map for lysozyme can be observed in figure I-6. Hydrophobic regions represented in yellow and hydrophilic in blue.

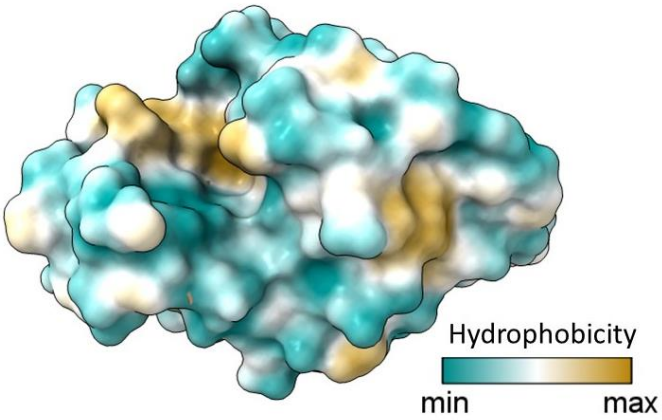

Figure I-6: Hydrophobicity scale for lysozyme molecule. Image created using ChimeraX.

As different interactions will be involved in function of surface chemistry, the kinetics and/or mechanism change will be dependent of the material. For example, for positively or negatively charged surfaces, electrostatic interactions will be more important when compared with hydrophobic ones. In this sense, adsorption kinetics will depend on thermodynamics parameters but also on protein, surface properties and environmental conditions[65].

Considering thermodynamic principle, spontaneous adsorption protein occurs when the process result in a decrease of Gibbs free energy (ΔG) of the system (protein, solvent and surface).[66] The Gibbs free energy changing is described as below:

$$\Delta G = \Delta H - T\Delta S \qquad \textit{equation (1)}$$

Where, T is the absolute temperature, ΔS is the change in entropy and ΔH is the enthalpy variation of the system. In this expression, interactions between protein and surface, protein and solvent and surface and solvent are taken into account [67].

Depending on the surface composition, adsorption phenomena are favored by different factors. For example, in nonpolar surfaces, the protein adsorbs with nonpolar groups faced to the surface, and adsorption is driven by hydrophobic interactions. To improve stabilization during the time, protein tends to increase the interactions of nonpolar amino acid residues against the materials and as consequence, the unfolding process with conformation changing happens. *Sivaraman et al.*[68], measured the change in helical structure of albumin on a hydrophobic surface (CH_3 self-assembled monolayer on gold) and it decreased from 66.5% to

14.4% with a β-sheet structure increase of approximately 27%. These results showed the destabilization of secondary structures due to hydrophobic interactions with material surface.

On polar surfaces, hydrogen bonds are formed between the polar amino acid residues of the protein and the polar groups of the surface. The protein, as macromolecule, can interact with the surface by different hydrogen-bondable groups at the same time. Then, it is spontaneous transformation with $\Delta G < 0$[67]. Unfolding protein process after adsorption on hydrophilic materials was also observed by *Fears et al.*[69].

For charged surfaces it is common to associate the energy of electrostatic attractions (i.e., ΔE) between opposite protein charges with surface as the main thermodynamic force. Protein can assume negative or positive net charge depending on the environment. If the pH is higher than protein isoelectric point (pI), the molecule has a net negative charge and if the pH is lower than the pI, protein has positive global charge. The protein will be neutral if pH equals its isoelectric point[70]. The point of view that electrostatic opposite charges interaction is the major phenomenon in adsorption thermodynamic ignores the presence of ions from salts in physiological solutions. Therefore, considering the salt presence, it is possible to affirm that adsorption is thermodynamically favored by an ion-exchange process where the ions on material surface are replaced by the charged proteins ions[67]. Considering electrostatic interactions between opposite protein and surface charges, protein orientation can be controlled depending on the organization of charged residues at the protein surface. *Zhou et al.*[71] performed *Monte Carlo* simulations to study adsorption and orientation of antibodies in charged surfaces and they found that in positive surfaces, antibodies presented a desired end-on orientation and in negative surface head-on was observed. They concluded that orientation depends on van der Waals and electrostatic interactions.

2.4.2 Kinetics of protein adsorption

Protein adsorption kinetic is the measure of protein amount adsorbed on the surface with time. There are direct and indirect ways to estimate the protein amount on surfaces. The most common technique is the Quartz Crystal Microbalance (QCM). It measures protein amount by frequency variation with time and it is an *in situ* technique. It means that all curve points are done with exactly the same environmental condition[72]. Desorption of adsorbed protein is also used to quantify it, normally, the surfaces are put in contact with protein solution, and they are collected in different time periods. After that, surfaces can be rinsed with a desorption solution

as Sodium dodecyl sulfate (SDS) and with this washing solution (containing the protein that was adsorbed before) quantification can be done using UV spectroscopy or colorimetric assays.

In the present work, protein adsorption kinetic was studied using the area of Amide I band obtained by FTIR-ATR spectroscopy. The area is proportional to the amount of protein on the surface[73–76], it means that kinetic curve can be construct as a graph of area of amide I versus time of adsorption.

Kinetic comprehension starts assuming that surface is equilibrated when in contact with protein solution and consequently, a saturation coverage will be established. In this sense, protein can be packed in a densely or loosely way, resulting in monolayers or multilayers[77]. Multilayers are found under conditions that induce protein aggregation and monolayers are formed when protein-protein interactions are weak or repulsive. It is the case when adsorption is done with pH different from pI due to similar global charge between proteins. Density of protein monolayer is also dependent of protein solution concentration and changes of protein conformation when adsorbed. At low concentration, for example, surface coverage is done slowly, so the adsorbed protein has time to change its conformation and to increase its interactions and footprint on the surface. It means that there will have less surface area available for adsorption of other molecules. On the other hand, high concentrated solutions will induce a rapid surface coverage and due to the lack of available surface and presence of neighboring proteins, structural changes will not be possible resulting in a denser protein layer [78–80].

Considering only the proteins that do not present attractive interactions with themselves, proteins start to populate the surface according to the theory of *random sequential adsorption* (RSA). Protein will adsorb only in the areas where there is no pre-adsorbed protein, it means that overlap does not happen on the beginning. If protein hit another adsorbed one, it backs to the solution volume. The probability to find an available site decreases with the increase of surface coverage and that is the reason why sometimes the *Langmuir adsorption isotherm* to gas molecules on surfaces can be followed. His theory elucidates that there is an increase on adsorbed molecules until certain time period where saturation is reached due to surface total coverage[81] but Langmuir isotherms suppose that the protein is unchanged during the process.

However, during experimental observations, overshoots and oscillations are reported. Overshoot is the situation where adsorption kinetics has a global maximum before reaching the saturation. Some works in literature explain this overshooting with a *time delay model*. With this model during the adsorption, the surface is temporally oversaturated and to reach the

equilibrium, desorption of pre-adsorbed molecules can occur[81]. It means that adsorption begins and after a certain period, desorption starts due to initial conformational change that forces the oversaturated surface situation. Desorption of a protein that had its native structure already modified makes the solution that had contact with these surfaces to present a higher number of denatured proteins. It means that surface contact can be also a stress factor responsible to the loss of stability and efficiency in solution. In addition to overshoot, oscillations on the ideal kinetic adsorption curve can also be observed due to lateral interactions and cooperative effects.

During this complex adsorption process, protein-protein and protein-surface interactions are the main keys to explain obtained results. The kinetics can be different depending on the protein used and the surface chemistry. This is why we proposed to modify the surface chemistry with the help of self-assembled monolayers for studying lysozyme adsorption.

2.4.3 Self-Assembled monolayer surfaces (SAMs)

Self-assembled monolayers (SAMs) are thin films formed on the surface with high molecular orientation and organization. SAMs are formed by the adsorption and assembly of molecules from a solution to the surface. SAMs surface preparation starts selecting the molecule to be used. In that case, head group should present higher affinity with surface and so, the monolayer can be built up directionally and homogeneously across the surface. alkyl chain between head and terminal group will determine the SAMs thickness. The terminal group (functional group) will give the surface its physical chemical properties as wettability and it can be used for further modification or interaction with external molecules[82]. With this controlled preparation, the surface chemistry and properties can be modified without impacting on physical characteristics of the substrate such as roughness.

Nowadays SAMs are being widely used to modify surfaces made of glass, silica and metals. They can be used in industry from biomedical applications to semiconductors. Metals like gold are generally modified using thiols/silane, on the other side, silicon and glass surfaces have their monolayer constructed by alkylsilanes[83] or phosphonates. Alkysilanes reacts by covalent attachment on hydroxylated surfaces. This covalent bond guarantees surfaces stability to be further used in aqueous solution[84]. To avoid the condensation of these molecules in a multilayer form, van der Waals interactions between organosilanes chains are required.

Monolayers are obtained using organosilanes with more than 10 carbon atoms and with small terminal groups to limit steric effects[85].

Böhmler et al. 2013[86] proposed to create chemically mixed SAMs surfaces. They created monolayers on silicon wafer exploiting the use of silane with non-nucleophilic functional groups (bromide) and methyl-terminated trichlorosilanes. The bromide groups were converted to NH_2 giving a surface with different ratios between amino and methyl groups. They optimized synthesis conditions to achieve monolayers with controlled chemical composition, silane organization and layer structure. The NH_2/CH_3 ratio was successfully achieve as the total conversion of Br-organosilanes happened. They showed variations in adhered bacterial numbers depending on the NH_2 surface amount.

In this work, the same mixed SAMs as proposed by *Böhmler et al.* were used in protein adsorption. However, borosilicate glass was used in place of silicon wafer. The goal is to obtain protein kinetic curve to surfaces containing 0, 25, 50, 75 and 100% of amino groups surface densities and to study adsorption and conformational changes on these substrates.

2.4.4 State of art for lysozyme surface adsorption

Conduction of experiments in the field of protein adsorption are indispensable to guarantee stability and efficiency of the product final. As already mentioned in the items above, environmental conditions as pH, ionic force, temperature, surface chemistry and protein charge can directly influence on thermodynamic and kinetic of protein adsorption. In that way, literature has a lot of works to understand the influence of these parameters, mainly surface properties, as wettability and surface charge. The goal is to determine the amount of adsorbed protein and the conformational changes depending on the surface and the conditions used during analysis.

In order to understand the influence of surface hydrophilicity on lysozyme adsorption, *Onwu et al. 2011*[87] exploited the adsorption capacity of this protein on silica and polystyrene surfaces varying concentration and ionic strength. The assay was done mixing silica and polystyrene particles with a volume of LSZ aqueous solution. After that, they quantified the adsorbed protein using the Lowry assay. For both surfaces, adsorption capacity increased with concentration, with bigger adsorbed amount on polystyrene. When ionic strength was increased, only a difference of silica isotherm was observed, suggesting that electrostatic

interaction play a major role in LSZ adsorption on silica and not on polystyrene. *Tangpasuthadol et al. 2003*[88] prepared chitosan films with different hydrophobicity. They studied the adsorption of lysozyme and bovine serum albumin on these films. It was observed an increase of protein amount adsorbed on hydrophobic surface when compared to the hydrophilic one. To the hydrophilic chitosan, LSZ adsorbed on higher amounts when compared to BSA because of electrostatic attraction between lysozyme positive charges and the negative ones from the surface (pH=7.4). The BSA has a global negative charge when in neutral pH, the electrostatic repulsion between the albumin and the hydrophilic chitosan explains its lower adsorption.

Ball et al. 1995[89] had already shown the major role of electrostatic interactions on lysozyme adsorption when they analyzed by FTIR the LSZ adsorbed into three different hydrophilic surfaces: silica, silicon and negatively charged polystyrene. In the test conditions, silicon crystal used in FTIR was negatively charged and the bigger amount of protein was found to be adsorbed on this substrate due to attractive electrostatic forces.

As important as measure the amount of adsorbed protein, understanding the adsorption kinetics curve allows the comprehension of the equilibrium phases to protein-surface interaction. *Yokoyama et al. 2003*[76] used Fourier Transform Infrared spectroscopy to quantify the lysozyme adsorbed on polytris(trimethylsiloxy)silylstyrene (pTSS) hydrophobic surface. They obtained a Langmuir model kinetic curve with a first increasing step and a second adsorption period that corresponds to the surface saturation. As two adsorption period were identified, they also evaluated the infrared spectra to have information about LSZ conformation. The protein that adsorbed in the first period had higher β-structure percentage when compared to the protein on solution. For proteins in the slower adsorption period (saturation), a higher β-sheets amount was observed. It indicates that protein adsorbed irreversibly in the faster stage and then, modified its conformation.

Other studies had reported the adsorption of lysozyme in two or more steps even to hydrophilic surfaces. *Ball and Ramsden, 2000*[90] observed a two-step kinetics to the adsorption of lysozyme on silica-titania surface. They showed that lysozyme quickly adsorbed to the surface until reached a constant amount (0.2 $\mu g.cm^{-2}$) and after the kinetic rate decreased. *Bentaleb et al. 1997*[91] also presented a multi-step adsorption of lysozyme on titanium oxide surfaces that they associated to different exchange kinetics between three coexisting conformations. In their work they also elucidated that the first step (the slowest one) could be

associated to the formation of a monolayer, while the second step is the beginning of a multilayer due to interactions between modified lysozyme on surface and protein on the solution.

Wang et al. 2022[92] used quartz crystal microbalance(QCM-D) to study lysozyme adsorption on surfaces such as borosilicate glass, polycarbonate (PC) and cellulose. With the same concentration of LSZ solution, higher adsorbed protein amounts were obtained on borosilicate glass followed by polycarbonate and cellulose. They showed that difference on adsorption should not be correlated only to hydrophobicity since borosilicate and cellulose are both very hydrophilic and presented opposite results on the amount of adsorbed lysozyme, while polycarbonate, a hydrophobic surface, had the intermediate value. Bigger adsorption into borosilicate glass was associated to attractive interaction between negative charged glass and positive lysozyme on solution. They explained that the reason why lysozyme does not adsorb on cellulose with higher amounts is that the interaction with this surface occurs through hydrogen bond interaction and LSZ in the folded state has only few hydrogen bonds acceptors or donors on surface as the most part of amino acids are already hydrated by water molecules from the solution.

There are a lot of studies in the literature that compare lysozyme adsorption on surfaces varying hydrophilicity. However, some of them omit the difference in characteristics such as roughness, geometric shape and distribution of chemical groups on the surface. *Sharma and Pattanayek 2017*[93] prepared self-assembled monolayers done on silicon wafers in order to obtain surfaces with the same roughness, well-controlled chemistry distribution and different surface energies. They evaluated the quantity and conformation of lysozyme and bovine serum albumin (BSA) that were adsorbed into these surfaces. Surfaces had amino, hydroxyl and octyl terminal groups. Surfaces were immersed in a PBS solution containing the proteins with the same concentration (1μM) and characterized by FTIR, ellipsometry and AFM. They concluded that on hydrophilic surfaces, taking into account ellipsometry measures, adsorption of both proteins was smaller when compared with more hydrophobic surfaces. The structure of the BSA was modified independently of the surface used while lysozyme was stable over a period of 24h.

Another approach to understand interactions between SAMs and lysozyme is the molecular simulations. *Xie et al. 2020*[94] investigated the adsorption of lysozyme on electrically responsive carboxyl/hydroxyl self-assembled monolayer using molecular simulation.

Electrostatic protein-surface interactions are depleted when strong negative electric field is applied, however the opposite is not true, positive electric field do not strengthen these interactions between LSZ and SAMs surface. A suggested explanation is that the hydrogen bonds formed within the surface chains, the binding of water molecules to form a water layer and the competitive adsorption from counter ions can decrease the interactions between protein and surface. They showed with the simulations that lysozyme orientation on surface could be controlled by applying positive or negative electric field in the system. Orientations as "back-on", "bottom-leaning" and "side-on" could be obtained.

The lack of experimental investigations of lysozyme adsorption on mixed self-assembled monolayer opens the gate to the importance of our investigation. The goal is to use SAMs varying the ratio between NH_2/CH_3 terminal groups to have surfaces with different wettability, surface energy and same roughness. Not only the kinetic curves will be constructed but it is also important to evaluate the secondary structure of LSZ after each contact time. SAMs were synthetized using a method developed by our group[86] and lysozyme adsorption was exploited by FTIR-ATR spectroscopy.

2.5. Protein characterization techniques

In order to conduct experiments and evaluate protein structure, some qualitative and quantitative techniques should be applied. For the part of the work where lysozyme was thermally, chemically and mechanically treated, only quantitative characterization was used and the conformational changing was evaluated through the enzymatic test against *Micrococcus Lysodeikticus*. For lysozyme adsorption into surfaces, both qualitative and quantitative techniques were used.

The most common assays used to quantify protein in solution are the colorimetric ones like the Lowry method[95], the Bradford method using the Coomassie blue G-250 dye–binding[96], the microBCA™, the biuret method[97] and the bicinchoninic acid (BCA) assay[98]. Each protein assay presents limitations and the selection of one of these should consider the sensitivity (lower detection limit), compatibility of protein with reagents used in the test and linearity of standard curve. Before choosing the method, it is also important to select the one which requires less manipulation and pre-treatments.

Apart from the chemical methods above, the amount of protein in solution can be evaluated by the UV-Vis spectroscopy at a wavelength of 280nm. It is a well-known technique that present as advantages the simplicity, fast measurement and low cost. Usually the absorbance at 280 nm is used to protein quantification as it corresponds to the tyrosine and tryptophan groups adsorption[99,100]. This technique mainly used in the literature, but some cautions should be taken due to disadvantages as low sensitivity. Once this technique is chosen for quantification, the analyst has to be sure that the solution has no big agglomerates, and that the sensitivity is high enough for the expected concentrations. In the present work, the UV-Vis spectroscopy was selected to quantification once it is the best method for the prepared samples.

In order to quantify proteins on surfaces some techniques as ellipsometry (ELM), optical waveguide lightmode spectroscopy (OWLS) and quartz crystal microbalance (QCM) can be used[101]. ELM through change of the light polarization state can measure the thickness of protein layer on surface and, as consequence, the mass of protein adsorbed can be calculated. It requires reflecting surfaces, homogeneous adsorbed layer and cannot be used with polymers. OWLS is a convenient technique with low cost, but only highly transparent planar surfaces can be investigated. Quartz crystal microbalance, in contrast to optical measures, is based on the change in oscillation frequency related to the mass load on a sensor. It presents high sensitivity, flexiblibilty (as soon as the electrode can be covered with the desired surface material), transparency, and reflectivity are not required. The bigger inconvenient of this technique is that water is considered in the given mass[65,101].

In addition to knowing the amount of protein on the surface, it is also crucial to understand if there has been any structural modification to the molecule. This structural modification occurs during adsorption due to molecule reorganization to improve protein-surface interaction leading on loss of ordered secondary structure. In this context, the techniques used are those capable of studying the secondary structure of the protein[65].

Circular dichroism (CD) is a technique that measures the difference of left and right circularly polarized light. It is known that the protein CD spectrum is a linear combination of individual secondary structures spectra since the amide chromophores of peptide chain when aligned in arrays have optical transitions that shift or split into multiple transitions. As consequence, each structural element has its specific CD spectrum. For example, β-sheet has negative bands at 218 nm and positive ones at 195 nm. On the other hand, α-helix presents negative bands in two regions at 222 and 208 nm and positive ones at 193 nm[102]. In literature, different research groups developed their own method to quantify the secondary structural

components[103–106] and so, it is not possible to compare the results of different methods. Furthermore, the β-sheet signals varies from each measure being less precise to quantify it when compared with α-helix[107]. Other disadvantage is that measures must be conducted in solution.

Protein vibrational spectra as the result of adsorption of energy by stretching and bending motions can be obtained by Fourier-transform infrared spectroscopy (FTIR). Each bond presents its characteristic wavenumber, and this value depends on inter and intramolecular effects, in the protein case, these interactions are related with peptide-bond angles and hydrogen-bonding patterns. Therefore, it is possible to estimate the secondary structure of a protein by the frequency of each component band[107]. The most studied and sensitive band for proteins is the Amide I, which appears in the range from 1600 to 1700 cm^{-1} approximately and is attributed to C=O stretching vibration of peptide bonds. Amide I is a broadband composed by the overlapping of different close bands that represent structural elements (α-helix, β-sheets, β-turns, among others)[108]. The width of each component band is large avoiding the separation during FTIR analysis. Thus, for spectra interpretation, peak fitting is required giving β-sheets signals from 1625 to 1635 cm^{-1}, α-helix at approximately 1655 cm^{-1}, unordered structure component at 1645 cm^{-1} and β-turns between 1670 and 1690 cm^{-1} [109,110].

To get the exact band values for each structural component, the second derivative of amide I region is one suggested method[108]. Peak positions can be easily find as the minimum of the second derivative function, taking into account the peaks with width bigger than 7 cm^{-1}, the one with smaller values may have arisen from spectrum noise[111–113]. Knowing the component peak values, the Fourier self-deconvolution (FSD) can be applied. The main challenge of this method is to select the conditions that achieve the best band narrowing assuming that the amide I is composed by the overlap of single components each one corresponding to one secondary structure. Thus, the approach is based on generation of *n* bands (according to the minimum of second derivative function) each one with its wavenumber and consideration of these values in a Gaussian or Lorentzian fit[111,113].

For protein adsorption on surfaces, ATR (Attenuated Total Reflectance) accessory is coupled with FTIR spectrometer to obtain protein spectrum directly on the surface. ATR is a non-destructive, surface contact method that does not require sample preparation. The spectral information is obtained by total reflection phenomena on a crystal that happens when the incident angle is greater than the critical angle. Figure I-7 shows the light transmission, reflection and refraction dependency on the sample and crystal refractive indices. Sample IR spectrum is result of the radiation at the reflection point that probes the sample with an

"evanescent wave." At a frequency within an absorption band the reflection will be attenuated, on the other hand at frequencies distant from absorption band, all light is reflected[114].

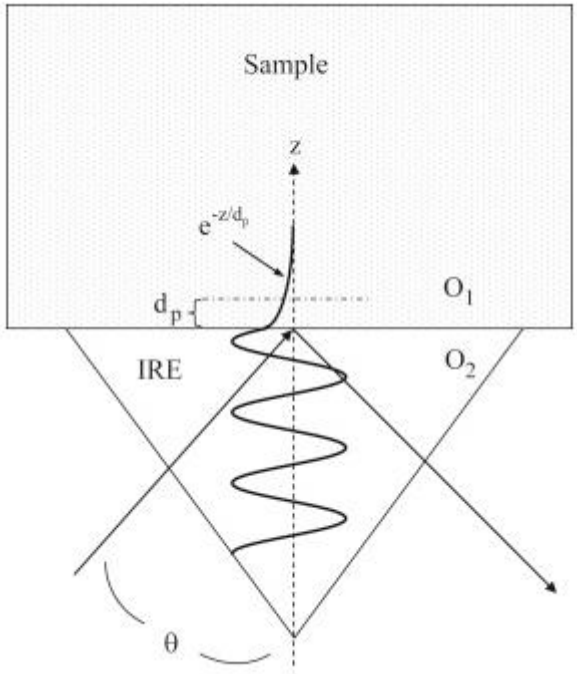

Figure I-7: Attenuated Total Reflectance accessory scheme.[114]

The contact with surface or action of denaturants can also induce aggregate formation. Identification of the presence of dimers, trimers, proteins in their oligomer form are commonly analyzed in solution. A technique that is already used for this purpose is size exclusion chromatography (SEC). The principle is based on high-performance liquid chromatography (HPLC) in which a silica porous membrane is used to separate molecules. In the case of SEC, molecules are separated by size as demonstrated in figure I-8. Molecules with big hydrodynamic radius are unable to go into the pores and are eluted rapidly (smaller retention time/volume) while molecules with small hydrodynamic radius are penetrating deeply into the pores, have a longer pathway and consequently higher elution times[115].

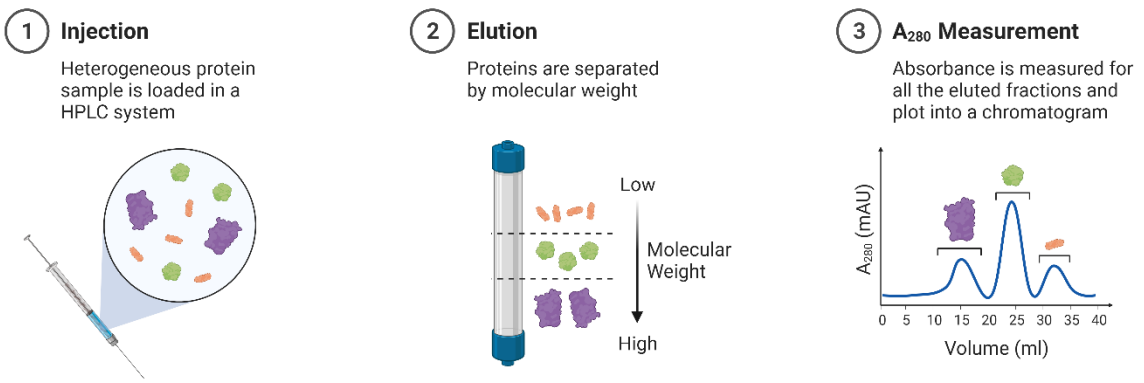

Figure I-8: SEC-HPLC principle demonstration. Created with BioRender.com.

Proteins are non-rigid molecules that can alter their tertiary and secondary structure to interact with surfaces. This statement also extends to the pore surface of the chromatography column and may cause variations in the size exclusion principle, such as retention time shift, peak tailing, asymmetry and even erroneous analysis of data due to alteration of protein structure. These are some reasons why, before any analysis, the method has to be optimized according to the protein studied. Secondary interactions with column can be limited by choosing an ideal column and mobile phase. Besides that, sensitivity and resolution can be increased by varying parameters as flow rate, injection volume and column temperature[115].

Another technique that gives information about hydrodynamic diameter of a molecule is the Dynamic Light Scattering (DLS). It has been reported as an efficient method to analyze protein aggregate in solution[116]. The principle of this technique is to measure the speed of particles in solution. The difference of particle sizes is estimated assuming the relation between the speed and the size of particles (Stokes-Einstein equation). These displacements make a visible monochromatic light to scatter in all directions as a function of size and shape of macromolecules. The scattering lights are recorded by a detector, in that case constructive or destructive fluctuations can be obtained. A digital auto-correlator creates the relationship between intensity fluctuations of scattered light and time to determine how rapidly the intensity fluctuates, which is related to the macromolecule's diffusion. Then, numerical methods are applied to extract the diameter of molecules obtained by the fit of autocorrelation function (decay of this function is proportional to the motion of particles and hence their dimensions)[116].

Bibliography

(1) Whitford, D. *Proteins Structure and Function*; John Wiley & Sons Ltd.: England, 2005.

(2) Rao, N. M. *Medical Biochemistry*, 2nd ed.; New Age International Publishers, 2006.

(3) Zhu, D.; Wu, Q.; Wang, N. Industrial Enzymes. In *Comprehensive Biotechnology, Second Edition*; Elsevier B.V., 2011; Vol. 3, pp 3–13. https://doi.org/10.1016/B978-0-08-088504-9.00182-3.

(4) Yada, R. Y. *Proteins in Food Processing*; Woodhead Publishing Limited, 2004.

(5) Leader, B.; Baca, Q. J.; Golan, D. E. Protein Therapeutics: A Summary and Pharmacological Classification. *Nat. Rev. Drug Discov.* **2008**, *7* (1), 21–39. https://doi.org/10.1038/nrd2399.

(6) Golan, D. E.; Tashjian, A. H.; Armstrong, E. J.; Armstrong, A. W. *Principles of Pharmacology: The Pathophysiologic Basis of Drug Therapy*, 2nd ed.; Lippincott Williams & Wilkins, 2007.

(7) Sava, G. Pharmacological Aspects and Therapeutic Applications of Lysozymes. *EXS* **1996**, 433–449.

(8) Okamoto, I.; Miyaji, H.; Miyata, S.; Shitomi, K.; Sugaya, T.; Ushijima, N.; Akasaka, T.; Enya, S.; Saita, S.; Kawasaki, H. Antibacterial and Antibiofilm Photodynamic Activities of Lysozyme-Au Nanoclusters/Rose Bengal Conjugates. *ACS Omega* **2021**, *6* (13), 9279–9290. https://doi.org/10.1021/acsomega.1c00838.

(9) Yang, Y. wei; Zhang, C. ning; Cao, Y. jia; Qu, Y. xia; Li, T. yi; Yang, T. ge; Geng, D.; Sun, Y. kun. Bidirectional Regulation of I-Type Lysozyme on Cutaneous Wound Healing. *Biomed. Pharmacother.* **2020**, *131*, 110700. https://doi.org/10.1016/j.biopha.2020.110700.

(10) Ragland, S. A.; Criss, A. K. From Bacterial Killing to Immune Modulation: Recent Insights into the Functions of Lysozyme. *PLoS Pathog.* **2017**, *13* (9), 1–22. https://doi.org/10.1371/journal.ppat.1006512.

(11) Wang, W. Protein Aggregation and Its Inhibition in Biopharmaceuticals. *Int. J. Pharm.* **2005**, *289*, 1–30.

(12) Wang, W. Instability, Stabilization, and Formulation of Liquid Protein Pharmaceuticals. *Int. J. Pharm.* **1999**, *185*, 129–188.

(13) Robinson, S. W.; Afzal, A. M.; Leader, D. P. Bioinformatics: Concepts, Methods, and Data. In *Handbook of Pharmacogenomics and Stratified Medicine*; Elsevier Inc., 2014; pp 259–287. https://doi.org/10.1016/B978-0-12-386882-4.00013-X.

(14) Floudas, C. A.; Fung, H. K.; McAllister, S. R.; Mönnigmann, M.; Rajgaria, R. Advances in Protein Structure Prediction and de Novo Protein Design: A Review. *Chem. Eng. Sci.* **2006**, *61* (3), 966–988. https://doi.org/10.1016/j.ces.2005.04.009.

(15) N. Cohen, G. *Microbial Biochemistry*, 3rd ed.; Springer Netherlands, 2014.

(16) Bandehagh, A.; Motie Noparvar, P.; Dorani Uliaie, E. Principles of Protein Folding. *J. Acad. Ind. Res.* **2013**, *2* (4), 216–220.

(17) Aminlari, L.; Mohammadi Hashemi, M.; Aminlari, M. Modified Lysozymes as Novel

Broad Spectrum Natural Antimicrobial Agents in Foods. *J. Food Sci.* **2014**, *79* (6), 1077–1090. https://doi.org/10.1111/1750-3841.12460.

(18) Wu, T.; Jiang, Q.; Wu, D.; Hu, Y.; Chen, S.; Ding, T.; Ye, X.; Liu, D.; Chen, J. What Is New in Lysozyme Research and Its Application in Food Industry? A Review. *Food Chem.* **2019**, *274* (September 2018), 698–709. https://doi.org/10.1016/j.foodchem.2018.09.017.

(19) Melinte, G.; Selvolini, G.; Cristea, C.; Marrazza, G. Aptasensors for Lysozyme Detection: Recent Advances. *Talanta* **2021**, *226* (January), 122169. https://doi.org/10.1016/j.talanta.2021.122169.

(20) Salazar, O.; Asenjo, J. A. Enzymatic Lysis of Microbial Cells. *Biotechnol. Lett.* **2007**, *29* (7), 985–994. https://doi.org/10.1007/s10529-007-9345-2.

(21) Lesnierowski, G.; Kijowski, J.; Cegielska-Radziejewska, R. Ultrafiltration-Modified Chicken Egg White Lysozyme and Its Antibacterial Action. *Int. J. Food Sci. Technol.* **2009**, *44* (2), 305–311. https://doi.org/10.1111/j.1365-2621.2008.01713.x.

(22) Phillips, D. C. The Three-Dimensional Structure of an Enzyme Molecule. *Sci. Am.* **1966**, *215* (5), 78–90. https://doi.org/10.1038/scientificamerican1166-78.

(23) Garrett, R. H.; Grisham, C. M. *Student Lecture Notebook for Biochemistry*; Brooks/Cole, 2005.

(24) de Espindola, A.; Dutournié, P.; Ponche, A. Impact of Industrial Stress Factors on Lysozyme Enzyme: Role of Denaturation Processes and Initial Protein Activity. *Sustain. Chem. Pharm.* **2023**, *31* (December 2022), 100964. https://doi.org/10.1016/j.scp.2022.100964.

(25) Karachi, A.; Rajaian, H.; Aminlari M, M.; Tabatabaee, A. Application of Lysozyme and Dextran Conjugated Lysozyme as Natural Antimicrobial Agents in the Treatment of Experimental Skin Wound in Mice. *Int. J. Phamaceutical Sci. Res.* **2013**, *4* (11), 4236. https://doi.org/10.13040/IJPSR.0975-8232.4(11).4236-44.

(26) Liao, A. H.; Hung, C. R.; Lin, C. F.; Lin, Y. C.; Chen, H. K. Treatment Effects of Lysozyme-Shelled Microbubbles and Ultrasound in Inflammatory Skin Disease. *Sci. Rep.* **2017**, *7*, 413–425.

(27) Ferraboschi, P.; Ciceri, S.; Grisenti, P. Applications of Lysozyme, an Innate Immune Defense Factor, as an Alternative Antibiotic. *Antibiotics* **2021**, *10* (12), 1–55. https://doi.org/10.3390/antibiotics10121534.

(28) Khorshidian, N.; Khanniri, E.; Koushki, M. R.; Sohrabvandi, S.; Yousefi, M. An Overview of Antimicrobial Activity of Lysozyme and Its Functionality in Cheese. *Front. Nutr.* **2022**, *9* (March). https://doi.org/10.3389/fnut.2022.833618.

(29) Abeyrathne, E. D. N. S.; Lee, H. Y.; Ahn, D. U. Egg White Proteins and Their Potential Use in Food Processing or as Nutraceutical and Pharmaceutical Agents-A Review. *Poult. Sci.* **2013**, *92* (12), 3292–3299. https://doi.org/10.3382/ps.2013-03391.

(30) Mangalassary, S.; Han, L.; Rieck, J.; Acton, J.; Dawson, P. Effect of Combining Nisin and/or Lysozyme with in-Package Pasteurization for Control of Listeria Monocytogenes in Ready-to-Eat Turkey Bologna during Refrigerated Storage. *Food Microbiol.* **2008**, *25*, 866–870.

(31) Min, S.; Harris, L. J.; Han, J. H.; Krochta, J. M. Listeria Monocytogenes Inhibition by Whey Protein Films and Coatings Incorporating Lysozyme. *J. Food Prot.* **2005**, *68* (11), 2317–2325.

(32) Carrillo, W.; García-Ruiz, A.; Recio, I.; Moreno-Arribas, M. V. Antibacterial Activity of Hen Egg White Lysozyme Modified by Heat and Enzymatic Treatments against Oenological Lactic Acid Bacteria and Acetic Acid Bacteria. *J. Food Prot.* **2014**, *77* (10), 1732–1739. https://doi.org/10.4315/0362-028X.JFP-14-009.

(33) Sarimov, R. M.; Binhi, V. N.; Matveeva, T. A.; Penkov, N. V.; Gudkov, S. V. Unfolding and Aggregation of Lysozyme under the Combined Action of Dithiothreitol and Guanidine Hydrochloride: Optical Studies. *Int. J. Mol. Sci.* **2021**, *22* (5), 1–16. https://doi.org/10.3390/ijms22052710.

(34) Biswas, B.; Muttathukattil, A. N.; Reddy, G.; Singh, P. C. Contrasting Effects of Guanidinium Chloride and Urea on the Activity and Unfolding of Lysozyme. *ACS Omega* **2018**, *3* (10), 14119–14126. https://doi.org/10.1021/acsomega.8b01911.

(35) Mañas, P.; Muñoz, B.; Sanz, D.; Condón, S. Inactivation of Lysozyme by Ultrasonic Waves under Pressure at Different Temperatures. *Enzyme Microb. Technol.* **2006**, *39* (6), 1177–1182. https://doi.org/10.1016/j.enzmictec.2005.11.053.

(36) Kessel, A.; Ben-tal, N. *Introduction to Proteins: Structure, Function, and Motion*, 2nd ed.; CRC Press, 2010.

(37) Mahler, H. C.; Friess, W.; Grauschopf, U.; Kiese, S. Protein Aggregation: Pathways, Induction Factors and Analysis. *J. Pharm. Sci.* **2009**, *98* (9), 2909–2934. https://doi.org/10.1002/jps.21566.

(38) Mitraki, A. *Protein Aggregation: From Inclusion Bodies to Amyloid and Biomaterials*, First.; Elsevier Inc., 2010; Vol. 79. https://doi.org/10.1016/S1876-1623(10)79003-9.

(39) Rašković, B.; Popović, M.; Ostojić, S.; Ancrossed D Signelković, B.; Tešević, V.; Polović, N. Fourier Transform Infrared Spectroscopy Provides an Evidence of Papain Denaturation and Aggregation during Cold Storage. *Spectrochim. Acta - Part A Mol. Biomol. Spectrosc.* **2015**, *150*, 238–246. https://doi.org/10.1016/j.saa.2015.05.061.

(40) Iqbal, A.; Murtaza, A.; Marszałek, K.; Iqbal, M. A.; Chughtai, M. F. J.; Hu, W.; Barba, F. J.; Bi, J.; Liu, X.; Xu, X. Inactivation and Structural Changes of Polyphenol Oxidase in Quince (Cydonia Oblonga Miller) Juice Subjected to Ultrasonic Treatment. *J. Sci. Food Agric.* **2020**, *100* (5), 2065–2073. https://doi.org/10.1002/jsfa.10229.

(41) Frachon, T.; Bruckert, F.; Le Masne, Q.; Monnin, E.; Weidenhaupt, M. Insulin Aggregation at a Dynamic Solid-Liquid-Air Triple Interface. *Langmuir* **2016**, *32* (49), 13009–13019. https://doi.org/10.1021/acs.langmuir.6b03314.

(42) Nault, L.; Guo, P.; Jain, B.; Bréchet, Y.; Bruckert, F.; Weidenhaupt, M. Human Insulin Adsorption Kinetics, Conformational Changes and Amyloidal Aggregate Formation on Hydrophobic Surfaces. *Acta Biomater.* **2013**, *9* (2), 5070–5079.

(43) Safavi Nic, S. S.; Buist, K. A.; Verdurmen, R. E. M.; Kuipers, J. A. M. Dynamic Model to Predict Heat-Induced Protein Denaturation and Fouling in a Direct Contact Steam Condensation Process. *Chem. Eng. Sci. X* **2020**, *8*, 100075. https://doi.org/10.1016/j.cesx.2020.100075.

(44) Zhao, W.; Yang, R. Comparative Study of Inactivation and Conformational Change of

Lysozyme Induced by Pulsed Electric Fields and Heat. *Eur. Food Res. Technol.* **2008**, *228* (1), 47–54. https://doi.org/10.1007/s00217-008-0905-z.

(45) Xing, L.; Lin, K.; Zhou, X.; Liu, S.; Luo, Y. Multistate Mechanism of Lysozyme Denaturation through Synchronous Analysis of Raman Spectra. *J. Phys. Chem. B* **2016**, *120* (41), 10660–10667. https://doi.org/10.1021/acs.jpcb.6b07900.

(46) Vilcacundo, R.; Méndez, P.; Reyes, W.; Romero, H.; Pinto, A.; Carrillo, W. Antibacterial Activity of Hen Egg White Lysozyme Denatured by Thermal and Chemical Treatments. *Sci. Pharm.* **2018**, *86* (4), 1–17. https://doi.org/10.3390/scipharm86040048.

(47) Subramanian, G. *Continuous Processing in Pharmaceutical Manufacturing*; Wiley-VCH Verlag GmbH & Co. KGaA, 2014.

(48) Freire, E.; Schön, A.; Hutchins, B. M.; Brown, R. K. Chemical Denaturation as a Tool in the Formulation Optimization of Biologics. *Drug Discov. Today* **2013**, *18* (19–20), 1007–1013. https://doi.org/10.1016/j.drudis.2013.06.005.

(49) Hamborg, L.; Horsted, E. W.; Johansson, K. E.; Willemoës, M.; Lindorff-Larsen, K.; Teilum, K. Global Analysis of Protein Stability by Temperature and Chemical Denaturation. *Anal. Biochem.* **2020**, *605* (July). https://doi.org/10.1016/j.ab.2020.113863.

(50) Bennion, B. J.; Daggett, V. The Molecular Basis for the Chemical Denaturation of Proteins by Urea. *Proc. Natl. Acad. Sci. U. S. A.* **2003**, *100* (9), 5142–5147. https://doi.org/10.1073/pnas.0930122100.

(51) Myers, J. K. Chemical Denaturation. *Mol. Life Sci.* **2014**, 1–7. https://doi.org/10.1007/978-1-4614-6436-5.

(52) Hédoux, A.; Krenzlin, S.; Paccou, L.; Guinet, Y.; Flament, M. P.; Siepmann, J. Influence of Urea and Guanidine Hydrochloride on Lysozyme Stability and Thermal Denaturation; A Correlation between Activity, Protein Dynamics and Conformational Changes. *Phys. Chem. Chem. Phys.* **2010**, *12* (40), 13189–13196. https://doi.org/10.1039/c0cp00602e.

(53) Siddaramaiah, M.; Satyamoorthy, K.; Rao, B. S. S.; Roy, S.; Chandra, S.; Mahato, K. K. Identification of Protein Secondary Structures by Laser Induced Autofluorescence: A Study of Urea and GnHCl Induced Protein Denaturation. *Spectrochim. Acta - Part A Mol. Biomol. Spectrosc.* **2017**, *174*, 44–53.

(54) Islam, M. N.; Zhang, M.; Adhikari, B. The Inactivation of Enzymes by Ultrasound-A Review of Potential Mechanisms. *Food Rev. Int.* **2014**, *30* (1), 1–21. https://doi.org/10.1080/87559129.2013.853772.

(55) Su, J.; Cavaco-Paulo, A. Effect of Ultrasound on Protein Functionality. *Ultrason. Sonochem.* **2021**, *76* (June), 105653. https://doi.org/10.1016/j.ultsonch.2021.105653.

(56) Munir, M.; Nadeem, M.; Qureshi, T. M.; Leong, T. S. H.; Gamlath, C. J.; Martin, G. J. O.; Ashokkumar, M. Effects of High Pressure, Microwave and Ultrasound Processing on Proteins and Enzyme Activity in Dairy Systems — A Review. *Innov. Food Sci. Emerg. Technol.* **2019**, *57* (July), 102192. https://doi.org/10.1016/j.ifset.2019.102192.

(57) Leong, T. S. H.; Martin, G. J. O.; Ashokkumar, M. Ultrasonic Encapsulation – A Review. *Ultrason. Sonochem.* **2017**, *35*, 605–614. https://doi.org/10.1016/j.ultsonch.2016.03.017.

(58) Krishnamurthy, R.; Lumpkin, J. A.; Sridhar, R. Inactivation of Lysozyme by Sonication under Conditions Relevant to Microencapsulation. *Int. J. Pharm.* **2000**, *205* (1–2), 23–34. https://doi.org/10.1016/S0378-5173(00)00473-7.

(59) Marchioni, C.; Riccardi, E.; Spinelli, S.; Dell'Unto, F.; Grimaldi, P.; Bedini, A.; Giliberti, C.; Giuliani, L.; Palomba, R.; Congiu Castellano, A. Structural Changes Induced in Proteins by Therapeutic Ultrasounds. *Ultrasonics* **2009**, *49* (6–7), 569–576. https://doi.org/10.1016/j.ultras.2009.02.003.

(60) Cheryan, M. *Ultrafiltration and Microfiltration HANDBOOK*, 2nd editio.; CRC Press, 1998.

(61) Charcosset, C. Membrane Processes in Biotechnology: An Overview. *Biotechnol. Adv.* **2006**, *24* (5), 482–492. https://doi.org/10.1016/j.biotechadv.2006.03.002.

(62) Meireles, M.; Aimar, P.; Sanchz, V. Albumin Denaturation during Ultrafiltration: Effects of Operating Conditions and Consequences on Membrane Fouling. *Biotechnol. Bioeng.* **1991**, *38*, 528–534.

(63) Cui, Z. Protein Separation Using Ultrafiltration — an Example of Multi-Scale Complex Systems. *China Particuology* **2005**, *3* (6), 343–348. https://doi.org/10.1016/s1672-2515(07)60213-9.

(64) Miron, S. M.; Dutournié, P.; Thabet, K.; Ponche, A. Filtration of Protein-Based Solutions with Ceramic Ultrafiltration Membrane. Study of Selectivity, Adsorption, and Protein Denaturation. *Comptes Rendus Chim.* **2019**, *22* (2–3), 198–205. https://doi.org/10.1016/j.crci.2018.09.011.

(65) Rabe, M.; Verdes, D.; Seeger, S. Understanding Protein Adsorption Phenomena at Solid Surfaces. *Adv. Colloid Interface Sci.* **2011**, *162* (1–2), 87–106. https://doi.org/10.1016/j.cis.2010.12.007.

(66) Barrick, D. *Biomolecular Thermodynamics: From Theory to Application*, 1st ed.; CRC Press, 2017.

(67) Latour, R. A. Fundamental Principles of the Thermodynamics and Kinetics of Protein Adsorption to Material Surfaces. *Colloids Surfaces B Biointerfaces* **2020**, *191* (March), 110992. https://doi.org/10.1016/j.colsurfb.2020.110992.

(68) Sivaraman, B.; Latour, R. A. The Adherence of Platelets to Adsorbed Albumin by Receptor-Mediated Recognition of Binding Sites Exposed by Adsorption-Induced Unfolding. *Biomaterials* **2010**, *31* (6), 1036–1044. https://doi.org/10.1016/j.biomaterials.2009.10.017.

(69) Fears, K. P.; Latour, R. A. Assessing the Influence of Adsorbed-State Conformation on the Bioactivity of Adsorbed Enzyme Layers. *Langmuir* **2009**, *25* (24), 13926–13933. https://doi.org/10.1021/la900799m.

(70) Norde, W.; Favier, J. P. Structure of Adsorbed and Desorbed Proteins. *Colloids and Surfaces* **1992**, *64* (1), 87–93. https://doi.org/10.1016/0166-6622(92)80164-W.

(71) Zhou, J.; Tsao, H. K.; Sheng, Y. J.; Jiang, S. Monte Carlo Simulations of Antibody Adsorption and Orientation on Charged Surfaces. *J. Chem. Phys.* **2004**, *121* (2), 1050–1057. https://doi.org/10.1063/1.1757434.

(72) Wang, W.; Zheng, S.; Li, J. Adsorption of Lysozyme and Antibodies at Material

Surfaces: Implications to Material Compatibility for Development of Biologics. *J. Drug Deliv. Sci. Technol.* **2022**, *73* (March), 103416. https://doi.org/10.1016/j.jddst.2022.103416.

(73) Lorenz-Fonfria, V. A. Infrared Difference Spectroscopy of Proteins: From Bands to Bonds. *Chem. Rev.* **2020**, *120* (7), 3466–3576. https://doi.org/10.1021/acs.chemrev.9b00449.

(74) Chittur, K. K. FTIR/ATR for Protein Adsorption to Biomaterial Surfaces. *Biomaterials* **1998**, *19* (4–5), 357–369. https://doi.org/10.1016/S0142-9612(97)00223-8.

(75) Ideris, N.; Ahmad, A. L.; Ooi, B. S.; Low, S. C. Correlation Study of PVDF Membrane Morphology with Protein Adsorption: Quantitative Analysis by FTIR/ATR Technique. *IOP Conf. Ser. Mater. Sci. Eng.* **2018**, *358* (1). https://doi.org/10.1088/1757-899X/358/1/012054.

(76) Yokoyama, Y.; Ishiguro, R.; Maeda, H.; Mukaiyama, M.; Kameyama, K.; Hiramatsu, K. Quantitative Analysis of Protein Adsorption on a Planar Surface by Fourier Transform Infrared Spectroscopy: Lysozyme Adsorbed on Hydrophobic Silicon-Containing Polymer. *J. Colloid Interface Sci.* **2003**, *268* (1), 23–32. https://doi.org/10.1016/j.jcis.2003.07.011.

(77) Facci, P.; Alliata, D.; Andolfi, L.; Schnyder, B.; Kötz, R. Formation and Characterization of Protein Monolayers on Oxygen-Exposing Surfaces by Multiple-Step Self-Chemisorption. *Surf. Sci.* **2002**, *504*, 282–292.

(78) Hinderliter, A.; May, S. Cooperative Adsorption of Proteins onto Lipid Membranes. *J. Phys. Condens. Matter* **2006**, *18*.

(79) Fair, B. D.; Jamieson, A. M. Studies of Protein Adsorption on Polystyrene Latex Surfaces. *J. Colloid Interface Sci.* **1980**, *77*, 525–534.

(80) Ramsden, J. J.; Maté, M. Kinetics of Monolayer Particle Deposition. *J. Chem. Soc. Faraday Trans.* **1998**, *94*, 783–788.

(81) Rabe, M.; Verdes, D.; Seeger, S. Understanding Protein Adsorption Phenomena at Solid Surfaces. *Adv. Colloid Interface Sci.* **2011**, *162* (1–2), 87–106. https://doi.org/10.1016/j.cis.2010.12.007.

(82) Hasan, A.; Pandey, L. M. *Self-Assembled Monolayers in Biomaterials*; Elsevier Ltd., 2018. https://doi.org/10.1016/B978-0-08-100716-7.00007-6.

(83) Park, J. W.; Kim, H.; Han, M. Polymeric Self-Assembled Monolayers Derived from Surface- Active Copolymers: A Modular Approach to Functionalized Surfaces. *Chem Soc Rev* **2010**, *39*, 2935–2947.

(84) Katsikogianni, M. G.; Missirlis, Y. F. Bacterial Adhesion onto Materials with Specific Surface Chemistries under Flow Conditions. *J. Mater. Sci. Mater. Med.* **2010**, *21*, 963–968.

(85) Schreiber, F. Structure and Growth of Self-Assembling Monolayers. *Prog. Surf. Sci.* **2000**, *65*, 151–257.

(86) Böhmler, J.; Ponche, A.; Anselme, K.; Ploux, L. Self-Assembled Molecular Platforms for Bacteria/Material Biointerface Studies: Importance to Control Functional Group Accessibility. *ACS Appl. Mater. Interfaces* **2013**, *5* (21), 10478–10488.

https://doi.org/10.1021/am401976g.

(87) Onwu, F. K.; Ogah, S. P. I. Adsorption of Lysozyme unto Silica and Polystyrene Surfaces in Aqueous Medium. *African J. Biotechnol.* **2011**, *10* (15), 3014–3021. https://doi.org/10.5897/AJB10.2102.

(88) Tangpasuthadol, V.; Pongchaisirikul, N.; Hoven, V. P. Surface Modification of Chitosan Films. Effects of Hydrophobicity on Protein Adsorption. *Carbohydr. Res.* **2003**, *338* (9), 937–942. https://doi.org/10.1016/S0008-6215(03)00038-7.

(89) Ball, A.; Jones, R. A. L. Conformational Changes in Adsorbed Proteins. *Langmuir* **1995**, *11* (9), 3542–3548. https://doi.org/10.1021/la00009a042.

(90) Ball, V.; Ramsden, J. J. Analysis of Hen Egg White Lysozyme Adsorption on Si(Ti)O2 | Aqueous Solution Interfaces at Low Ionic Strength: A Biphasic Reaction Related to Solution Self-Association. *Colloids Surfaces B Biointerfaces* **2000**, *17* (2), 81–94.

(91) Bentaleb, A.; Ball, V.; Haikel, Y.; Voegel, J. C.; Schaaf, P. Kinetics of the Homogeneous Exchange of Lysozyme Adsorbed on a Titanium Oxide Surface. *Langmuir* **1997**, *13* (4), 729–735.

(92) Wang, W.; Zheng, S.; Li, J. Adsorption of Lysozyme and Antibodies at Material Surfaces: Implications to Material Compatibility for Development of Biologics. *J. Drug Deliv. Sci. Technol.* **2022**, *73* (May). https://doi.org/10.1016/j.jddst.2022.103416.

(93) Sharma, I.; Pattanayek, S. K. Effect of Surface Energy of Solid Surfaces on the Micro- and Macroscopic Properties of Adsorbed BSA and Lysozyme. *Biophysical Chemistry*. 2017, pp 14–22. https://doi.org/10.1016/j.bpc.2017.03.011.

(94) Xie, Y.; Gong, W.; Jin, J.; Zhao, Z.; Li, Z.; Zhou, J. Molecular Simulations of Lysozyme Adsorption on an Electrically Responsive Mixed Self-Assembled Monolayer. *Appl. Surf. Sci.* **2020**, *506* (December 2019), 144962. https://doi.org/10.1016/j.apsusc.2019.144962.

(95) Lowry, O. H.; Rosebrough, N. J.; Farr, A. L.; Randall, L. J. Protein Measurement with the Folin Phenol Reagent. *J. Biol. Chem.* **1951**, *193*, 265–275.

(96) Badford, M. A Rapid and Sensitive Method for the Quantitation of Microgram Quantities of Protein Utilizing the Principle of Protein-Dye Binding. *Anal. Biochem.* **1976**, *72*, 248–254.

(97) Gornall, A. G. Determination of Serum Proteins by Means of the Biuret Reaction. *J. Biol. Chem.* **1949**, *177*, 751–766.

(98) Smith, P. K.; Krohn, R. I.; Hermanson, G. T.; Mallia, A. K.; Gartner, F. H.; Provenzano, M. D.; Fujimoto, E. K.; Goeke, N. M.; Olson, B. J.; Klenk, D. C. Measurement of Protein Using Bicinchoninic Acid. *Anal. Biochem.* **1985**, *150*, 76–85.

(99) Derylo-Marczewska, A.; Chrzanowska, A.; Marczewski, A. W. Morphological, Structural and Physiochemical Characteristics of the Surface of Mesocellular Silica Foam with the Adsorbed OVA and BSA Proteins. *Microporous Mesoporous Mater.* **2020**, *293*, 109769.

(100) Moradi, O.; Modarress, H.; Noroozi, M. Experimental Study of Albumin and Lysozyme Adsorption onto Acrylic Acid (AA) and 2-Hydroxyethyl Methacrylate (HEMA) Surfaces. *J. Colloid Interface Sci.* **2004**, *271*, 16–19.

(101) Zheng, K.; Kapp, M.; Boccaccini, A. R. Protein Interactions with Bioactive Glass

Surfaces: A Review. *Appl. Mater. Today* **2019**, *15*, 350–371. https://doi.org/10.1016/j.apmt.2019.02.003.

(102) Greenfield, N. J. Using Circular Dichroism Spectra to Estimate Protein Secondary Structure. *Nat. Protoc.* **2007**, *1* (6), 2876–2890. https://doi.org/10.1038/nprot.2006.202.

(103) Greenfield, N. J.; Fasman, G. D. Computed Circular Dichroism Spectra for the Evaluation of Protein Conformation. *Biochemistry* **1969**, *8*, 4108–4116.

(104) Chen, Y. H.; Yang, J. T. A New Approach to the Calculation of Secondary Structures of Globular Proteins by Optical Rotatory Dispersion and Circular Dichroism. *Biochem. Biophys. Res. Commun.* **1971**, *44*, 1285–1291.

(105) Manavalan, P.; Johnson, W. C. Variable Selection Method Improves the Prediction of Protein Secondary Structure from Circular Dichroism. *Anal. Biochem.* **1987**, *167*, 76–85.

(106) Sreerama, N.; Venyaminov, S. Y.; Woody, R. W. Estimation of Protein Secondary Structure from CD Spectra: Inclusion of Denatured Proteins with Native Proteins in the Analysis. *Anal. Biochem.* **2000**, *287*, 243–251.

(107) Pelton, J. T.; McLean, L. R. Spectroscopic Methods for Analysis of Protein Secondary Structure. *Anal. Biochem.* **2000**, *277* (2), 167–176. https://doi.org/10.1006/abio.1999.4320.

(108) Susi, H.; Byler, D. M. Resolution-Enhanced Fourier Transform Infrared Spectroscopy of Enzymes. *Methods Enzymol.* **1985**, *130* (1950), 290–311.

(109) Roach, P.; Farrar, D.; Perry, C. C. Interpretation of Protein Adsorption: Surface-Induced Conformational Changes. *J. Am. Chem. Soc.* **2005**, *127* (22), 8168–8173. https://doi.org/10.1021/ja042898o.

(110) Komorek, P.; Martin, E.; Jachimska, B. Adsorption and Conformation Behavior of Lysozyme on a Gold Surface Determined by QCM-D, MP-SPR, and FTIR. *Int. J. Mol. Sci.* **2021**, *22* (3), 1–17. https://doi.org/10.3390/ijms22031322.

(111) Kong, J.; Yu, S. Fourier Transform Infrared Spectroscopic Analysis of Protein Secondary Structures. *Acta Biochim. Biophys. Sin. (Shanghai).* **2007**, *39* (8), 549–559. https://doi.org/10.1111/j.1745-7270.2007.00320.x.

(112) Guo, C.; Guo, X.; Chu, W.; Jiang, N.; Li, H. Spectroscopic Study of Conformation Changes of Bovine Serum Albumin in Aqueous Environment. *Chinese Chem. Lett.* **2019**, *30* (6), 1302–1306. https://doi.org/10.1016/j.cclet.2019.02.023.

(113) Lu, R.; Li, W. W.; Katzir, A.; Raichlin, Y.; Yu, H. Q.; Mizaikoff, B. Probing the Secondary Structure of Bovine Serum Albumin during Heat-Induced Denaturation Using Mid-Infrared Fiberoptic Sensors. *Analyst* **2015**, *140* (3), 765–770. https://doi.org/10.1039/c4an01495b.

(114) Larkin, P. J. Instrumentation and Sampling Methods. In *Infrared and Raman Spectroscopy*; Elsevier, 2018; pp 29–61.

(115) Hong, P.; Koza, S.; Bouvier, E. S. P. A Review Size-Exclusion Chromatography for the Analysis of Protein Biotherapeutics and Their Aggregates. *J. Liq. Chromatogr. Relat. Technol.* **2012**, *35* (20), 2923–2950. https://doi.org/10.1080/10826076.2012.743724.

(116) Lorber, B.; Fischer, F.; Bailly, M.; Roy, H.; Kern, D. Protein Analysis by Dynamic Light

Scattering: Methods and Techniques for Students. *Biochem. Mol. Biol. Educ.* **2012**, *40* (6), 372–382. https://doi.org/10.1002/bmb.20644.

Chapter II – Materials and Methods

Résumé Chapitre II.

Matériels & Méthodes

Ce chapitre présente les matériels, les techniques et protocoles expérimentaux utilisés durant cette étude. Il est divisé en deux parties, la première présente les matériels et techniques utilisées pour étudier l'influence de différents facteurs de stress en solution et la seconde est relative à l'étude des interactions entre la protéine et différentes surfaces sous différentes conditions hydrodynamiques.

1- Etude de l'influence de différents facteurs de stress

Après une présentation des différents produits utilisés dans cette étude, la méthodologie mise en place pour chaque traitement est présentée. Ces traitements sont en rapport avec les traitements classiques utilisés lors de la préparation et le conditionnement de solutions protéiques dans les industries pharmaceutiques et alimentaires. Les traitements thermiques sont réalisés en chauffant la solution à 70 ou 90°C pendant une heure. Après refroidissement à température ambiante, la solution est filtrée pour éliminer les agrégats insolubles avant analyse. Deux dénaturants chimiques ont été utilisés (urée et le chlorure de guanidinium) pour étudier le comportement du lysozyme en présence d'un stress chimique. Des essais de filtration ont été réalisés en utilisant des membranes commerciales d'ultrafiltration à bas seuil de coupure en dioxyde de titane (1 kDa). La membrane est préalablement conditionnée à l'eau déminéralisée jusqu'à stabilisation des ces propriétés hydrauliques. Au cours des essais de filtration de la solution de lysozyme, des tests additionnels sont réalisés pour assurer le suivi des propriétés hydrauliques (filtration eau pure) et de sélectivité (filtration soluté neutre, Vitamine B12) de la membrane. La solution filtrée et la solution non filtrée sont prélevées pour analyse. Des traitements de durée variable (3 à 45 minutes) par ultrasons ont été réalisés sur des solutions de lysozyme. Pour éviter une élévation de température importante, le système est arrêté 5 minutes toutes les 3 minutes de traitement. Après traitement, les solutions sont filtrées pour retirer les agrégats insolubles avant analyse de la solution.

A la suite, les techniques d'analyse des solutions traitées sont présentées ; Spectroscopie UV-visible pour quantifier la quantité de lysozyme présent en solution, Chromatographie Liquide

équipée d'une colonne d'exclusion stérique pour analyser les quantités et la taille des différentes espèces présentes.

L'activité enzymatique (antibactérienne) des solutions filtrées est étudiée suivant un test normé mettant en présence la solution de lysozyme avec une solution de bactéries Gram-positive (Micrococcus Lysodeikticus). La diminution de la turbidité de la solution due à la lyse bactérienne est mesurée par spectrométrie dans le domaine visible. L'activité enzymatique est déduite de la vitesse de diminution de l'absorbance de la solution. Différents tests ont été réalisés afin de rechercher les conditions optimales d'utilisation de cette technique (concentration, dilution et modèle cinétique). A des fins de comparaison, un index d'activité a été mis en place (rapport entre l'activité enzymatique de la solution étudiée et celle de la solution référence).

2- Interactions protéines/surfaces sous différentes conditions hydrodynamiques

Dans toutes les opérations industrielles de réalisation de solutions protéiques (fabrication, purification, stérilisation, conditionnement, stockage et administration), le contact de la solution avec des matériaux est récurrent. Cette partie d'étude a donc pour but d'étudier les interactions entre la protéine (Lysozyme) et différents matériaux pour différentes conditions hydrodynamiques. Tout d'abord, les essais ont été réalisés en mode statique avec plusieurs matériaux à hydrophilicité variable, allant du très hydrophile (le verre) au très hydrophobe (le PDMS). Ces surfaces (monocouches auto-assemblées) ont été préparées à partir de verre borosilicate immergé dans une solution contenant deux organosilanes (dont l'un contient du brome) en proportion contrôlée. Après conversion du brome en groupe fonctionnel azoté, puis réduction et amination, les surfaces présentes à fois des groupements fonctionnels amine (hydrophile) et méthyle (hydrophobe). Les différents ratios entre les quantités relatives de ces deux groupements fonctionnels utilisés sont 0, 25, 50, 75, 100%. Après réalisation, ces différentes surfaces ont été caractérisées par microscopie de force atomique (rugosité), spectroscopie de photoélectrons X (stoechiométrie de surface) et des essais de mouillabilité avec 3 liquides ont été effectués (mesure d'hydrophilicité et des contributions polaires et apolaire de la tension de surface).
Les tests en statique ont été réalisés en plaçant plusieurs mêmes surfaces dans une solution de lysozyme et en les retirant après différents temps d'immersion pour analyse.

Les tests en écoulement sont réalisés dans une cellule développée au laboratoire qui permet de mettre en contact une plaque plane de 8×8 cm (du matériau à étudier) avec la solution protéique (avec ou sans écoulement) et de la retirer pour analyser la quantité de protéine adsorbée à sa surface. Deux matériaux ont été étudiés ; le verre et le polydimethylsiloxane (PDMS, polymère silicone) en écoulement laminaire, turbulent et turbulent diphasique (mélange air/eau). A l'issue du traitement, la plaque est retirée, rincée puis séchée avant analyse.

Que ce soit pour les tests statiques ou en mode dynamique, les quantités de protéines adsorbées en surface du matériau sont estimée par intégration du pic amide I obtenu par spectroscopie infra-rouge à transformée de Fourier (Réflectance totale atténuée). Dans un second temps, un ajustement numérique en 6 composantes est réalisée afin d'estimer les éventuelles modifications de structures secondaires de la protéine.

Part I – Influence of stress factors on Lysozyme antibacterial activity in solution

1. Materials

1.1 Proteins

Two lysozymes were used from Sigma-Aldrich. Table II-1 presents information regarding each one.

Table II-1. Basic information on the proteins used in the present work.

Product	**Antibacterial activity (units.mg^{-1})**	**Molar mass (g.mol^{-1})**	**Stokes radius (Å)**	**Purity (%)**	**Name used in the present work**
Lysozyme from chicken egg white, powder (crystalline)	70000	14300	19.0	98	LSZ 7.10^4
Lysozyme from chicken egg white, dialyzed, lyophilized, powder	100000				LSZ 1.10^5

1.2 Chemicals

In addition to the lysozyme, other chemical reagents were used and their essential information are shown in table II-2.

Table II-2. Information about chemical reagents used.

Product	**Molecular formula**	**Molar mass ($g.mol^{-1}$)**	**Supplier**	**Purity (%)**
Urea	CH_4N_2O	60.06	Sigma-Aldrich	98.0
Guanidine Hydrochloride	$CH_5N_3.HCl$	95.53	Sigma-Aldrich	98.0
Sodium chloride	NaCl	58.44	Sigma-Aldrich	99.5
Sodium azide	NaN_3	65.01	Acros Organics	99.0
Vitamin B12	$C_{63}H_{88}CoN_{14}O_{14}P$	1355.38	Alfa Aesar	98.0
Sodium phosphate monobasic	NaH_2PO_4	119.98	Sigma-Aldrich	99.0
Sodium phosphate dibasic	Na_2HPO_4	141.96	Sigma-Aldrich	99.0
Phosphate buffered saline tablet	-	-	Sigma-Aldrich	-
Micrococcus Lysodeikticus ATCC	-	-	Sigma-Aldrich	-

2. Solution preparation and modification

2.1 Native solution

Lysozyme native solution was prepared in deionized water (18 MΩ) considering concentration of 0.025 mM (0.36 $mg.mL^{-1}$). The amount of lysozyme (LSZ 1.10^5 or LSZ 7.10^4) was dissolved in water under continuous agitation (magnetic stirring) during 15 minutes. The calculated concentration uncertainty is less than 1%.

2.2 Thermal treatment

Thermally denatured lysozyme was prepared by heating native solution at 70°C (LSZ 70) and 90°C (LSZ 90) for 1 hour with magnetic stirring. A thermocouple was used to guarantee the accuracy of the solution temperature. After one hour, the solution was cooled down until room temperature and filtrated with a syringe filter (sterile and non-pyrogenic Polyethersulfone membrane with pore size of 0.2 µm) to eliminate any insoluble aggregate.

2.3 Chemical treatment

Chemical treatment was performed by adding a mass of urea or guanidine hydrochloric in 15 mL of LSZ native solution to reach chosen concentrations: 2, 6 and 10 $mol.L^{-1}$. The reaction media was magnetically stirred during 30 minutes. Solutions were filtered with syringe filter with a pore size of 0.2 µm.

2.4 Ultrasonic treatment

Lysozyme native solution (150 mL) was mechanically treated by ultrasonification using an ultrasonic processor Sonics Vibra cell VCX 500 with amplitude of 60% and a probe of ½" diameter. Durations of 3, 15, 30 and 45 minutes of ultrasonification were studied. The treatment is stopped during 5 minutes every 3 minutes to avoid overheating. The temperature was checked after each cycle and it was between 45 and 55°C (the temperature at which lysozyme is still stable). Every 3 minutes of ultrasound, a total energy of 8000 J was delivered to the solution. After the treatment, samples were filtered with a 0.2 µm syringe filter to eliminate aggregates.

2.5 Ultrafiltration

Filtrations were performed using an ultrafiltration pilot-plant provided by TIA Industries (Bollène, France). Figure II-1 presents the real pre-industrial setup made of stainless steel, equipped with a feed tank with capacity of 5L, a 3 Frame Plunger pump, a cooling unit composed of a heat exchanger and a refrigeration system, four manual valves (one to control transmembrane pressure and 3 to empty the pilot), two manometers and a thermometer to measure or control the pressure and temperature, respectively.

Figure II-1: Setup of the ultrafiltration pilot-plant.

The volumetric pump provides the circulation of the feed solution. The flow rate was controlled by an analogic sensor. The transmembrane pressure was adjusted between 4 and 12 bar using a manual valve. A part of the solution goes through the membrane (permeate) and the other part called retentate is rejected by the membrane. The permeate and retentate are sampled for analysis and fed back to the tank to operate with constant concentration (steady state).

The chosen membrane, supplied by TAMI Industries (Nyons, France), is a tubular mono channel one with a commercial cut-off of 1 kDa; It consists in a macro porous support in alumina coated by an active layer (TiO_2).

Before any filtration, a conditioning step is required to stabilize the hydraulic properties. This step is requisite for reaching steady membrane performances and it consists in the filtration of deionized water filtration at constant pressure (6 bar), temperature (25°C) and flow rate (500 L/h). During the experiment, the flow rate of filtrated water (permeation flux) is measured. The conditioning step was completed when the permeation flux (J_v) does not change (approximately 2 days of filtration). After that, water filtration was done increasing the transmembrane pressure (ΔP) and measuring the permeation flux. The initial hydraulic permeability (L_P) was determined as the slope of the linear curve (permeation flux versus applied pressure) according to the Darcy's law (equation 1).

$$J_V = \frac{L_P}{\mu} \Delta P \qquad \text{Equation 1}$$

Where μ s the dynamic viscosity of water at room temperature (25°C).

After stabilization of membrane properties, the selectivity of the membrane was studied by measuring the rejection rate of the target compound(s). For this, permeate and retentate are sampled and analyzed by UV-visible spectroscopy and the observed rejection rate is calculated from equation 2.

$$R_{obs} = \left(1 - (A_{perm}/A_{ret})\right) \qquad \text{Equation 2}$$

Where: R_{obs} is the observed rejection rate, A_{perm} is the absorbance for the permeate and A_{ret} is the absorbance of the retentate (absorbance values were obtained at 360 and 280 nm for Vitamin B12 and lysozyme, respectively).

According to the literature, the selectivity performances of NF/UF (low cut-off) membranes is due to three effects, i.e. steric, electric and dielectric effects. The first one is investigated by conducting filtration of aqueous solutions containing a neutral solute (Vitamin B12). In this case, electric and dielectric effects can be neglected and the rejection of the molecule is only due to steric hindrance. The experiments were performed using a concentration of 0.009 mM of Vitamin B12, filtrated at a constant flow rate (700 L/h), temperature (25°C) and pressure varying from 4 to 12 bar. At each different applied pressure, a part of retentate and permeate solutions were sampled to further analysis.

Lysozyme solutions were filtrated with similar conditions as vitamin B12 solution and the membrane performances were obtained using equations 1 and 2.

2.6 LSZ 7.10^4 dialysis

Lysozyme with smaller initial activity (7.10^4 units.mg^{-1}) was dialyzed in order to have the same informed purification process as the lysozyme with higher activity (LSZ 1.10^5). For the dialysis, a membrane Spectrum™ Labs Spectra/Por™ 1 6-8 kD MWCO supplied by Thermo Fischer Scientific was used. The membrane was rehydrated 30 minutes in deionized

water and rinsed several times to eliminate any trace of sodium azide preservative. Then, the membrane was filled with 100 mL of a 4.3 $mg.mL^{-1}$ LSZ aqueous solution, sealed and added in a beaker containing 3 L of water with magnetic stirring. Dialysis was done during 3 days changing external water in 6 cycles, 4 cycles of 3 hours and 2 overnight. The LSZ 7.10^4 solution concentration was measured with UV spectroscopy at a wavelength of 280 nm, diluted to obtain a solution of 0.025 mM and used for an ultrafiltration experiment.

3. Characterization techniques

3.1 UV-Vis spectroscopy

Lysozyme quantification after each modification were conducted using UV-Vis spectroscopy (Perkin Elmer Lambda 750, resolution of 0.17 nm, quartz cell). Using the Lambert-Beer law and a calibration curve, concentration of LSZ solutions were determined by measuring the absorbance in triplicate at 280 nm. The experimental concentration was used to perform dilutions for enzymatic tests. The calibration curve for the two LSZ sources are presented in figure II-2.

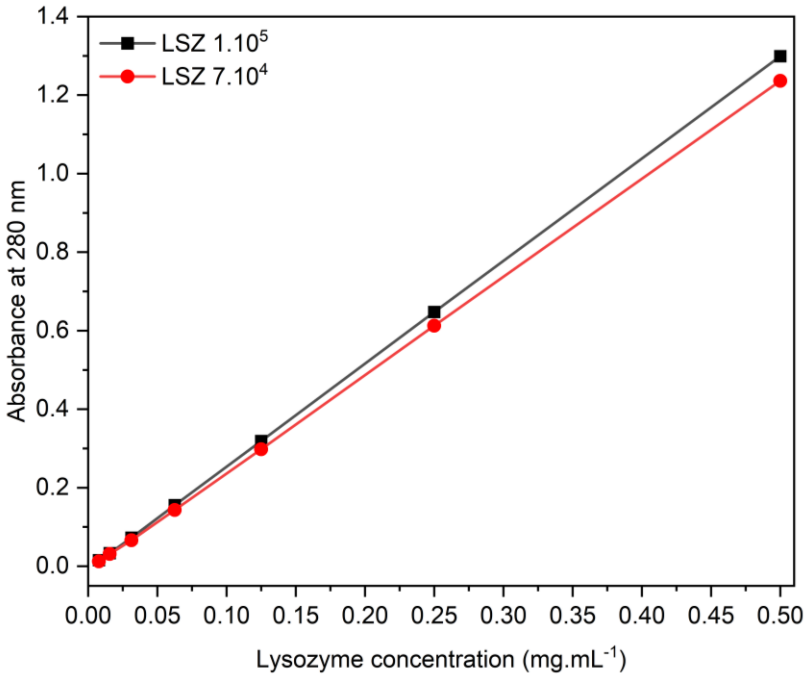

Figure II-2: Calibration curve of lysozymes.

After each treatment, as mentioned before, a filtration step was conducted with a 0.2 μm syringe filter. In order to obtain the amount of insoluble aggregates that were formed and eliminated in this step, protein amount in solution before and after filtration was obtained using UV spectroscopy. The percentage of insoluble aggregates ($\%A_{in}$) was calculated according to equation 3.

$$\%A_{in} = \left(\frac{[LSZ]_0 - [LSZ]_f}{[LSZ]_0}\right) \times 100 \qquad \text{Equation 3}$$

Where $[LSZ]_0$ is the treated lysozyme concentration before filtration and $[LSZ]_f$ is the concentration of the same solution after filtration.

UV-Vis spectroscopy was also used to obtain the absorbance values used for membrane selectivity calculation (R). The absorbance was measured at 360 nm for vitamin B12 and 280 nm for lysozyme.

3.2 Size-Exclusion High Performance Liquid Chromatography analysis (SEC-HPLC)

The prepared and modified solutions were analyzed using the technique of High Performance Liquid Chromatography (HPLC) with a size exclusion column. Agilent 1100 Series chain equipped with a quaternary pump and the ultraviolet and fluorescent detectors was used. The column was an Agilent AdvanceBio SEC 130 Å, 2.7 μm, 4.6x300 nm.

The UV detector was set to 280 nm (specific absorption from the amino acids tyrosine and tryptophan) to detect lysozyme. For the fluorescence detector, emission was fixed at 340 nm and excitation at 280nm[1–3]. Sample injection volume was fixed to 100μL, flow rate to 0.7 $mL.min^{-1}$ with analysis time of 20 minutes and column temperature at 30°C.

Elution order in SEC columns normally follows molecular weight. The largest molecules elute first because they are not able to penetrate deeply in the column pores as the smallest ones. Small molecules diffuse further into the pores and, as consequence, they are eluted as the last. This theory only considers the effect of size and not the possible interactions between molecules and the column or the hydrodynamic radius of the molecule in the mobile phase. As proteins are molecules that contain amino acids with different chemical groups like

acids, bases with hydrophobic, hydrophilic or neutral chain, mobile phase must be chosen to avoid undesired interactions with the column.

For the selected column, 150 mM PBS buffer is recommended for protein separation and analysis. However, the pH of the buffer (pH=7.2) is smaller than lysozyme pI, causing the LSZ to be, globally, positively charged during the test and, in this case, secondary interactions with the column happen and the protein is not eluted before 20 minutes (Figure II-3 red curve). To avoid interaction with the column, increasing ionic force can be a solution and the effect of sodium chloride in the mobile phase was studied. NaCl was used as it is found in literature as good candidate for ionic strength regulation in mobile phase for protein analysis [4,5]. Sodium chloride can be used to balance ionic interactions between protein and column.

The optimization was done varying NaCl concentration from 0 to 0.5 M with a fixed concentration of PBS (0.15M). The NaCl concentration of 0.5 M is the maximum tolerated by the column according to manufacturer. The preparation of PBS buffer was done by dissolving 7.56 g of NaH_2PO_4 and 12.35 g of Na_2HPO_4 in 800 mL of demineralized water. The pH was measured and corrected as 7.00 (when necessary) with a 2.0 M NaOH aqueous solution. After pH correction, the volume was completed to 1.00 L and 0.005 wt% of NaN_3 was added. For the optimization, a second bottle of 0.15 M PBS with NaN_3 was prepared containing 1.00 M of NaCl. Mobile phase with different concentrations of NaCl was obtained by mixing different ratio of the two previous solution.

The results are presented in figure II-3 and it was observed that below a NaCl concentration of 0.3 M, LSZ is not fully recovered in 20 minutes of test. Above a NaCl concentration of 0.3 M the retention time is stable (around 15 min.) and the area of the peak constant. This indicates that the maximum recovery of LSZ is obtained for higher NaCl concentration. To avoid the use of extreme condition (0.5 M maximum NaCl concentration), all analyses were conducted containing 0.3 M of NaCl in the mobile phase.

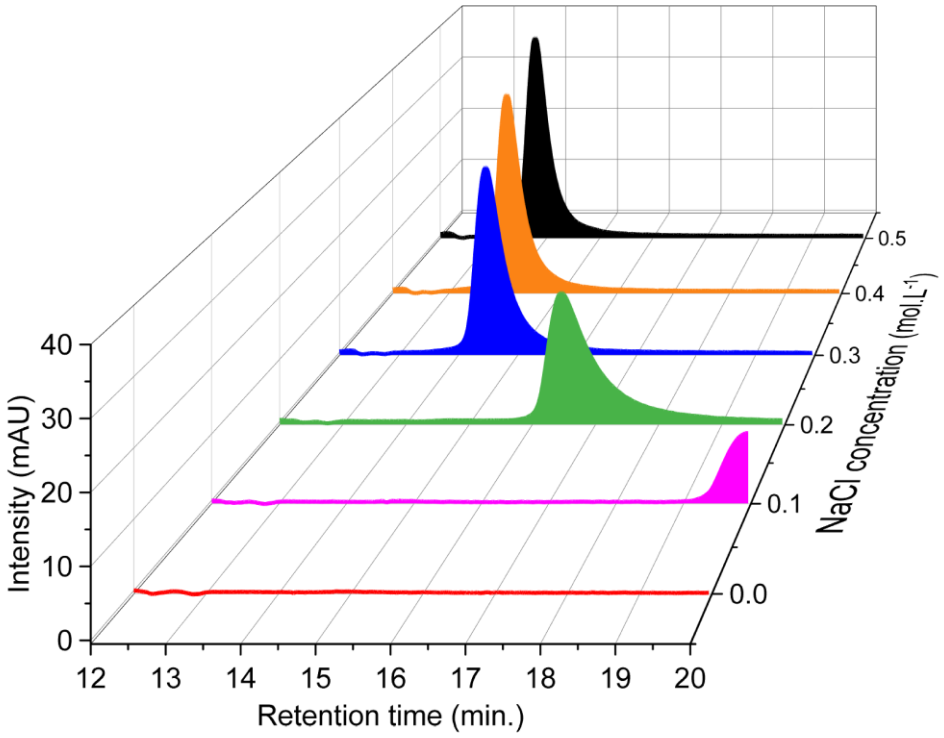

Figure II-3: Lysozyme chromatograms during SEC mobile phase optimization with different NaCl concentrations.

3.2.1 Data treatment

The peak profile for the untreated lysozyme (reference) is presented in figure II-4. Peak fitting was done by a Gaussian shape with 3 imposed components centered at 14.95, 15.15 and 15.4 minutes, respectively in Origin Pro Software. Selected range for all samples was from 14.25 to 16.00 minutes with baseline correction. The constraints for the automatic detection of peak center position were ±0.10 minutes with constant full width at half maximum (FWHM) between the three peaks. The fitting procedure was performed by iterative least-squares calculation following the input parameters of Gaussian components.

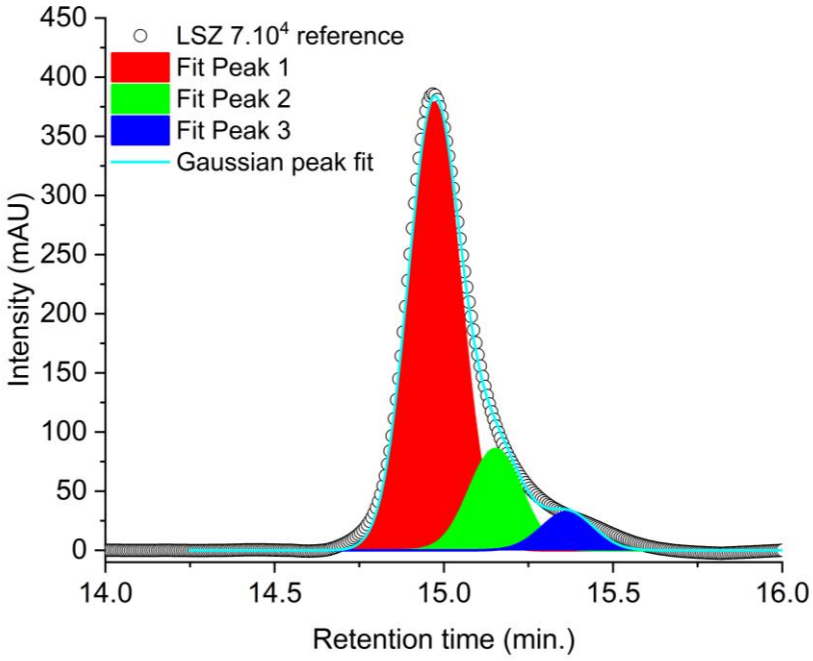

Figure II-4: Gaussian peak fitting for an untreated lysozyme (reference).

The presence of more than one component in different elution times for the reference was not expected as only lysozyme was injected in the column. This asymmetry can be associated with interactions remaining between the lysozyme and the column even after optimization of the mobile phase. While adding NaCl in the mobile phase can reduce the electrostatic effects, secondary interactions as hydrophobic and hydrogen bond ones can be responsible for this peak asymmetry and the presence of more than one component for an optimal Gaussian fit. To confirm the peak shape three reference solutions were analyzed in 3 different days and with new mobile phase preparation with the same result observed. As consequence, this model was established for all analysis.

SEC-HPLC chromatograms for LSZ 7.10^4 and LSZ 1.10^5 treated with ultrasound showed an extra component in the peak profile at 14.70 minutes. For the samples that presented this component, the fitting was done as above including the new imposed peak as the example below (figure II-5).

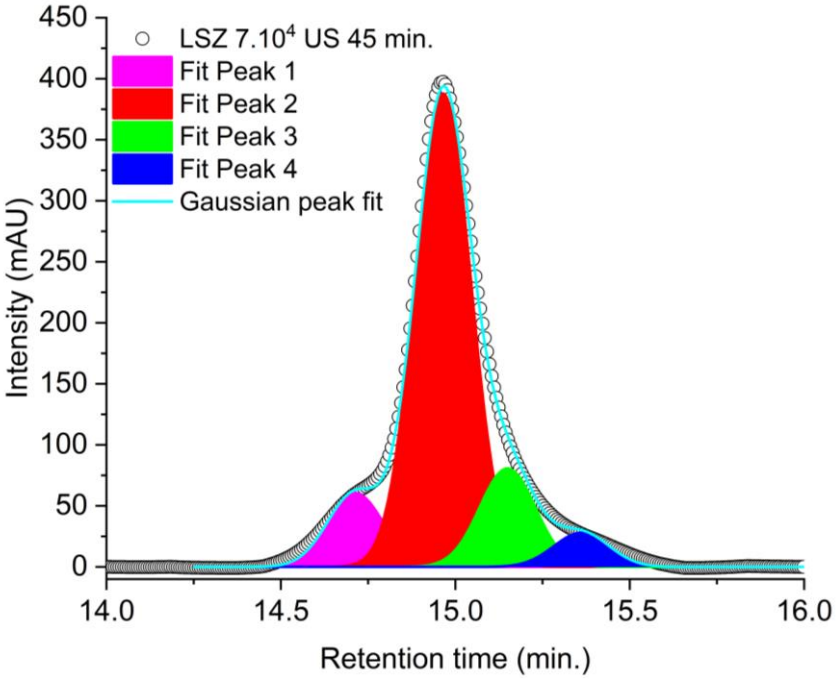

Figure II-5: Example of a Gaussian peak fitting for a lysozyme treated with ultrasound.

Considering the principle of size-exclusion columns in which molecules with higher hydrodynamic volume are eluted at smaller elution time, the peak centered at 14.70 minutes that appeared after ultrasound treatment corresponds to aggregated compounds. The percentage of aggregate formation was calculated by the ratio between the area of this peak (at 14.70 min.) and the sum of the area of all peaks of the chromatogram. An error associated with this determination was estimated as the standard deviation of the percentage obtained from 5 replicates (ultrasonic treatment of 5 different solutions).

3.3 Enzymatic activity measurements

Test parameters optimization

The antibacterial action of lysozyme occurs through an enzymatic process, where the lysozyme is the enzyme and *Micrococcus Lysodeikticus* (gram-positive bacteria), is the substrate. Enzyme transforms the substrate in a new product and its action can be measured by product formation or substrate consumption, in the present investigation, the second parameter was evaluated.

The antibacterial activity of lysozyme was determined by the decrease in turbidity of a *Micrococcus Lysodeikticus* (*ML*) suspension at 450 nm for 10 minutes with 15 seconds intervals

using a UV-Vis reader apparatus (MultiScan FC from Thermo Fischer). The decrease of turbidity at 450 nm of *ML* suspension is associated with the lysis of cell membranes under the LSZ action. Lysozyme is damaging the integrity of the cell wall and thereby acts as a bactericidal agent consuming the substrate.

The assay was conducted in a microplate to allow simultaneous measures between replicates (5 replicates in 3 different experiment days).

The concentration chosen for bacteria suspension was 0.3 $mg.mL^{-1}$ giving an initial absorbance of 0.36 at 450nm , the microplate was shaken 30s before the measure and during the test the solutions were incubated at 30°C. According to *Bisswang et al.* and *Rogers et al.*, enzyme concentration should be lower than the substrate, in that case, the concentration of LSZ cannot be bigger than 0.3 $mg.mL^{-1}$.[6,7]. Enzymatic tests were realized by changing the protein concentration to values of 0.001, 0.002, 0.005, 0.01, 0.02, 0.05, 0.10, 0.20 and 0.30 $mg.mL^{-1}$.

The evolution of *ML* lysis (absorbance decrease) versus time is presented in the figure II-6. The curves are presented as the mean of 15 different measures ± standard deviation.

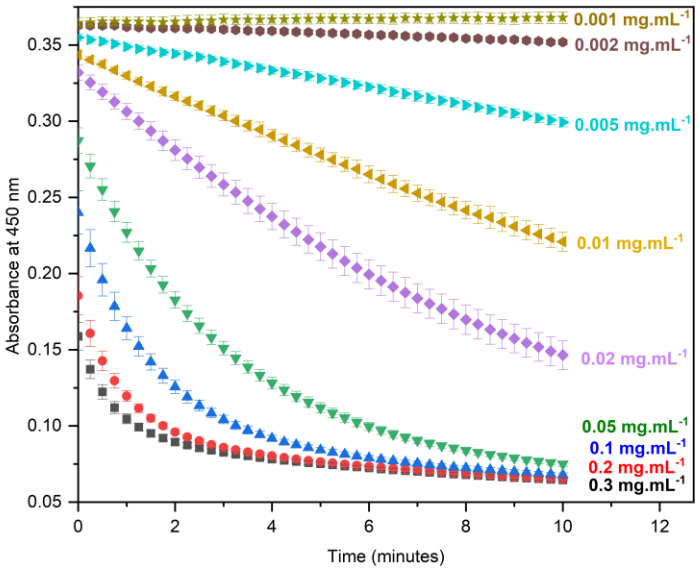

Figure II-6: Absorbance of *ML* suspension versus time with different lysozyme concentration (each point is the average of 15 measurements ± standard deviation).

It was observed in fig. II-6 that for concentrations higher than 0.02 mg.mL^{-1} the steady state (linear part of the curve) last less than 2 minutes, showing that the concentration of enzyme (LSZ) was too high and the substrate depletion was achieved very rapidly. Considering that the lysozyme activity is calculated with the slope of linear part of the curve and that before the measure a dead time exists between the reaction beginning and the detection, big amounts of enzyme increases the reaction rate, and the linear part of the curves is not detected due to the higher dead time. Slope values of linear part for the different concentrations are showed in figure II-7. The standard deviations are in agreement with the ones in figure II-6, showing that the smaller the concentration of the enzyme, smaller is the measure error. Furthermore, the linearity between lysozyme action velocity and amount is observed just until 0.02 mg.mL^{-1} indicating that concentrations between 0.002 and 0.02 mg.mL^{-1} should be considered as the best for the enzymatic assay. In this interval, the enzymatic activity is linearly dependent on the lysozyme concentration.

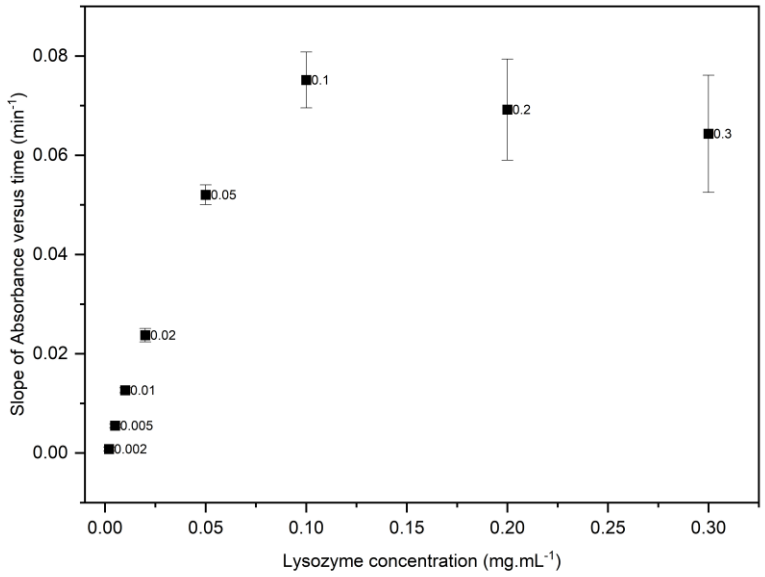

Figure II-7: Initial derivative of absorbance versus time as a function of lysozyme concentrations (n=15).

The theoretical activity for the lysozyme used in the optimization is 7.10^4 units.mg^{-1} (supplier data) and to see which condition gives the more accurate value, using the equation 4, the activity was calculated with the slope of 15 measures for each concentration. In the equation,

A_u is the activity in units.mg^{-1}, $|slope|$ is the modulus of the slope of the graph absorbance versus time and m_{LZS} is the mass of lysozyme in the test well. The figure II-8 present the results.

$$A_u = \frac{|slope|.1000}{m_{LZS}} \qquad \text{Equation 4}$$

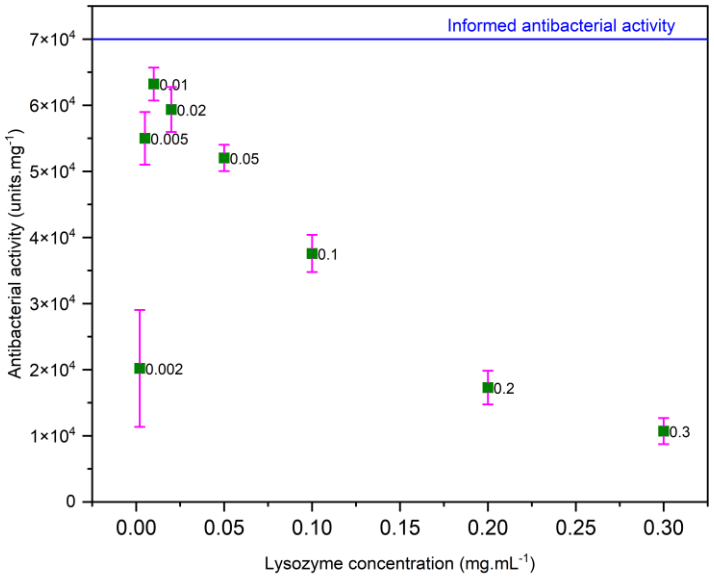

Figure II-8: Lysozyme calculated activity values with different concentrations (n=15).

Results in figure II-8 show that the maximum LSZ activity is obtained for a concentration of 0.01 mg.mL^{-1} and this concentration was used for all the following tests. Using this method, the activities average found for native LSZ 1.10^5 and LSZ 7.10^4 were 91000 and 66000 units.mg^{-1} respectively, very close from the theoretical values of 100 000 and 70000 given by the manufacturer.

Optimized enzymatic activity determination

20 µL of lysozyme aqueous solution (0.01 mg.mL^{-1}) were added in the wells quickly followed by addition of 200 µL of bacteria culture in PBS 10 mM (0.3 mg.mL^{-1}). The solutions were shaken during 30 seconds before measurement and incubated at 30°C. The absorbance reading time was 10 minutes with 15 seconds of intervals. The assays were repeated 15 times (3 different days with 5 replicates).

The reaction rate was estimated by the slope of linear part from A_{450nm} versus time graph. The activity of lysozyme (A_u) is calculated considering that one unit is defined as a decrease in absorbance at 450 nm of 0.001 min^{-1}. The value in units was divided by the mass of lysozyme in the well giving A_u in $units.mg^{-1}$ (equation 4).

An activity index is calculated by normalizing the antibacterial activity of the sample with the one of the reference (equation 5).

$$I_{Au} = \frac{A_u}{A_{u_{reference}}} \qquad \text{Equation 5}$$

Where: I_{Au} is the index of activity, A_u is the activity of the lysozyme after different treatments, $A_{u\ reference}$ is the activity of the reference lysozyme (untreated lysozyme).

Statistical data analysis

The activity index was calculated with the slope of each curve, the mean and standard deviation were obtained on 15 replicates and a box plot was used to present the results. A hypothesis test to compare the data group of reference and sample was done applying a two sample t-test with 95% of confidence interval on Origin 2021 Pro.

Part II – Interaction between lysozyme and surfaces under different hydrodynamic conditions

1. Materials and sample preparation

1.1 Protein solution

To study the interaction between protein and surface, lysozyme with higher biological activity (LSZ 1.10^5) supplied by Sigma-Aldrich was chosen. The mass corresponding to each concentration used (0.36, 1.00 and 2.00 $mg.mL^{-1}$) was dissolved in deionized water and magnetic stirring was maintained for 15 minutes before using the solution.

1.2 Surface materials for adsorption kinetics tests

The substrates used for protein adsorption tests were glass and PDMS.

PDMS surfaces were prepared using the Sylgard^{TM}184 kit from Dow Corning Corporation. The silicone elastomer was mixed with the curing agent in a 10:1 mass ratio. The mixture was done using 20 g of elastomer and it was poured in a flat polystyrene box. To eliminate bubbles, the box was gently tapped and then left at room temperature for 1 hour. After this period, silicone sheet has been thermally treated at 70°C during 6h. The substrate with a thickness of approximately 5mm was cut in rectangular pieces of 10x20 mm.

Pre-cut 15x15 mm cover slips (borosilicate glass) were purchased from Menzel-Gläser. They were used without treatment (and named glass in the current work) or modified with Self-Assembled Monolayer (SAM).[8,9] The goal of this syntheses is to control the ratio between NH_2 and CH_3 on the surface and as consequence the wettability while keeping the surface roughness constant. SAMs with 0, 25, 50, 75 and 100% of amine groups at the surface were prepared (Figure II-9). Surfaces were called Glass X% NH_2 "X" being the percentage of amino groups according to the synthesis. The SAMs fabrication was divided in 4 steps as presented below.

Step 1: Surface cleaning

Borosilicate cover slips were immersed in chloroform ($CHCl_3$ from Carlo Erba) and ultrasonically cleaned during 10 minutes to remove any trace of organic impurities. They were dried with compressed air and, treated 30 minutes with UV/Ozone ProCleaner Plus (Bioforce

Nanoscience) to eliminate contaminants and to increase the surface density of hydroxyl groups –OH on the substrate surface[9].

Step 2: Silanization and surface functionalization with bromide different densities

Just after the UV/O_3 treatment, surfaces were immersed in a solution 30/70 (volume ratio) $CHCl_3$/*n*-heptane ($CHCl_3$ from Carlo Erba and *n*-heptane from VWR chemicals) containing 11-bromoundecyltrichlorosilane and/or undecyltrichlorosilane (both purchased from ABCR, Germany) during 4h at 6°C. The use of Br-organosilane, as already presented by the group, allows a better control of surface chemistry and monolayer formation when compared to direct addition of amino-silane[8]. Silane total concentration was maintained as 1 mM and molar ratio between 11-bromoundecyltrichlorosilane and undecyltrichlorosilane was dependent on the desired percentage of bromide on the surface. In that case, percentage of bromide results in the percentage of $–NH_2$ on the end of synthesis and for the present work, the densities chosen were 0, 25, 50, 75 and 100% (Figure II-9). It means that when bromide density is 0%, the surface is completely covered with $–CH_3$ groups.

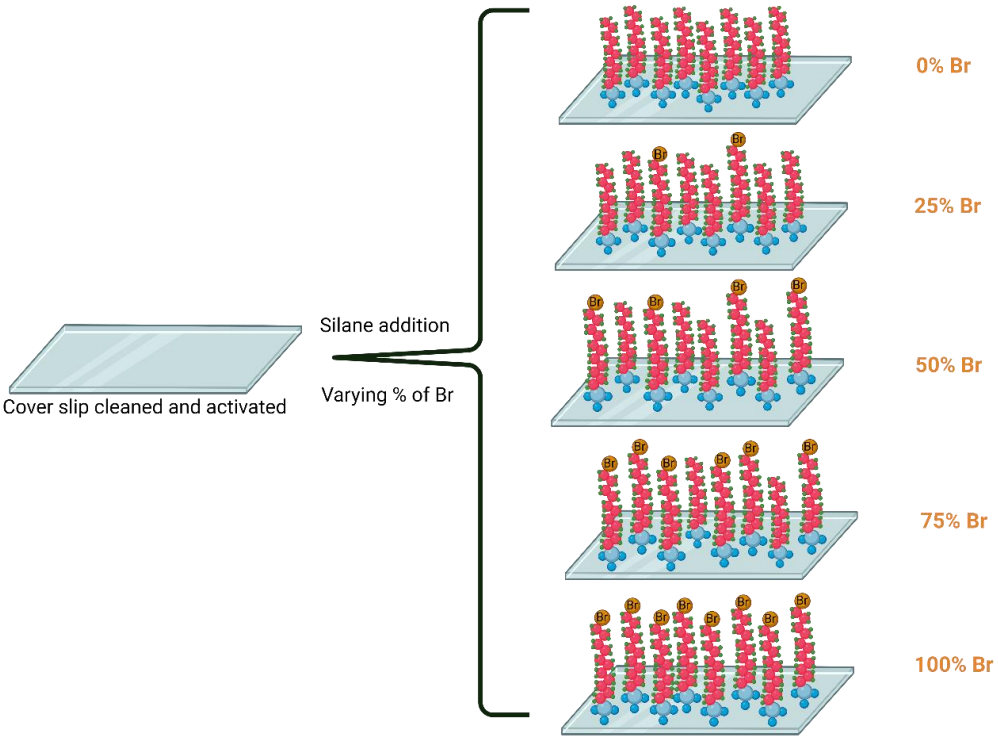

Figure II-9: Scheme of surfaces containing different bromide densities. Created with BioRender.com.

After the immersion period of 4h, surfaces were rinsed with chloroform followed by hot MilliQ water, dried using compressed nitrogen and baked in an oven for 1h at 105°C to favor the reaction between adjacent silanes.

Step 3: Conversion of bromide into azide (N_3) groups

After step 2, surfaces were immersed on dimethylformamide (Carlo Erba) solution containing 0.1 M of sodium azide (Acros Organics, 99%) for 72h at room temperature and with mechanical stirring (Heidolph Rotamax 120 shaker). Then, surfaces were rinsed with acetone (Sigma-Aldrich, Germany) followed by MilliQ water and dried using nitrogen stream. Bromine groups on sample surface are converted into azide groups via nucleophilic substitution reaction as exemplified in figure II-10. Previous articles have shown that 72h of reaction was necessary on silicon wafer substrates to obtain at leat 95% conversion of bromine groups[8].

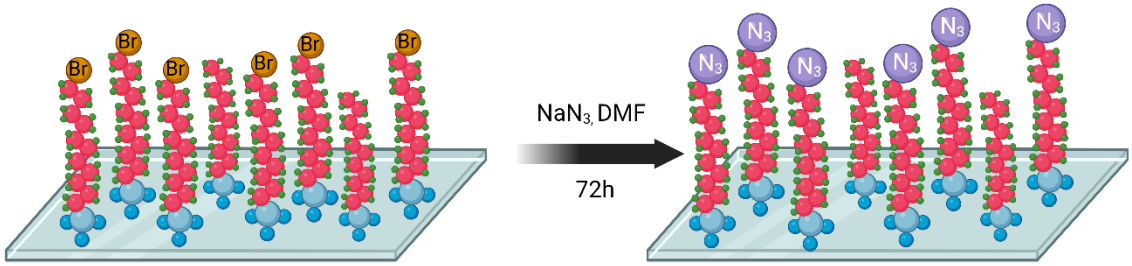

Figure II-10: Bromine conversion into azide on coverslip surfaces. SAMs fabrication step 3. Created with BioRender.com.

Step 4: Azide reduction and amination

Azide surfaces were immersed overnight in a THF anhydride solution containing 0.2 M of lithium aluminum hydride at room temperature. This step reduces azide into amine groups (Step 4, figure II-11). After this period, samples were immersed in THF for at least 12h at room temperature. Lithium complexes on the surface were removed by hydrolysis for 1 h in a 10% solution of hydrochloric acid (HCl, 37%, Sigma-Aldrich). Samples were rinsed with MilliQ water, ethanol and dried under nitrogen stream. After the reduction step and rinsing, samples were covered with trimethylamine for 24h at room temperature to convert NH_3^+ into NH_2. Finally, surfaces were rinsed with MilliQ water and ethanol and dried with nitrogen.

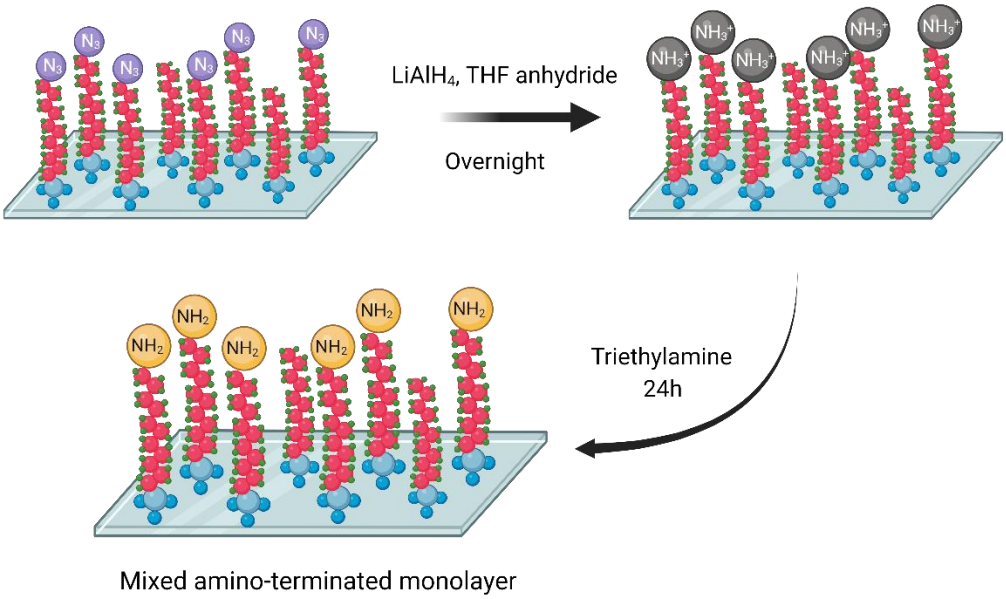

Figure II-11: Simplified scheme presenting azide reduction and surface amination to reach the final surface with an amino-terminated monolayer. Created with BioRender.com.

1.3 Surface materials for dynamic mode and plate channels

Dynamic mode test was done in a flow cell with 8x8 cm surfaces of PDMS and glass. The solution passed in the surface through 5 different channels with a constant flow rate and for the chosen periods. After that, the surface was removed from the flow cell, rinsed with water, dried and analyzed by FTIR-ATR spectroscopy. 25 points were analyzed (5 points in each channel along the flow path) as shown in figure II-12.

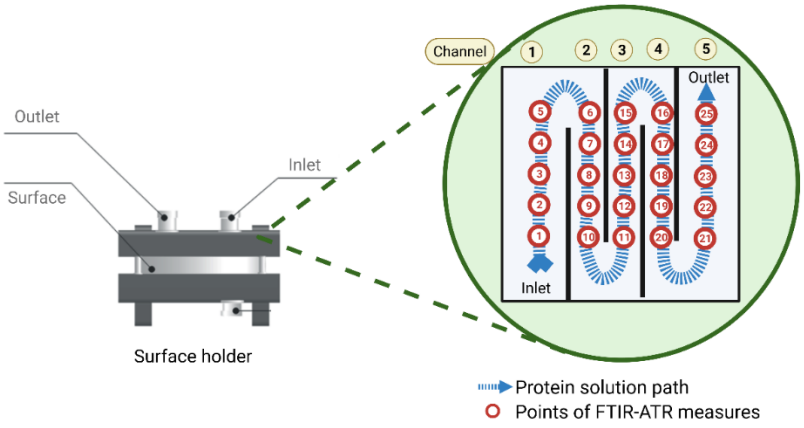

Figure II-12: Surface with schematic channels and chosen points for further FTIR-ATR analysis. Created with BioRender.com.

2. Protocols

2.1 Static mode – Adsorption kinetics test

Adsorption kinetics test was done in static mode; it means that no flow rate was applied. Before the start of the test, PDMS surfaces were washed with ethanol and water, glass surfaces were let in ultrasound bath during 10 minutes in chloroform and after rinsed with ethanol and water. Modified glass surfaces were not cleaned after the SAMs fabrication but freshly prepared and tested within 1 week.

The test consisted of immersing 11 surfaces of each material in 500 mL of lysozyme solution. Three different lysozyme concentrations were used: 0.36, 1.00 and 2.00 $mg.mL^{-1}$ for PDMS and glass. For the SAMs surfaces lysozyme concentration of 1.00 $mg.mL^{-1}$ was used. After different period of immersion (5 and 30 minutes, 1 and 5 hours, 1, 2, 3, 7, 9, 14 and 21 days), the surface was removed from the solution, rinsed with deionized water, dried at room temperature and analyzed in three points by FTIR-ATR.

2.2 Dynamic mode – Pilot-plant setup

Hydrodynamic influence on protein adsorption was studied using a laboratory pilot-plant setup as presented in figure II-13.

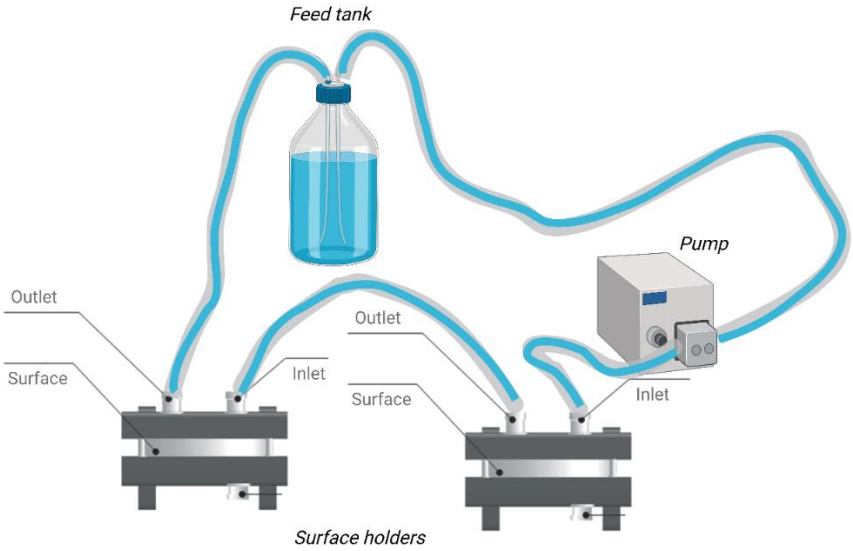

Figure II-13: Pilot-plant setup simple representation. Scheme to study the combination of surface contact and shear stress on protein adsorption and denaturation. Created with BioRender.com.

The laboratory pilot is composed by a feed tank bottle made of borosilicate glass (with 1L of capacity), a gear pump (Ismatec, Reglo-Z Digital Gear Pump) responsible for the transport of feeding solution from the tank through the whole system and two surface holders. The protein solution followed the path in the surface as described on figure II-9 going in the inlet and out from the outlet.

After installed in the surface holders, glass or PDMS were cleaned by adding deionized water in the feed tank and passing the solution with a velocity of 500 $mL.min^{-1}$. The water was changed 3 times and the cleaning was done one day long before the experiment. To study the influence of shear stress on the pre-adsorbed lysozyme, two surfaces were analyzed in series (as presented in figure II-13). Protein solution was added in the tank and the experiment started with flow rate at 50.6 $mL.min^{-1}$. This period was called laminar flow. The time and lysozyme concentration for each surface were chosen according to the adsorption kinetic test done in the static mode. Laminar flow time and concentration for each surface are described on the table II-3 below.

Table II-3. Lysozyme concentration and time used during laminar flow for different surfaces.

Surface	**Lysozyme concentration ($mg.mL^{-1}$)**	**Time of laminar low ($50.6\ mL.min^{-1}$)**
PDMS	0.36	9 days
Glass	1.00	3 days

One of the surfaces, after the laminar flow, was removed from the system, rinsed with deionized water, dried and analyzed by FTIR-ATR. The other surface was left in the surface holder and the flow rate was increased to 3.0 $L.min^{-1}$ (turbulent flow, Re > Rc = 2500) during 5h. After this period, the surface was collected, rinsed with water, dried and analyzed by FTIR-ATR.

Reynolds numbers were calculated considering that the channels are rectangular (l×e, l >> e). The experiments were performed in two flow regimes (laminar and turbulent) according to the Reynolds number $Re = \frac{2\rho q_v}{\mu(l+e)}$.

With q_v the flow rate, ρ and μ are the density and the dynamic viscosity of the fluid, respectively.

- In laminar flow (q_v= 50.6 $mL.min^{-1}$, Re=153 < Rc) and established flow (L/2e > 0.06 Re), the velocity profile is parabolic, the shear stress is $\tau = \frac{6\mu q_v}{le^2}$.

- In turbulent flow (q_v= 3 $L.min^{-1}$, Re=9170 > Rc) and established flow (L/2e > 0.63 $Re^{0.25}$), the velocity profile is linear in the viscous sub-layer, logarithmic in the buffer layer and parabolic in the central portion of the channel. The shear stress is $\tau = \rho U_\tau^2$ with U_τ the friction velocity.

3. Techniques of surface analysis

3.1 FTIR-ATR

To evaluate the protein adsorbed on studied surfaces, infrared spectrophotometer model Nicolet iS50 from Thermo Fischer was used with a VariGATR grazing angle accessory equipped with a germanium crystal. The spectra range was between 4000 and 650 cm^{-1}, the measurements were done with 64 scans and resolution of 4 cm^{-1}. To avoid water vapor

interference in detector, nitrogen flux was used. The background was discounted directly before the measure and a bare surface was used for this purpose.

3.1.1 Data treatment

The polypeptide chain gives rise to nine infrared vibrational bands called amide A, B, and amide I to VII. Among them, the amide I and II bands are the most prominent of protein backbone because amide I is related with C=O stretching vibrations of peptide linkages and amide II derives from in-plane NH bending and C-N stretching vibrations. Amide I frequencies were found to be closely related with protein secondary structure and besides that, its intensity and area are proportional to the protein amount.[10,11]

For the estimation of protein quantity adsorbed on surfaces during the time, amide I area (cm^{-1}) was used. Baseline of amide I band was corrected from 1600 to 1700 cm^{-1} with OriginPro 2022 and the area was obtained by peak integration. For each studied time and surface, 3 spectra were done choosing random surface points. For the kinetics curves, the area of Amide I band was plotted versus time and the standard deviation was calculated on 3 different measure points on the same surface.

Lysozyme secondary structure was determined assuming that amide I band is the linear sum of secondary structure elements and that the percentage of each component is only related with spectral intensity[10].Using the same range (from 1600 to 1700 cm^{-1}), baseline of amide I band and applying a Gaussian fit, the optimal model was constructed imposing 6 peak components with their assignment described in table II-4.

Table II-4: Assignments of Gaussian fit imposed peaks.

Amide I wavenumber (cm^{-1})	**Secondary structure**
1620	β-sheet intermolecular
1632	β-sheet intramolecular
1643	Random coil
1656	α-helix
1672	β-turn
1688	β-turn

Peak positions were forced to be positive and constrained to ±2 cm^{-1} of variation, bandwidth was imposed to be constant for the 6 peaks and limited to 32 cm^{-1} in order to distinguish one structural component from another. After all parameters were set, curve fitting was performed by iterative least-squares calculation. One example of this model fitting is presented below (figure II-14).

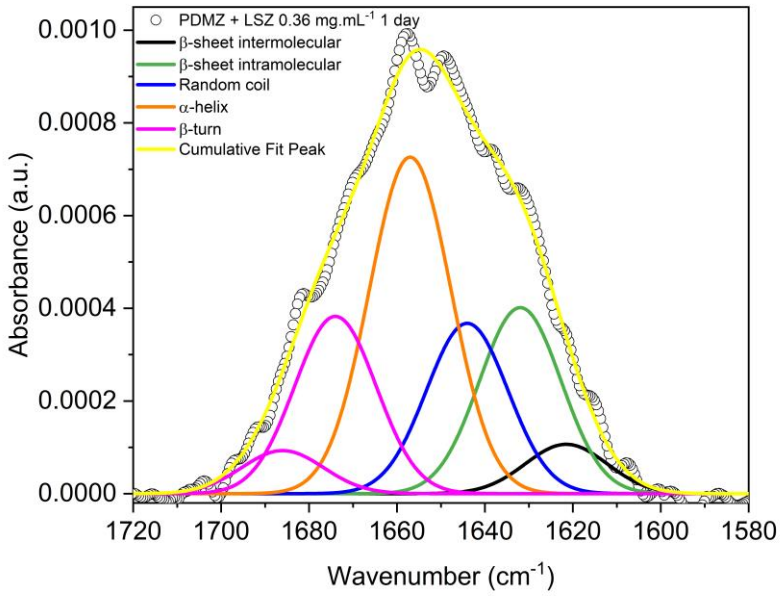

Figure II-14: Model of Amide I band fitted with Gaussian function to determine lysozyme secondary structure.

The percentage of each structural component (β-sheet, α-helix, etc.) was calculated by dividing the area of the peak by the total area of the amide I band.

3.2 Dynamic light scattering (DLS)

Dynamic light scattering (DLS) was used to determine the hydrodynamic radius of lysozyme and to detect the formation of aggregates in solution after surface adsorption kinetics test. Taking this into account, 100 µL of LSZ solution was added in the sample cell (made of a silica prism and backscattered light detection) of a VASCO^{TM} nanoparticle size analyzer from Cordouan Technologies. Measurements were done at 25°C with wavelength of 657 nm and

scattered light angle at 135°. Statistical mode was chosen with 5 acquisitions and noise limitation of 2%.

Hydrodynamic diameter was calculated directly in the Software NanoQ using the SBL algorithm that looks for multi-modal and multi dispersity size distribution and considering the 5 acquisitions.

3.3 Atomic force microscopy (AFM)

SAMs surfaces were analyzed using a digital instrument FlexAFM from NanoSurf equipped with a C3000i controller. Topographies were obtained by tapping mode AFM imaging under ambient conditions using standard silicon probes (k~13-77 $N.m^{-1}$), having a resonant frequency between 200 and 400 kHz and a tip radius smaller than 10 nm. The scan size used was 1x1 μm. Average roughness was obtained with the software Gwyddion version 2.60.

3.4 X-ray Photoelectron Spectroscopy (XPS)

X-ray Photoelectron Spectroscopy (XPS) analysis was conducted with a spectrometer model VG SCIENTA SES-2002 equipped with a concentric hemispherical analyzer. Incident radiation was generated by a monochromatic Al Kα x-ray source (1486.6 eV) operating at 420 W (14kV; 30 mA). Photo-emitted electrons were collected at a 90° take-off angle from the substrate with electron detection in the constant analyzer energy mode (FAT). Widescan spectrum signal was recorded with a pass energy of 500 eV and 100 eV for core level spectra. The analyzed surface was a rectangular area of 24 mm^2 (4x6 mm) and the base pressure during the measure was about 10^{-9} mbar.

The spectrometer energy scale was calibrated using the Ag 3d5/2, Au 4f7/2 and Cu 2p3/2 core level peaks, setting at binding energies of 368.2, 84.0 and 932.6 eV, respectively. The peak areas were determined with linear background using CASAXPS version 2.3.18 software. Peak integration of each component taking into account transmission factor of the spectrometer, mean free path and Scofield sensitivity factors was used to obtain the surface composition in atomic percentages. Binding energies (BE) are referenced to C1s peak at 285.0 eV.

3.5 Contact angle

Wettability of bare and modified glass surfaces were assessed by contact angle measurements using the sessile drop method at room temperature. Contact angle was obtained using a DSA100 (Krüss. Germany) goniometer coupled with a camera and an image analyzer software. The static contact angle (θ) was obtained some seconds after deposing a 2 µL liquid droplet on the surface. The values were calculated by fitting a circle on the shape of the drop and the results were obtained as an average of 6 independent measures for each surface.

Surface energy could be calculated from the measure of contact angle between the surface and three different liquids: water, diiodomethane and ethylene glycol. Lifshitz-van der Waals theory was used. According to this theory, the interaction energy (ΔG) between the liquid and the surface can be described by equation 6.

$$\Delta G = -A_{LS}(1+\cos\theta)\gamma = -2A_{LS}(\sqrt{\gamma_S^{LW}\gamma_L^{LW}} + \sqrt{\gamma_S^{+}\gamma_L^{-}} + \sqrt{\gamma_S^{-}\gamma_L^{+}}) \qquad \text{Equation 6}$$

Where A_{LS} is the contact area between the liquid and the surface, γ_S and γ_L are the apparent surface tension on the interface solid/gas and liquid/gas, respectively. LW is the apolar van der Waals interactions and the polar contribution is divided on two components γ^+ (electron acceptor) and γ^- (electron donor).

First, a simple measure of contact angle between a liquid and the surface can give the value of interaction energy (ΔG). To obtain the different contributions ($\gamma_S^{LW}, \gamma_S^{+}$ and γ_S^{-}) , three liquids with different polarities should be used. The values of surface tension components for each liquid were extracted from the literature[12] and are shown in table II-5.

Table II-5: Apolar and polar surface tension components for water, ethylene glycol and diiodomethane[12,13].

Liquid	γ^{LW}	γ^{+}	γ^{-}
Water	21.8	25.5	25.5
Diiodomethane	50.8	0.0	0.0
Ethylene Glycol	29.0	1.92	47.0

Bibliography

(1) Pellegrino, L.; Tirelli, A. A Sensitive HPLC Method to Detect Hen's Egg White Lysozyme in Milk and Dairy Products. *Int. Dairy J.* **2000**, *10* (7), 435–442. https://doi.org/10.1016/S0958-6946(00)00065-0.

(2) Yue, Q.; Niu, L.; Li, X.; Shao, X.; Xie, X.; Song, Z. Study on the Interaction Mechanism of Lysozyme and Bromophenol Blue by Fluorescence Spectroscopy. *J. Fluoresc.* **2008**, *18* (1), 11–15. https://doi.org/10.1007/s10895-007-0228-7.

(3) Jain, N.; Bhattacharya, M.; Mukhopadhyay, S. Kinetics of Surfactant-Induced Aggregation of Lysozyme Studied by Fluorescence Spectroscopy. *J. Fluoresc.* **2011**, *21* (2), 615–625. https://doi.org/10.1007/s10895-010-0749-3.

(4) Goyon, A.; Fekete, S.; Beck, A.; Veuthey, J. L.; Guillarme, D. Unraveling the Mysteries of Modern Size Exclusion Chromatography - the Way to Achieve Confident Characterization of Therapeutic Proteins. *J. Chromatogr. B Anal. Technol. Biomed. Life Sci.* **2018**, *1092* (June), 368–378. https://doi.org/10.1016/j.jchromb.2018.06.029.

(5) Arakawa, T.; Ejima, D.; Li, T.; Philo, J. S. The Critical Role of Mobile Phase Composition in Size Exclusion Chromatography of Protein Pharmaceuticals. *J. Pharm. Sci.* **2010**, *99* (4), 1674–1692. https://doi.org/10.1002/jps.

(6) Rogers, A.; Gibon, Y. Enzyme Kinetics: Theory and Practice. In *Plant Metabolic Networks*; Springer Science+Business Media, 2009; pp 1–331. https://doi.org/10.1007/978-0-387-78745-9.

(7) Bisswanger, H. *Practical Enzymology*; Wiley-VCH Verlag & Co. KGaA, 2011.

(8) Böhmler, J.; Ponche, A.; Anselme, K.; Ploux, L. Self-Assembled Molecular Platforms for Bacteria/Material Biointerface Studies: Importance to Control Functional Group Accessibility. *ACS Appl. Mater. Interfaces* **2013**, *5* (21), 10478–10488. https://doi.org/10.1021/am401976g.

(9) Tomasovic, L.; Fioux, P.; Gilbert, F.; Jacquet, D.; Verchère, D.; Bally-Le Gall, F.; Ponche, A. Self-Assembled Monolayers with a Controlled Density of Hydroxyl Groups: A Relevant Model to Investigate the Adhesion Properties of Epoxy Adhesives. *J. Phys. Chem. C* **2022**, *126* (6), 3227–3234. https://doi.org/10.1021/acs.jpcc.1c10432.

(10) Kong, J.; Yu, S. Fourier Transform Infrared Spectroscopic Analysis of Protein Secondary Structures. *Acta Biochim. Biophys. Sin. (Shanghai).* **2007**, *39* (8), 549–559. https://doi.org/10.1111/j.1745-7270.2007.00320.x.

(11) Lu, R.; Li, W. W.; Katzir, A.; Raichlin, Y.; Yu, H. Q.; Mizaikoff, B. Probing the Secondary Structure of Bovine Serum Albumin during Heat-Induced Denaturation Using Mid-Infrared Fiberoptic Sensors. *Analyst* **2015**, *140* (3), 765–770. https://doi.org/10.1039/c4an01495b.

(12) Kwok, D. Y.; Lee, Y.; Neumann, A. W. Evaluation of the Lifshitz-van Der Waals/Acid-Base Approach to Determine Interfacial Tensions. 2. Interfacial Tensions of Liquid-Liquid Systems. *Langmuir* **1998**, *14* (9), 2548–2553. https://doi.org/10.1021/la970460e.

(13) Dutournié, P.; Said, A.; Daou, T. J.; Bikaï, J.; Limousy, L. Hydraulic Performance Modifications of a Zeolite Membrane after an Alkaline Treatment: Contribution of Polar and Apolar Surface Tension Components. *Adv. Mater. Sci. Eng.* **2015**, *2015*. https://doi.org/10.1155/2015/524259.

Chapter III – Evaluation of enzymatic activity under different stress factors

Résumé Chapitre III.

Evaluation de l'activité enzymatique du lysozyme sous différents facteurs de stress

Ce chapitre présente l'étude de l'effet de différents facteurs de stress sur l'activité enzymatique du lysozyme. Plusieurs facteurs de stress ont été étudiés (chimiques, thermiques et mécaniques). Afin de compléter les informations obtenues via l'activité antibactérienne, la formation d'agrégats solubles et insolubles a été étudiée et quantifiée.

Pour ce faire, les solutions de protéines traitées sont préalablement filtrées afin d'éliminer les agrégats insolubles. L'activité antibactérienne du lysozyme de la partie filtrée a été mesurée en présence d'un facteur de stress en utilisant le test optimisé et la méthode présentés dans le chapitre précédent. La solution filtrée est également analysée par chromatographie liquide afin d'évaluer la taille des espèces en solution et d'en déduire la quantité d'agrégats solubles.

Ces essais ont été réalisés à partir de deux sources de lysozyme, provenant du même fabricant et présentant des activités antibactériennes différentes (10^5 vs. 7 10^4 unités / mg).

Traitements thermiques :

L'étude a été réalisée sur des solutions non traitées (référence) et traitées à 70°C et 90°C. Seules les solutions traitées à 90°C présentent une diminution de l'activité enzymatique (entre 20 et 30%) par rapport à la solution référence. En parallèle, le pourcentage d'agrégats insolubles est faible, n'excédant pas 3% pour toutes les solutions étudiées. Les analyses chromatographiques montrent une augmentation du rayon hydrodynamique du lysozyme après le traitement à 90°C.

Dénaturation chimique :

L'effet de deux dénaturants chimiques a été étudié (l'urée et le chlorure de guanidinium). Les résultats obtenus sont similaires pour les deux sources de lysozyme et montrent une faible diminution de l'activité enzymatique pour le traitement avec l'urée et une décroissance importante avec le sel de guanidine (30-35%) et ce d'autant plus que la concentration saline est importante. En parallèle, le pourcentage d'agrégats insolubles est important pour les deux dénaturants et augmente avec la concentration (jusqu'à 45% pour le chlorure de guanidinium 10 M). Ces résultats montrent que les mécanismes de dénaturation sont différents en présence de ces deux produits chimiques.

Traitement par ultrasons :

Différents temps de traitement ont été appliqués aux solutions de lysozyme (3,15,30 et 45 minutes). Il apparait que l'activité enzymatique du lysozyme commence à diminuer après 15 minutes de traitement et ce d'autant plus que le temps de traitement est long. Il semblerait qu'il y ait une différence entre les deux sources de lysozyme. En effet, après 15 minutes de traitement, l'index d'activité de LSZ 7 10^4 reste inchangé, alors que celui de LSZ 10^5 varie avec la pression transmembranaire. La quantité d'agrégats insolubles est relativement faible (maximum de 7%) mais augmente avec le temps de traitement. L'analyse par chromatographie liquide en exclusion stérique montre la présence d'un pic à des temps de rétention plus courts dont l'aire augmente en fonction du temps de traitement. Ce pic est associé à la formation d'agrégats solubles dont la proportion est estimée par ajustement du pic. La comparaison de la diminution de l'activité enzymatique de la solution avec la quantité d'agrégats solubles montre que cette diminution d'activité ne peut être expliquée que par la seule formation d'agrégats.

Ultrafiltration des solutions de lysozyme :

Une étude précédente réalisée avec des solutions de lysozyme 10^5 a montré que l'activité enzymatique des solutions ultrafiltrées (perméat) était plus faible que la solution référence. De plus, il apparaît que plus la pression transmembranaire appliquée est importante plus l'activité antibactérienne de la solution est faible (perte d'activité de 40-50% à 12 bar). De même, l'analyse chromatographique des solutions filtrées montrait un décalage de pic. Au contraire,la solution non filtrée (rétentat) ne présentait aucune modification de son activité antibactérienne. Après vérification et validation de ces résultats, les mêmes analyses ont été effectuées avec le lysozyme 7 10^4 avec les mêmes membranes dans les mêmes conditions. Les résultats ne montrent aucune modification de l'activité enzymatique du lysozyme des solutions ultrafiltrées. Ces résultats montrent que le comportement et les propriétés des deux lysozymes est différent face à cette opération unitaire.

Afin de comprendre l'origine de ce fait, des analyses et essais complémentaires ont été réalisés, par exemple après dialyse de la solution de lysozyme 7 10^4. Les résultats restent inchangés et ne permettent donc pas d'expliquer la différence de comportement des deux lysozymes.

Ce chapitre se termine par une synthèse des modifications d'activité enzymatique obtenues pour les divers traitements étudiés. Ces résultats mettent en exergue qu'aucun traitement n'inactive complètement le lysozyme et que chacun d'eux agit de manière différente sur les protéines.

This chapter presents the effect of different stress factors on the lysozyme antibacterial activity. The goal here is to study the consequences in terms of lysozyme activity loss of some common stresses used in the industry like temperature (for pasteurization), ultrasound (for homogenization before microencapsulation process) and ultrafiltration (for concentration, purification and separation). As presented in the materials and methods part, a biological assay was optimized and to evaluate its potential to follow lysozyme loss of activity, chemical denaturation with known denaturants as urea and guanidinium hydrochloride has been studied.

For mechanical treatments (ultrasound and ultrafiltration) some different results were observed for the lysozymes presented in materials and methods (LSZ 1.10^5 and LSZ 7.10^4). The information provided by the supplier (Sigma-Aldrich) is that the two lysozymes are from the same source (chicken hen egg-white), however, the purification process was different, LSZ 1.10^5 being dialyzed and crystallized and LSZ 7.10^4 was lyophilized without dialysis step. As a result of unknown production details, one lysozyme has an initial antibacterial activity against *Micrococcus Lysodeikticus* of 100,000 units.mg^{-1} (called LSZ 1.10^5) and the other 70,000 units.mg^{-1} (LSZ 7.10^4).

1. Quantification of insoluble aggregates after each modification

Between the modification applied to the lysozyme solutions and the performance of the biological tests, the solutions were filtered to eliminate large aggregates. Insoluble aggregates may interfere with the biological test since it relies on a measure of turbidity.

Despite this, it is interesting to quantify the insoluble aggregates after each modification as it is an indication of strong denaturation and consequent loss of function. Aggregation is a challenge for biopharmaceutical production and formulation of therapeutic protein and peptides since they can cause immune reactions, decrease product efficacy with consequent increase of production cost.

A protein can undergo various aggregation pathways depending on the applied stress. Aggregates are the result of the accumulation of partially and/or completely unfolded proteins. At the beginning, reversible oligomers are formed due to exposure of hydrophobic amino acids. Different protein chains can interact via strong hydrophobic contacts and satisfy their hydrogen bonding needs forming irreversible, non-native oligomers that can stay as just dimers/oligomers or can grow through different mechanisms[1–4]. We have evaluated after filtration the amount of insoluble aggregates formed in the solution. The quantity can give an insight about the

denaturation pathway and the efficiency for the denatured form to induce aggregates of large size.

Table III-1 presents the percentage of insoluble aggregates of both LSZ 1.10^5 and LSZ 7.10^4 created after thermal, chemical and mechanical (ultrasound) treatments.

Table III-1: Percentage of insoluble aggregates quantified by UV spectroscopy at 280 nm after applied stress factors (n=5) for the two commercial lysozymes.

	Percentage of insoluble aggregates formation after solution modification (%)	
Applied modification	***LSZ 1.10^5***	***LSZ 7.10^4***
Thermal treatment at 70°C	2.4 ± 0.2	0.0 ± 0.2
Thermal treatment at 90°C	3.3 ± 0.2	1.5 ± 0.2
Chemical treatment with urea 2M	12.4 ± 0.2	11.2 ± 0.2
Chemical treatment with urea 6M	25.1 ± 0.2	24.0 ± 0.2
Chemical treatment with urea 10M	35.5 ± 0.2	33.4 ± 0.2
Chemical treatment with GdHCl 2M	12.0 ± 0.2	11.2 ± 0.2
Chemical treatment with GdHCl 6M	34.5 ± 0.2	27.8 ± 0.2
Chemical treatment with GdHCl 10M	45.2 ± 0.2	44.2 ± 0.2
Ultrasound treatment during 3 minutes	4.1 ± 0.2	2.7 ± 0.2
Ultrasound treatment during 15 minutes	4.4 ± 0.2	3.1 ± 0.2
Ultrasound treatment during 30 minutes	3.9 ± 0.2	5.5 ± 0.2
Ultrasound treatment during 45 minutes	5.8 ± 0.2	7.4 ± 0.2

Chemical treatments formed a large quantity of insoluble aggregates. Chemical interactions can disrupt the tertiary and secondary protein structures by unfolding the native configuration[5–8]. On the other side, thermal treatment formed very few insoluble aggregates.

For the two sources of lysozyme, the number of aggregates formed in the chemical and thermal treatment were proportional to the denaturant concentration and temperature, respectively. These results were expected and consistent with the literature. The increase of concentration and temperature can induce a higher modification on protein secondary structure. Higher temperatures induce an increase of system entropy and as consequence, a bigger

disorder and loss of protein stability. Chemical denaturants act directly with protein chain through hydrogen bonds and electrostatic interactions and the higher the number of molecules, the higher the chemical interactions occurring simultaneously.

The results were similar for the two lysozymes when submitted to thermal and chemical treatments. This indicates that the initial properties of the two lysozyme are sufficiently close to give the same results and that the aggregation pathway looks similar.

In the ultrasound treatment a different behavior was observed for both lysozymes. On the beginning (until 30 minutes for LSZ 1.10^5 and 15 minutes for LSZ 7.10^4), the amount of insoluble aggregates was maintained almost constant. It indicates a different denaturation mechanism when compared to the chemical and thermal treatments. It can be suggested that the thermal and chemical denaturation mechanism leads to a one-order insoluble aggregate formation, as it is completely dependent on the treatment conditions (temperature and concentration). However, for the US modification, even with increase of treatment period the LSZ seems to keep stable until a specific point. Another indication that different unfolding mechanisms are happening is that the only observed difference between the two lysozymes was during ultrasound. LSZ 1.10^5 seems to be stable to aggregate formation until 30 minutes (presenting almost the same percentage since 3 minutes) and LSZ 7.10^4 presented the same result until 15 minutes.

These results are in agreement with the literature. Mañas et al.[9] studied the influence of ultrasound combined with external applied pressure or temperature. They observed that ultrasound treatment does not present a proportional behavior between LSZ modification and time. They showed an initial phase with slow modification followed by a second phase with higher and linear LSZ inactivation with treatment time. In the present work, the same was observed however, this first phase was different when comparing LSZ 1.10^5 and LSZ 7.10^4.

Highlights:

- Thermal and ultrasound treatments induce formation of insoluble aggregates.
- Higher amount of insoluble aggregates is obtained for chemical denaturation (up to 45%).
- The amount of insoluble aggregates formed increases with operating conditions (temperature, concentration or ultrasonic treatment duration).
- Both lysozymes presented similar results, except for ultrasound treatment were LSZ 1.10^5 seems to be more stable (until 30 minutes).

2. Antibacterial activity for modified lysozymes

2.1 Thermal treatment

In addition to insoluble aggregate formation, antibacterial activity after each stress factor was investigated. The goal is to explore the possibility to differentiate the effects of the treatment on the protein.

The enzymatic assay curves for solutions thermally treated are shown in figure III-1 for LSZ 7.10^4 and plotted with standard deviation for 15 different measures (5 replicates in 3 different days). During the first five minutes of the test, the absorbance decrease is linear. The slope of the linear part decreases between the reference (LSZ native) and the 90°C thermally treated lysozyme (LSZ 90) reveals a loss of activity of the protein remaining in solution after the filtration step and removal of aggregates. The loss of activity is detected by a lower slope of the curve Absorbance vs Time.

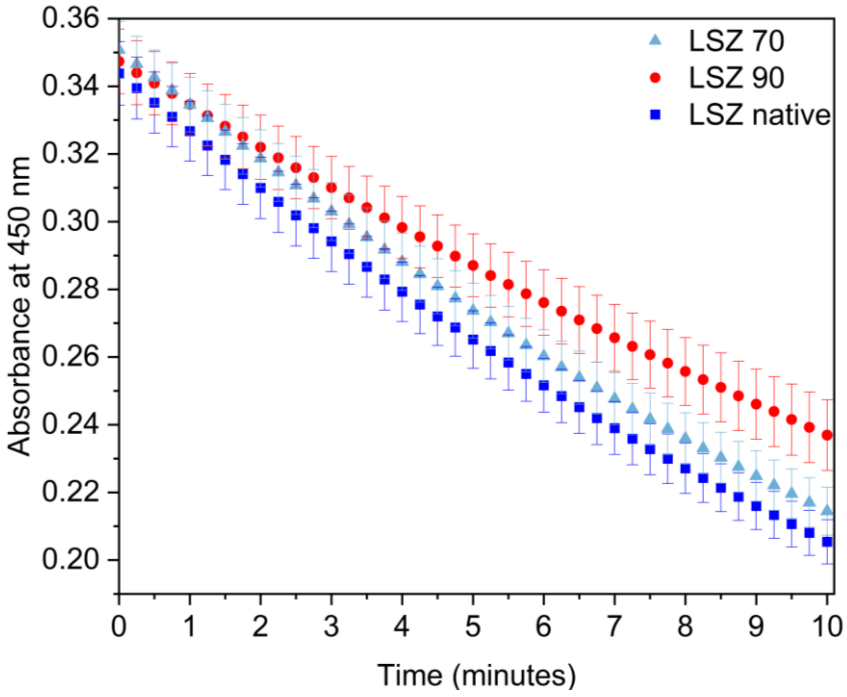

Figure III-1: Enzymatic assay curves for lysozyme (LSZ 7.10^4) solutions thermally treated.

From these results, the antibacterial activity index is calculated by dividing activity value of each measure by activity value of native LSZ (see item 3.3 in Materials and methods

part). Figure III-2 presents the box plot of LSZ activity index after treatment at 70°C (LSZ 70) and 90°C (LSZ 90), compared to the activity of the native LSZ at room temperature (reference).

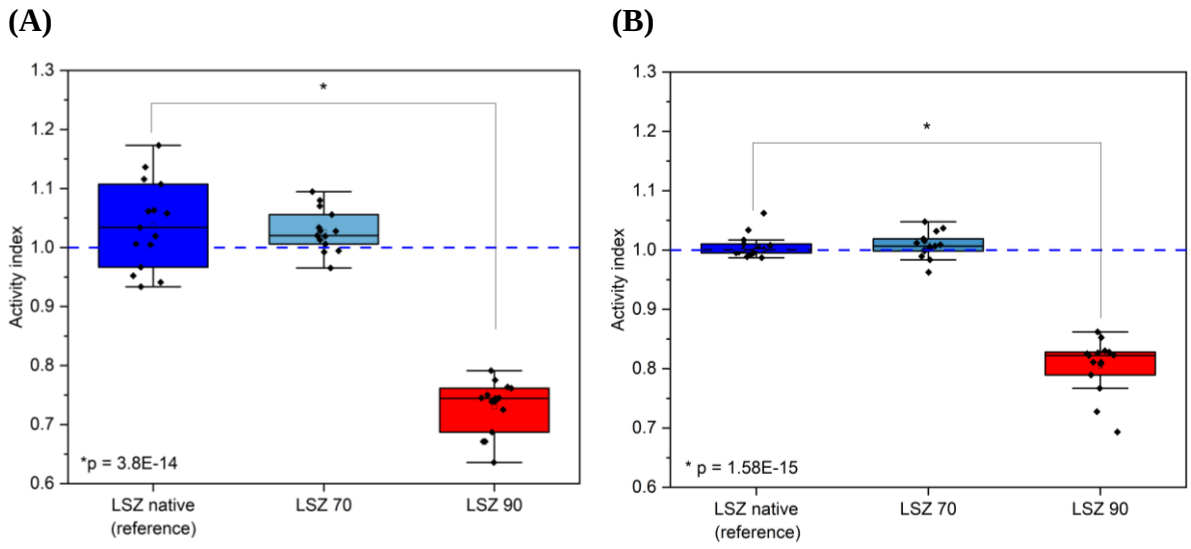

Figure III-2: Lysozyme antibacterial activity after thermal modifications using LSZ 1.10^5 (A) and LSZ 7.10^4 (B) (n=15).

Comparing both LSZ with the reference, the same average activity was found after a treatment at 70°C, meaning that until this temperature, no change in antibacterial activity was observed. On the contrary, a statistical difference ($p<10^{-14}$) was observed between the untreated lysozyme (reference) and the two lysozymes treated at 90°C. In that case, a loss of activity around 20% was obtained.

The activity loss with the temperature is in agreement with previous works in the literature [8,10–12]. *Xing at al.*[7] combined Raman spectroscopy with the antibacterial activity assay to state that thermal denaturation is a three-step mechanism that begins at 74°C. That is the reason why no changes in activity was observed in the present study when temperature of 70°C was applied (fig III-2, LSZ 70). The correlation of antibacterial activity decrease with aggregate formation is commonly found in literature. This is because, when aggregated, proteins have fewer active sites available to perform the enzymatic reaction against the bacterial cell wall. In our study, as the solutions were filtered before the activity test, the reduction could only be attributed to soluble aggregates as insoluble aggregates were removed with a 0.20 µm filter.

In order to investigate if soluble aggregates were in the test solution, SEC-HPLC experiments were conducted after thermal treatment and are presented in figure III-3.

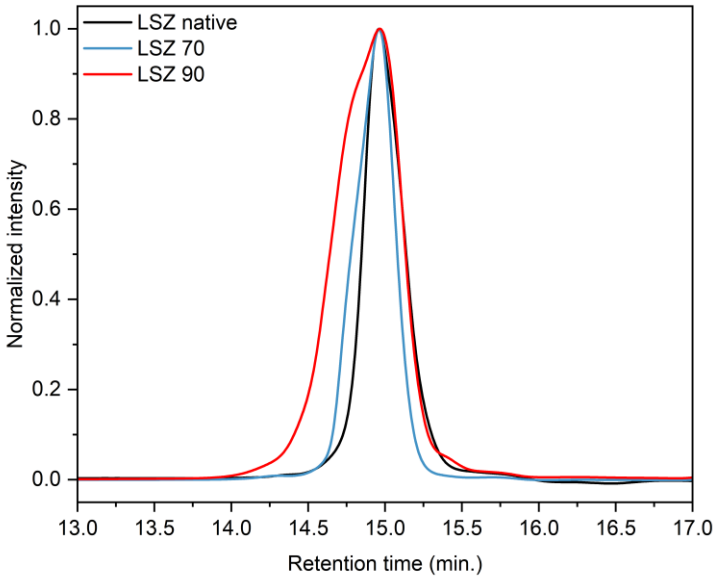

Figure III-3: SEC-HPLC chromatograms of lysozyme (LSZ 7.10^4) solutions thermally treated at 70 and 90°C.

A monomeric peak without presence of oligomers or aggregates was obtained for native and LSZ 70 solutions. Comparing all the chromatograms, the center of the peak was not shifted. The difference between native and thermal treated lysozyme is in the shape of the peak where a shoulder at shorter retention time is observed. This shoulder at lower values of retention time for LSZ 90 indicates an increase of the hydrodynamic volume of lysozyme that could be linked to a conformational change. Thus, antibacterial activity loss can be directly correlated to LSZ tertiary structure modification and the local modification of the environment around the active site.

Highlights:

- No modification was observed for both lysozymes until 70°
- The antibacterial activity decreases about 20% after 1 hour at 90°C,
- The hydrodynamic radius increases after treatment at 90°C.
- The results are in agreement with the literature.

2.2 Chemical denaturation

Two different denaturants were studied (urea and guanidine hydrochloride). They have been well studied in the literature, and in the present work, they were used to verify the results of our test. To understand the maximum loss in biological activity, the concentration of denaturants was varied from 2 to 10 M. The graphs of absorbance at 450 nm versus time are presented in figure III-4 for the two sources of lysozyme.

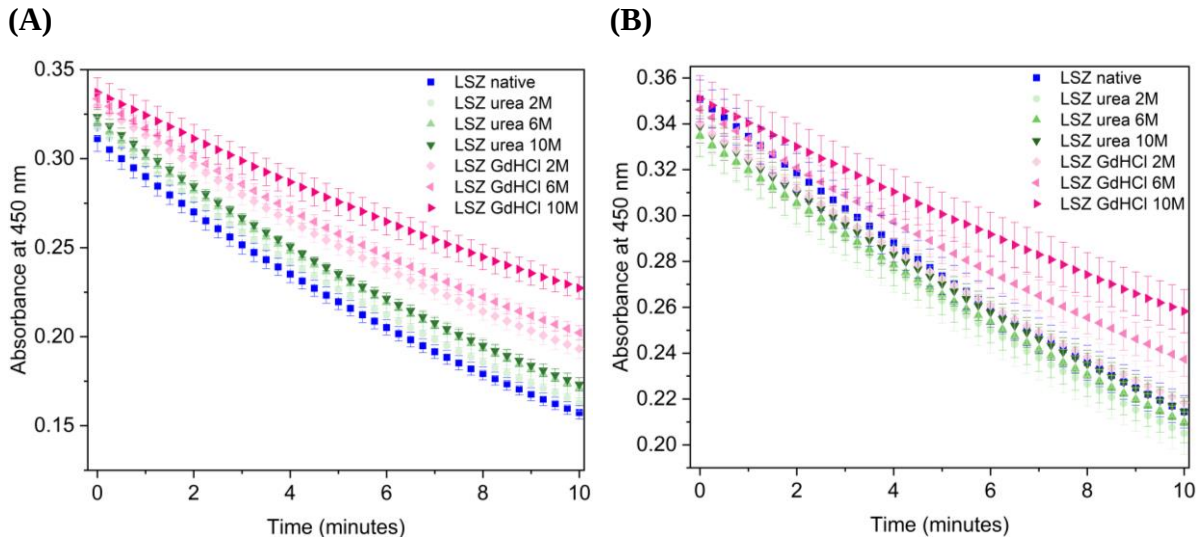

Figure III-4: Enzymatic assay curves for lysozyme solutions chemically treated (A) LSZ 1.10^5 and (B) LSZ 7.10^4 (n=15).

The slopes of the curves in figure III-4 were obtained and compared. Independently on the studied LSZ, it was possible to observe that LSZ treated with urea solutions had a similar behavior as the reference (green and blue dots).

Figure III-5 presents the activity index calculated for all experimental points with the statistical analysis.

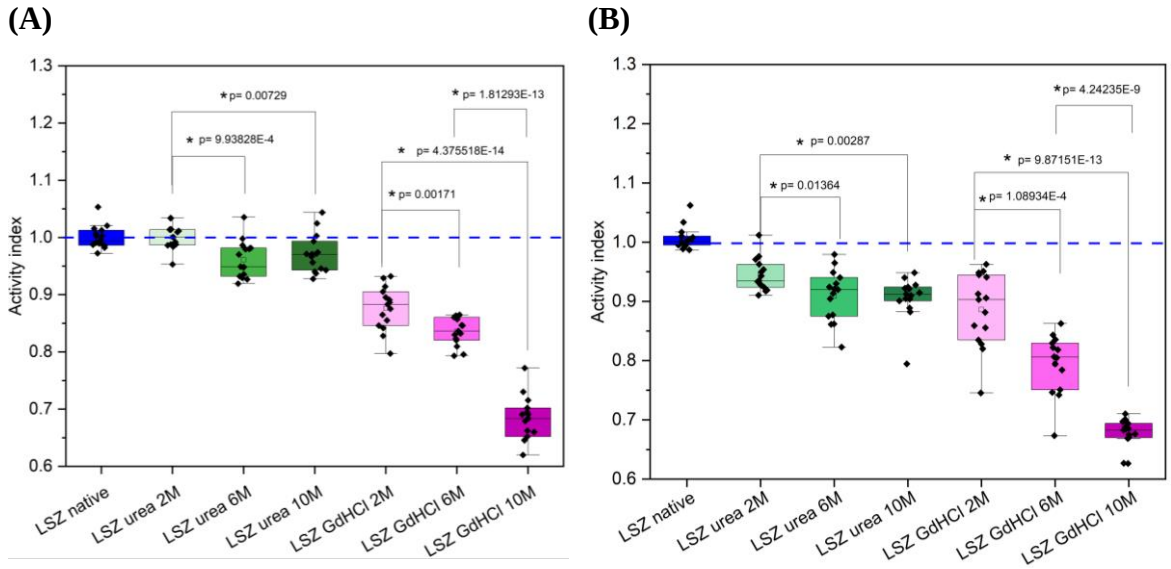

Figure III-5: Lysozyme antibacterial activity after chemical modifications using LSZ 1.10^5 (A) and LSZ 7.10^4 (B) (n=15).

For LSZ 1.10^5 with urea, the antibacterial loss is very low and limited to 5%. This value rises to 10% for LSZ 7.10^4 and suggests that the two proteins behave differently with respect to the test.

On the contrary, guanidine hydrochloride induced a significant activity loss (around 30% using 10M) directly proportional to its concentration for both molecules. This difference between urea and guanidine hydrochloride suggests two distinct mechanisms of interaction of these reagents with the protein.

These results with those presented in table III-1 show that both denaturants result in a different way of lysozyme conformational change. Indeed, insoluble aggregates were formed and increased with denaturant concentration (up to 40% of the total amount of protein in solution). However, the influence of these modifications on the antibacterial activity was different according to the chemical denaturant used. It shows that it is not only structure modification that can interfere on the antibacterial action of lysozyme and it proves that the enzymatic assay optimized in this work is able to identify different unfolding mechanisms.

Siddaramaiah et al. [6] used laser induced autofluorescence to evaluate the secondary structure of α-helix and β-sheet rich proteins after denaturation with urea and guanidine hydrochloride. They observed that urea causes more conformational changes in proteins that presents a high amount in β-sheet secondary structure than in proteins rich in α-helix. Lysozyme

can be characterized as a protein rich in α-helix (Figure III-6). This explains why urea did not influence LSZ activity in the same way as GdHCl.

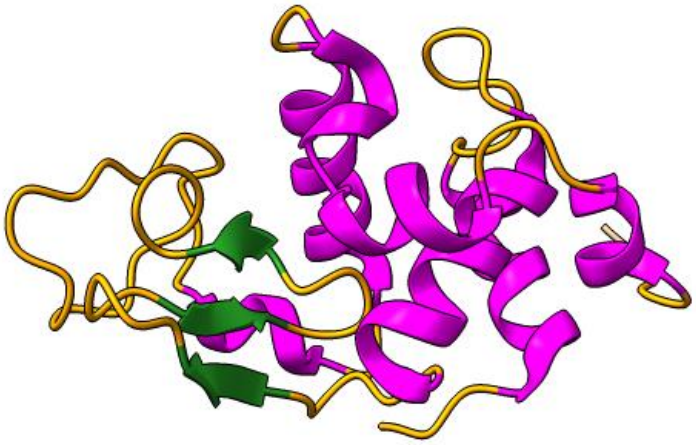

Figure III-6: Lysozyme secondary structures. Presentation of α-helix in pink, β-sheet in green and random coil in orange. Figure created with ChimeraX.

The enzymatic activity depends also on the active site integrity (correct distance between the residues Asp-52 and Glu-35 that participates on bacteria lysis) and environment. Hédoux et al.[5] compared the two denaturants using Raman spectroscopy and microcalorimetry. They observed that urea changes the tertiary structure of lysozyme while guanidine hydrochloride can also modify the secondary structure. Using Raman spectroscopy, Xing et al. [7] stated a multi-step chemical denaturation. For low GdHCl concentrations, the salt interacts with the protein surface, changing the environment of the side groups and as consequence induces a conformational change (tertiary structure modification). Then, the microenvironment of all the side groups is modified in function of GdHCl concentration. The secondary structure changes at high concentration, enough to alter the conformation of the skeleton groups as well as the disulfide bonds.

As presented in the introductive part, the antibacterial property is less affected by changes in tertiary structure compared to changes in secondary structure. This explains the linear dependence of antibacterial activity to guanidine concentration: as the amount of guanidine increases, the secondary structure of the protein suffers more modifications and consequently the antimicrobial activity decreases. But we have also to mention that a complete loss of antimicrobial activity is never observed.

Highlights:

- The optimized enzymatic test is able to show protein denaturation coming from different mechanisms (urea vs. GdHCl).
- The enzymatic test is a useful tool to complement results from HPLC and UV spectrometry.
- Urea induced a limited lysozyme activity loss (max. of 10% to LSZ 7.10^4).
- The higher the concentration of GdHCl, the lower the activity of lysozyme after the treatment. Values around 35% of activity loss were observed.
- LSZ 1.10^5 and LSZ 7.10^4 presented similar results.

2.3 Mechanical modification by ultrasound

Mechanical treatments (ultrasound and ultrafiltration) were also performed to evaluate if similar conclusions can be drawn.

2.3.1 Antibacterial activity

Ultrasound treatment was applied during different times (3, 15, 30 and 45 minutes) and the results of antibacterial test of treated solutions are presented in figures III-7. When ultrasound is applied, enzymes can be denatured by shear forces of cavitation, that is, the formation and collapse of bubbles or by free radicals formed during water sonolysis.

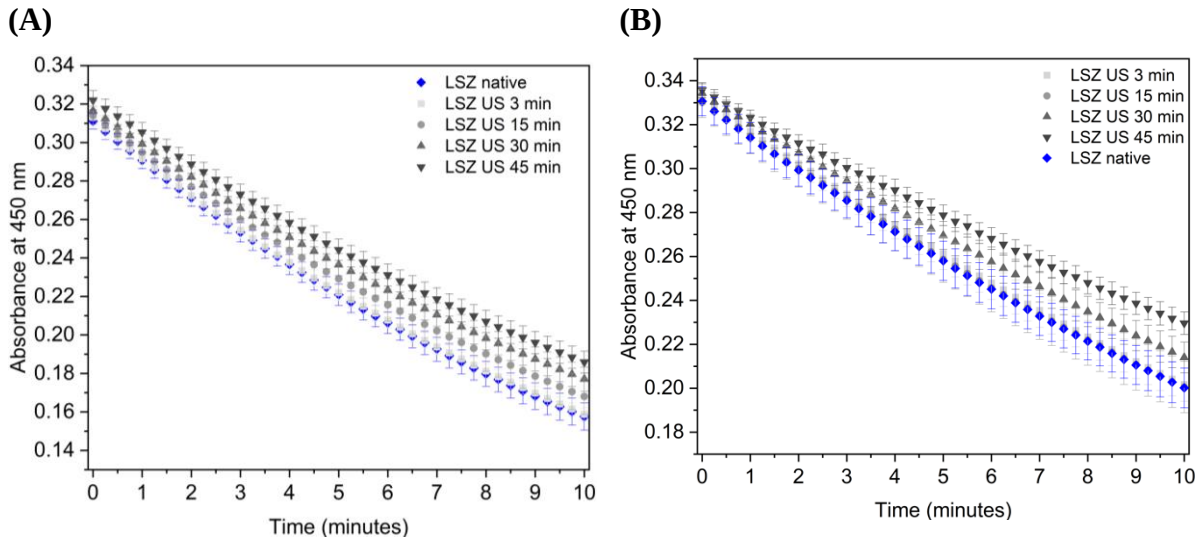

Figure III-7: Enzymatic assay curves for lysozyme solutions mechanically treated with ultrasound (A) LSZ 1.10^5 and (B) LSZ 7.10^4 (n=15).

The results of antibacterial activity index are presented as a box plot in figure III-8.

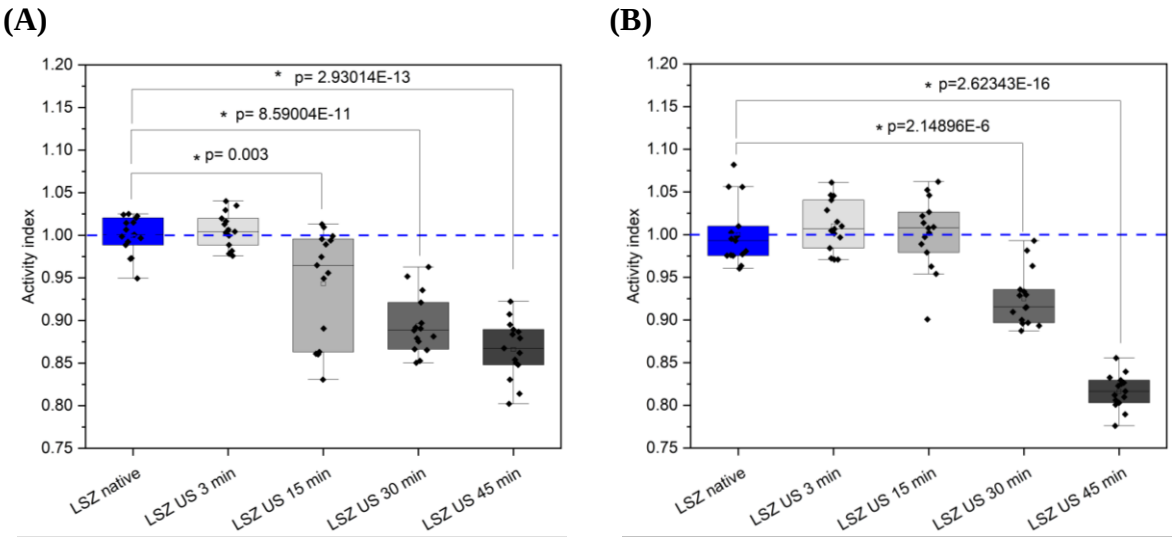

Figure III-8: Lysozyme antibacterial activity after ultrasound treatment for LSZ 1.10^5 (A) and LSZ 7.10^4 (B) (n=15).

No statistical difference was observed between reference, 3 and 15 minutes of US treatment for LSZ 7.10^4. Activity decrease is only observed after 30 minutes, with a maximum around 18% at 45 minutes. On the other hand, a slight decrease in enzymatic activity was observed starting from 15 minutes for the LSZ 1.10^5 compared to the reference (native lysozyme). LSZ 7.10^4 seems to be stable during a longer time than LSZ 1.10^5. However, the treatment at 30 and 45 minutes presented close values for both LSZ, around 10 and 15%, respectively.

Krishnamurthy at al.[13] observed a similar behavior of LSZ inactivation increase with the time of ultrasonic treatment and they also studied the inclusion of an organic solvent, methylene chloride, to mimic the first step of the encapsulation process. They observed that the presence of an organic solvent can increase the antibacterial activity loss of lysozyme and formed insoluble precipitate. However, on their investigation, no aggregate, fragment or hydrodynamic volume change of the protein were found in the soluble fraction, and they affirm that ultrasonification modifies mainly the secondary structure. The hypothesis of secondary

structure modification with ultrasound was also elucidated by *Marchioni et al.*[14]. The authors have implemented ultrasonic treatment during 10, 20, 30, 40, 50 and 60 minutes for different proteins including lysozyme. A change in the secondary structure after 20 minutes could be detected using circular dichroism spectroscopy, mainly with a decrease in α-helix content.

In our work, the activity decrease was in the same timescale as the literature. After 15 minutes, insoluble aggregates were formed for a lysozyme aqueous solution. Formation of insoluble aggregates did not seem to follow a linear increasing with ultrasound time and enzymatic activity of soluble fraction also shown a stability period (around 15 minutes), meaning that as showed by Mañas et al.[9], there is an initial phase with slow loss of enzymatic activity followed by a sudden increase of inactivation rate (see Figure III-8). The difference between our studied lysozymes on the first phase suggests that there are some stabilizing effects on LSZ 7.10^4 that are not present on LSZ 1.10^5.

These results show that for industrial procedures where ultrasound is used such as microencapsulation, homogenization and sterilization, the time of treatment should be taken into account as well as the initial state of the protein to avoid changes in final biological activity and aggregation.

Highlights:

- LSZ 7.10^4 preserved its antibacterial activity for a longer period than LSZ 1.10^5 after an ultrasonic treatment.
- After the period of 3 min. for LSZ 7.10^4 and 15 min. for LSZ 1.10^5, the decrease of activity was linear with processing time.

In addition to insoluble aggregates, soluble ones are frequently associated with loss of activity. To verify whether this type of aggregate was present in our test, HPLC measurements were performed. The results are presented on the next item (2.3.2).

2.3.2 Study of soluble aggregates formation

In order to confirm that the activity loss detected after ultrasonic treatment is due to soluble aggregates, the soluble fraction was analyzed by SEC-HPLC and the results are presented in figure III-9.

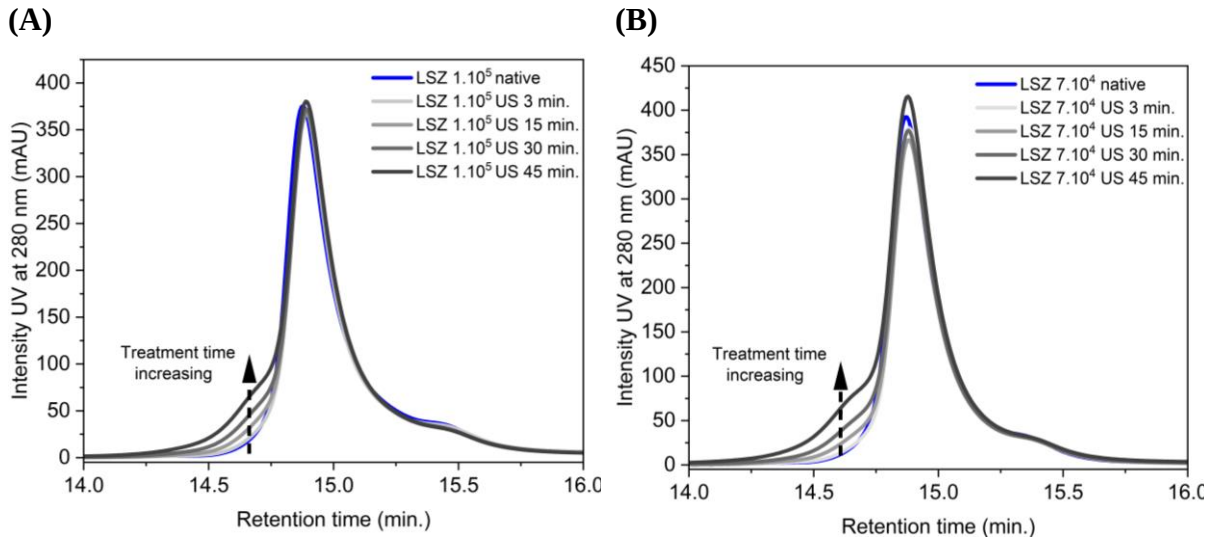

Figure III-9: SEC-HPLC chromatograms for LSZ 1.10^5 (A) and LSZ 7.10^4 (B) after ultrasound treatment.

A peak shoulder was observed for both sources of lysozyme after 15 minutes of treatment with retention time at approximately 14.7 minutes. The peak intensity increased with treatment duration. Area of the peaks were quantified by a deconvolution method explained on item 3.1.2 of materials and methods chapter. This peak was associated with the formation of soluble aggregates. The proportion of soluble aggregates increases since the beginning of the treatment as shown in figure III-10. It can suggest that on the beginning there is no direct relationship between aggregates in the solution and activity decrease as both LSZ were enzymatically stable until almost 15 minutes.

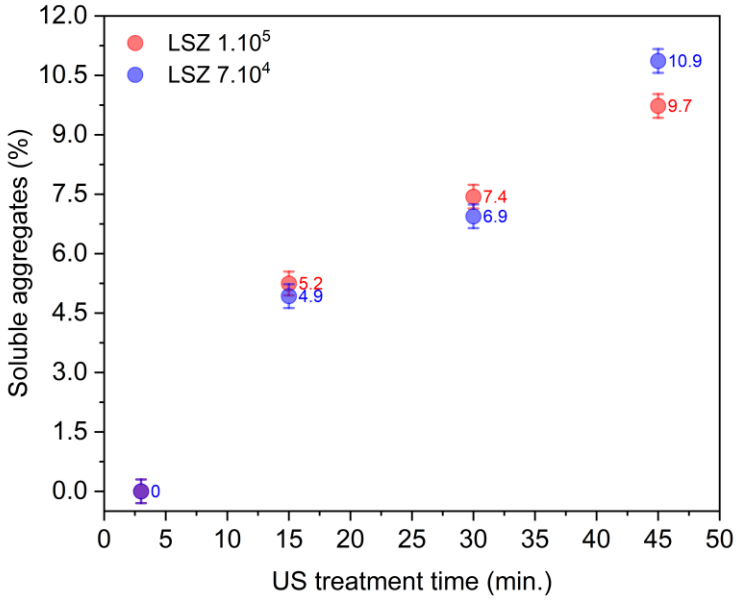

Figure III-10: Soluble aggregates formation versus US treatment period for LSZ 1.10^5 and LSZ 7.10^4. Average and standard deviation based on 5 independent experiments.

A possible relationship between soluble aggregate amount with enzymatic activity decrease was studied by plotting antibacterial activity index versus percentage of aggregates (Figure III-11).

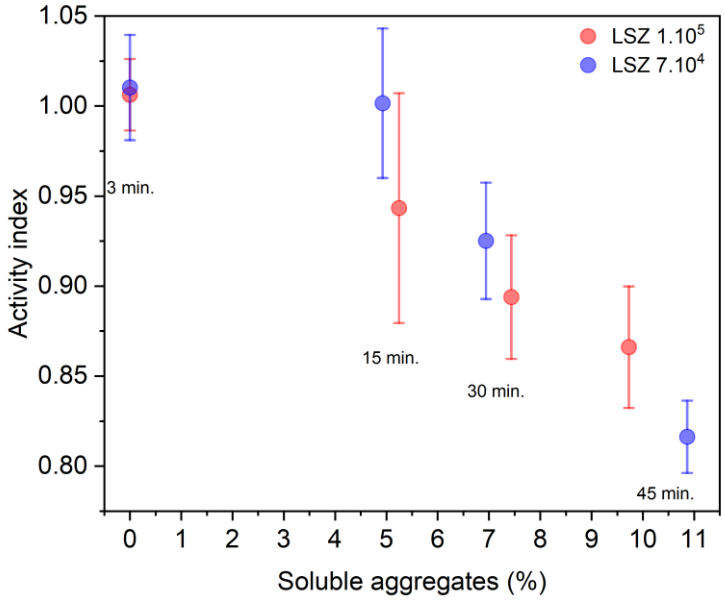

Figure III-11: Relationship between soluble aggregates and antibacterial activity loss for LSZ 1.10^5 and LSZ 7.10^4.

LSZ 7.10^4 maintained its initial activity for up to 15 minutes even with soluble aggregates in solution (around 5% of aggregates). It seems that for this lysozyme, a two-step denaturing process occurs. In the literature, ultrasound denaturation is characterized by a slow activity decrease at the beginning followed by a faster inactivation process[9]. On the other hand, LSZ 1.10^5 started to lose its activity just after 15 minutes of treatment even if the aggregate formation was slower than that for LSZ 7.10^4.

For both lysozymes after 30 minutes, the bigger the soluble aggregate amount, the lower the antibacterial activity. There seems to be a difference of stability between these two products on the initial step. There are two possible explanations: both LSZ follows the same mechanism but the initial slow step is faster for LSZ 1.10^5 which can be explained by stabilizing factors present on LSZ 7.10^4 that are not on the other, or, the initial conformation of them is different and ultrasound cavitation have a different impact on the two molecules.

Mañas et al.[9] proposed that the first inactivation phase occurs due to implosion of bubbles during cavitation that form hot spots where high pressures can unfold the initial conformation of lysozyme by shear forces. The protein unfolding occurs along the interfacial area of microbubbles, leading the protein more hydrophobic and it can easily aggregate. This

initial unfolding was observed to cause small effects on enzymatic activity when compare to the second phase that is characterized by breakage of disulfide bonds. Breakage of disulfide bonds after protein ultrasonication were supported by other authors in the literature.[15,16]

We suggest that LSZ 7.10^4 has a slight more stable initial conformation when compared to LSZ 1.10^5. This assumption can be reinforced by the percentage of insoluble aggregates at the beginning of ultrasonic treatment. The value is lower for LSZ 7.10^4 at the beginning but higher for long duration. This difference is more evident and pronounced during mechanical stress application as it could be observed by ultrasound and will be also presented on the next item about ultrafiltration.

Highlights:

- With the US treatment, soluble and insoluble aggregates were formed.
- The higher amount of soluble aggregates (11%) was observed for LSZ 7.10^4 within 45 minutes.
- Loss of antibacterial activity, soluble and insoluble aggregates formation are dependent of the US treatment duration.

2.4 Mechanical modification with ultrafiltration

2.4.1 Filtration study of native lysozyme

Ultrafiltration is a pressure driven separation mainly used in industrial processes. In this case, the treatment consists in a combination of mechanical stress and surface contact between the protein and the membrane pores surface. In a previous work of the team, the relationship between hydraulic properties of the membrane and the antibacterial activity lysozyme was studied varying the membrane used[17]. It was found that lysozyme (LSZ 1.10^5) after filtration lost part of its antibacterial activity with pressure increasing and this behavior was observed just for the membranes with small real cut-off.

In order to better understand which membrane parameter influence more the LSZ modification, in the present work the data of 3 membranes were compared with antibacterial assay results. Three commercial similar membranes were considered M1, M2 and M3 and their permeability and selectivity are presented in table III-2 after vitamin B12 filtration

Table III-2. Membrane properties determined by VB12 filtration and pure water filtration.

Membrane	**Rejection rate (%)**	**Permeation flux (10^{-14} $m^3.m^{-2}.s^{-1}$)**
M1	54	5.5
M2	56	2.9
M3	59	5.4

Membranes M1, M2 and M3 presented similar selectivity performances (around 50%) and it could be affirmed that they have small pores. To understand which parameter between rejection rate and permeation flux interferes more in the antibacterial activity, the enzymatic test was conducted for retentate and permeate solutions. The retentate solutions are not passing in the pores and no changes of activity have been detected in previous works (results not presented here)[17–19]. On the contrary, the activity loss increased with applied pressure for lysozyme in permeate solutions passing through small pores. The dependence to the pressure is equivalent for the membranes with comparable values of rejection rate or pore size (see fig. III-12).

Figure III-12 shows the antibacterial index (average of 9 measures) for LSZ 1.10^5 permeates filtered in different pressures ranging from 4 to 12 bar. The results of the linear fit (absolute slope) for each membrane are shown in the colored boxes (left side figure III-12).

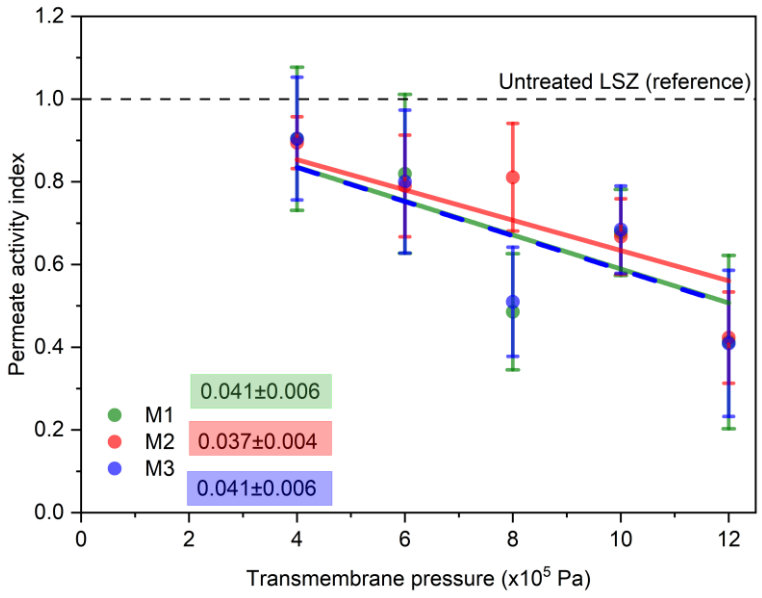

Figure III-12: Evolution of antibacterial activity index for LSZ 1.10^5 permeate solutions in different membranes and applied pressures (n=15).

For M1, M2 and M3, the maximum of activity loss was approximately 60% for 12 bar pressure. In addition, a linear relationship between activity index and pressure was observed and the slopes were 0.041, 0.037 and 0.041 for M1, M2 and M3 respectively. The similarity between slope values indicates that the parameter of the membrane that plays a major role in antibacterial lysozyme action is the pore size and so, the steric hindrance.

Additional investigations were carried out by modifying the initial conditions of lysozyme and doing the ultrafiltration with membranes that present selectivity higher than 50%. In this way, UF operations were conducted with the second lysozyme source (LSZ 7.10^4). Successive treatments were also considered to evaluate if these modifications can induce a bigger loss of activity. For example, what could happen if ultrafiltration was done with a thermally modified protein?

Highlights:

- Antibacterial activity decreases with transmembrane pressure.
- Ultrafiltration at 12 bar induced high activity loss (50%) for LSZ 1.10^5.
- The activity decrease was linear for a transmembrane pressure between 2 and 12 bars.

2.4.2 Antibacterial activity after ultrafiltration – Comparing LSZ 1.10^5 and LSZ 7.10^4

In order to evaluate the impact of ultrafiltration (mechanical stress combined with surface interaction), experiments for both lysozyme sources were performed using membranes with similar initial properties. Table III-3 presents the membrane performances before and during different LSZ filtration cycles.

Table III-3. Selectivity and permeability of similar membranes during filtration of LSZ 1.10^5 and LSZ 7.10^4.

LSZ 1.10^5		
Solution	*Rejection rate (%)*	*Hydraulic permeability (10^{-14} $m^3.m^{-2}$)*
Vitamin B12	60	4.1
LSZ 1st filtration	85	3.6
LSZ 2nd filtration	93	3.3
LSZ 3rd filtration	98	3.1
LSZ 7.10^4		
Solution	*Rejection rate (%)*	*Hydraulic permeability (10^{-14} $m^3.m^{-2}$)*
Vitamin B12	59	1.7
LSZ 1st filtration	61	1.4
LSZ 2nd filtration	77	1.4
LSZ 3rd filtration	80	1.3

The membranes used are low-cut off UF ones (1 kDa as informed by the supplier). Theoretically, these membranes should fully reject a protein of 14kDa like lysozyme. Indeed, from a steric hindrance point of view, the rejection rate of vitamin B12 solution indicates that the average pore size is above 1.5 nm [20]. The stokes radius of the protein is 1.85 nm. In theory, the protein should not go through the pores of this membrane.

An interesting result was obtained comparing the two lysozymes. Even being both the same protein obtained from the same manufacturer and biological source, their respective behaviors during UF operation were different. While for the LSZ 1.10^5 filtration the retention rate increased for each cycle almost until a total rejection, for the LSZ 7.10^4, the increase in rejection rate evolves differently as observed in table III-3. This increase in rejection rate is due to protein adsorption in membrane pores as successive filtration tests were carried out. It seems that interactions between membrane surface and lysozyme with higher activity (LSZ 1.10^5) are stronger and favorable when compared to lower activity lysozyme (LSZ 7.10^4). The differences obtained from manufacturer between these two proteins are only the initial activity value and the purification process, while one was dialyzed (LSZ 1.10^5), the other one was not (LSZ 7.10^4). The differences between the two lysozymes could be explained by the small amount of low molecular weight residues present in the non-dialyzed sample. These residues may interact with the protein and the pore surface. This would avoid protein-surface interactions, limiting protein

adsorption, resulting in a limited reduction in pores size after consecutive filtrations and avoiding high rejection rates (Table III-3).

In order to evaluate the effect of different adsorption behavior in the final antibacterial activity, the operation was conducted varying the pressure from 4 to 12 bar. The results presented in figure III-13 (LSZ 1.10^5 in red and LSZ 7.10^4 in blue) correspond to solutions of the 3rd filtration.

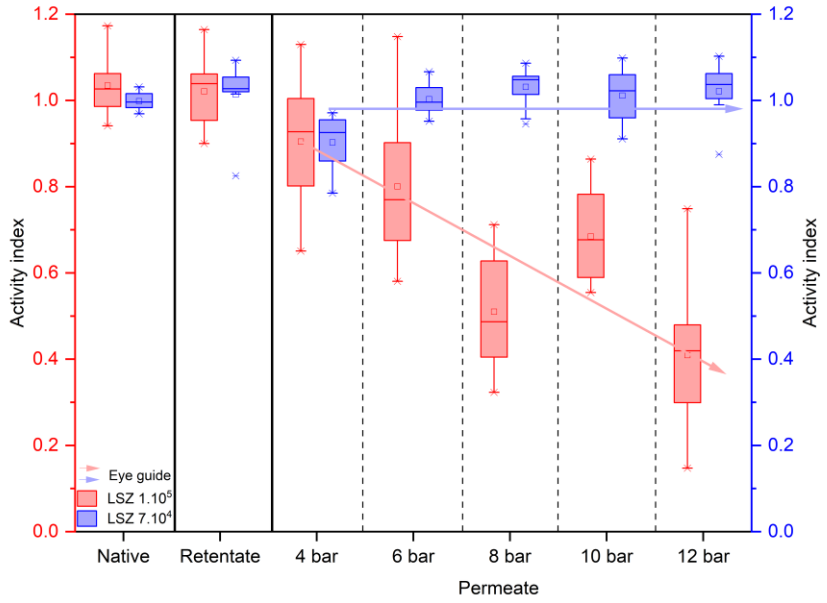

Figure III-13: Lysozyme antibacterial activity after ultrafiltration of LSZ 1.10^5 (red boxes) and LSZ 7.10^4 (blue boxes) solutions at room temperature (n=15).

The retentate solutions are the part of the protein solution rejected by the membrane. These solutions circulate in the filtration system during filtration (2 hours in a turbulent flow regime). The permeates are solutions that passed through the pores and sampled at different transmembrane pressures. Comparing the retentate of the two lysozymes with the native reference solution, no difference was observed. It means that the shearing forces due to the turbulent flow or the contact with the metallic surface (stainless steel) of the tubes do not lead to enough changes in the lysozyme structure that triggers a modification of its activity.

However, in the permeate a decrease of antibacterial activity proportional to the increase of transmembrane pressure was observed only for LSZ 1.10^5. This activity loss can be associated with the forced passage of LSZ into the pores due to applied pressure. On the contrary and surprisingly, the LSZ 7.10^4 maintained its activity suggesting that its structure was stable even after ultrafiltration in the permeate solutions.

As informed by the supplier, the LSZ 7.10^4 did not go through the dialysis process like the LSZ 1.10^5. One suggestion for this greater stability of non-dialyzed lysozyme is that small molecules in low amount are present and can interact preferentially with the pore surface avoiding LSZ-surface interaction or adsorption, as evidenced by the changes in hydraulic properties (table 1). Another possibility is that small molecules can interact directly with the protein and, in this case, the interaction can avoid the contact of lysozyme with the pores or even protect the structure from being modified during filtration. Instead, the LSZ 1.10^5 solution was dialyzed (purification process informed by the manufacturer) and the small molecules able to stabilized the protein were eliminated.

In order to evaluate if this difference between lysozymes could be due to purification step, the ultrafiltration of LSZ 7.10^4 dialyzed was done and the results are presented in the item 2.4.4.

Highlights:

- During ultrafiltration, only antibacterial activity of LSZ 1.10^5 permeate decreases
- No modification of activity index of LSZ 7.10^4 is observed after ultrafiltration.
- Small molecules are likely to be present and change the interactions between lysozyme and his environment.

2.4.3 SEC-HPLC chromatograms for lysozyme solutions after ultrafiltration

LSZ 1.10^5 and LSZ 7.10^4 were analyzed by SEC-HPLC chromatography before (native) and after ultrafiltration at 12 bar. For the treated solution, retentate and permeate were evaluated and the results are presented in figure III-14.

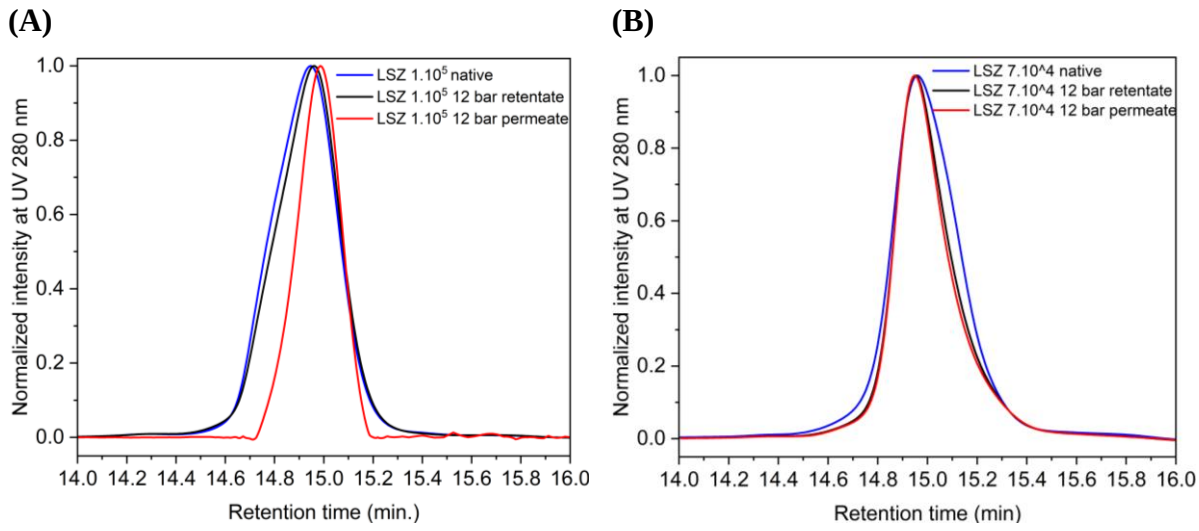

Figure III-14: SEC-HPLC chromatograms for LSZ 1.10^5 (A) and LSZ 7.10^4 (B) after ultrafiltration treatment.

A peak shape modification and a slight shift (0.04 minutes) was observed on chromatograms in figure III-14 when we compared the permeate with retentate or native solutions for LSZ 1.10^5. Retentate and native solutions presented similar chromatography peaks indicating one more time that turbulent flow on feed tank could not change lysozyme conformation after approximately 2 hours of experiments. Permeate peak shifted to higher retention time: it means that the lysozyme that passed through the pore has a smaller hydrodynamic radius when compared to the retentate. This decrease of hydrodynamic radius can be associated to a partial unfolding process caused by the forced passage of protein into the membrane's pore. This modification is associated with a reduction on antibacterial activity depending on the pressure (fig III-13).

On the other hand, the chromatograms for the LSZ 7.10^4 showed the same retention time for all solutions. The permeate and retentate peaks can be superimposed. These results indicate that independently of the stress caused on LSZ 7.10^4 during ultrafiltration, the hydrodynamic radius was maintained.

Transmembrane pressure and porous interaction influence on activity depend on the raw material that was filtrated. It can also be affirmed that the activity decrease with pressure for LSZ 1.10^5 can be associated to a population with smaller hydrodynamic radius in HPLC after passage through the pores.

Highlights:

- HPLC chromatograms showed a shift on retention time only after filtration the of LSZ 1.10^5 (permeate).
- The activity loss can be associated to a conformational change that reduce the hydrodynamic radius.
- For LSZ 7.10^4, native, retentate and permeate chromatograms were superimposed.

2.4.4 Filtration study of dialyzed LSZ 7.10^4

The difference between the two lysozymes is the dialysis step. LSZ 1.10^5 was dialyzed, whereas LSZ 7.10^4 was not. Therefore, this second one was dialyzed to understand the influence of this purification step on the ultrafiltration results.

Figure III-15 presents the SEC-HPLC chromatograms for LSZ 7.10^4 before and after dialysis. It is observed that the main LSZ peak kept the shape and position but a small peak around 15.4 minutes is present for non-dialyzed samples. This peak at higher elution time and so, smaller hydrodynamic radius can be associated with small molecules present in the samples. These small molecules are removed after dialysis through a membrane with 6-8 kD cut-off.

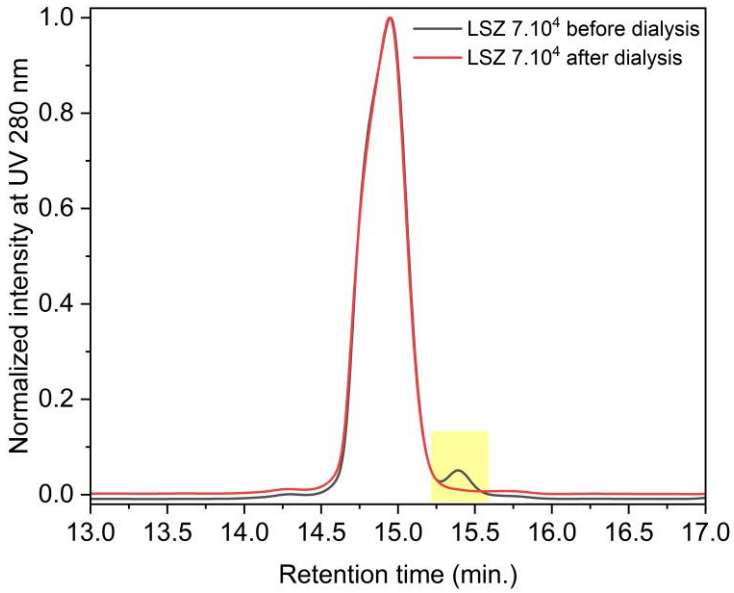

Figure III-15: SEC-HPLC chromatograms for LSZ 7.10^4 before and after dialysis.

Ultrafiltration of LSZ 7.10^4 with and without dialysis was done with the same membrane and the results of membrane hydraulic properties are presented on table III-4.

Table III-4. Selectivity and permeability for filtration of LSZ 7.10^4 before and after dialysis in the same membrane.

LSZ 7.10^4 before dialysis		
Solution	*Rejection rate (%)*	*Hydraulic permeability (10^{-14} $m^3.m^{-2}$)*
Vitamin B12	82	1.8
LSZ filtration	92	2.0
LSZ 7.10^4 after dialysis		
Solution	*Rejection rate (%)*	*Hydraulic permeability (10^{-14} $m^3.m^{-2}$)*
Vitamin B12	78	2.4
LSZ filtration	98	1.6

After filtration of dialyzed LSZ 7.10^4, the membrane hydraulic permeability decreases and the observed rejection rate is 98% as for filtrations of LSZ 1.10^5 solution. By contrast, filtration of LSZ 7.10^4 shows never observed trend (increase of hydraulic permeability and transmission about 8%).

Permeate solutions from LSZ 7.10^4 dialyzed were collected and the enzymatic activity was measured. The figure III-16 present the results of activity index. Independently of the pressure used, the retentate presented the same activity as the native lysozyme. For the permeates, as the selectivity was higher for smaller transmembrane pressures it was not possible to collect samples from 4, 6 and 8 bar, so just solutions from 10 and 12 bar were analyzed according to their antibacterial activity.

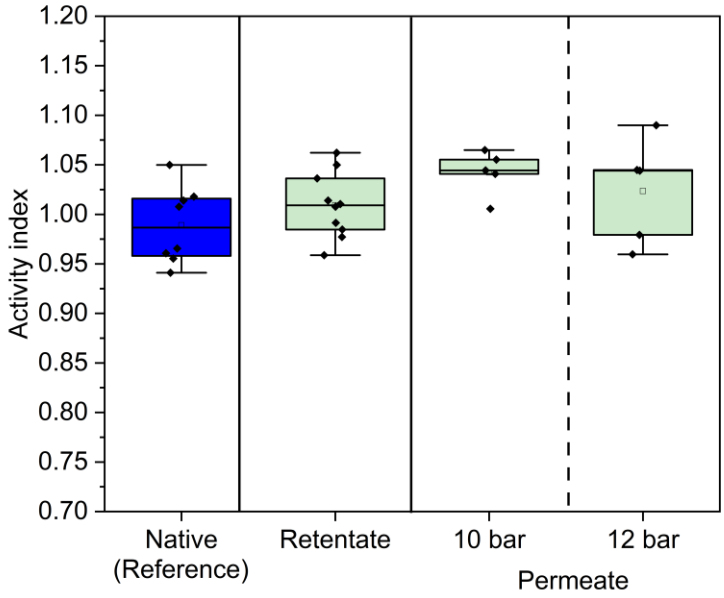

Figure III-16: Lysozyme antibacterial activity after ultrafiltration of LSZ 7.10^4 dialyzed solution at room temperature (n=15).

Figure III-16 shows the antibacterial activity after ultrafiltration of dialyzed LSZ 7.10^4. No difference was observed compared to the reference. It means that even if the dialyzed LSZ 7.10^4 presented a similar behavior (in terms of hydraulic performances and selectivity) as LSZ 1.10^5, the antibacterial activity is not affected by the ultrafiltration process. Further investigations should be done to understand the reason why these lysozymes presented different stability towards mechanical stresses.

Highlights:

- SEC-HPLC chromatograms show that small molecules were eliminated from the LSZ 7.10^4 solution after dialysis.
- Membrane selectivity and hydraulic performances are similar after filtration of dialyzed solution or LSZ 1.10^5.
- No change in antibacterial activity was detected after filtration of dialyzed LSZ 7.10^4.

2.4.5 Filtration study of thermally treated lysozyme

For both lysozyme sources, the thermal treatment presented exactly the same result in terms of antibacterial activity and according to the literature, the changes in the protein conformation are irreversible. Thinking about that, the combination of ultrafiltration and thermal treatment was done to understand if the obtained conformation changes using UF could also occur when a thermally modified lysozyme is filtrated.

Figure III-17 presents the antibacterial activity for LSZ solutions filtered after thermal modifications at 70 and 90°C. As mentioned earlier in the topic about thermal treatment, solutions treated at 70°C did not suffer any modification of activity and when it goes to ultrafiltration, no modification can be detected in the retentate. The activities obtained for the two LSZ retentate solutions are then identical to the reference ones. The results for the permeate after 70°C thermal treatment are the same that the ones obtained with ultrafiltration treatment alone. LSZ 7.10^4 activity in the permeate after 12 bar ultrafiltration is comparable to LSZ reference activity. On the contrary, LSZ 1.10^5 exhibits a loss of activity of approximately 40% in the permeate after a thermal treatment at 70°C. Considering the standard deviation obtained for ultrafiltration experiments in triplicate, this loss of activity is comparable to the decrease of activity for LSZ 1.10^5 exposed to ultrafiltration only, confirming that thermal treatment at 70°C did not modify the chemical structure of LSZ.

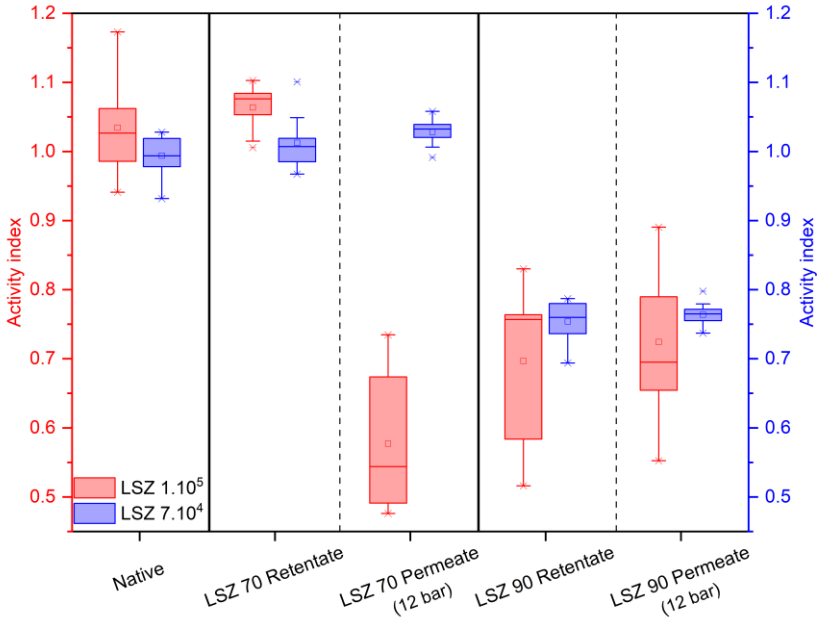

Figure III-17: Lysozyme antibacterial activity after ultrafiltration of pre-treated LSZ solutions at 70°C and 90°C (red boxes for LSZ 1.10^5 and blue boxes for LSZ 7.10^4 solutions) (n=15).

When lysozyme solution was pre heated at 90°C, activity loss around 30% was observed for the two sources of lysozyme. This activity loss is not modified after filtration. Permeate (12 bar) and retentate presents the same activity (activity index around 0.7). This indicates that the ultrafiltration could not induce any additional effect in the antibacterial action loss after thermal treatment at 90°C.

It also shows that the conformational changes are different for the two types of denaturation. Thermal treatment at 90°C gives activity index with values comparable to guanidinium chloride at a concentration of 10M (activity index around 0.7) but ultrafiltration at a pressure of 12 bar can decrease activity index to lower value around 0.4. Unsurprisingly, one can expect important conformational changes for lysozyme in the pores as evidenced with LSZ 1.10^5 but the singular lack of activity loss of LSZ 7.10^4 after permeation at 12 bar has to be further investigated.

Highlights:

- UF of solutions treated at 70°C presented similar results to the filtration of a native lysozyme.
- No additional activity modification after ultrafiltration of lysozyme solutions treated at 90°C.
- Ultrafiltration impact on lysozyme activity depends on its initial state.

3. Activity scale after modifications and general discussion

An activity scale was done to compare all the stress factors studied in the present chapter (figure III-18). It was observed that for modifications using GdHCl 10M, heating at 90°C and ultrafiltration using 12 bar as transmembrane pressure caused the higher biological activity loss on lysozyme. It means that these processes were the most modifying ones in the extreme conditions used. Smaller concentration, temperature and transmembrane pressure caused less modifications on lysozyme activity meaning that for these treatments, applied conditions should be carefully studied before their use.

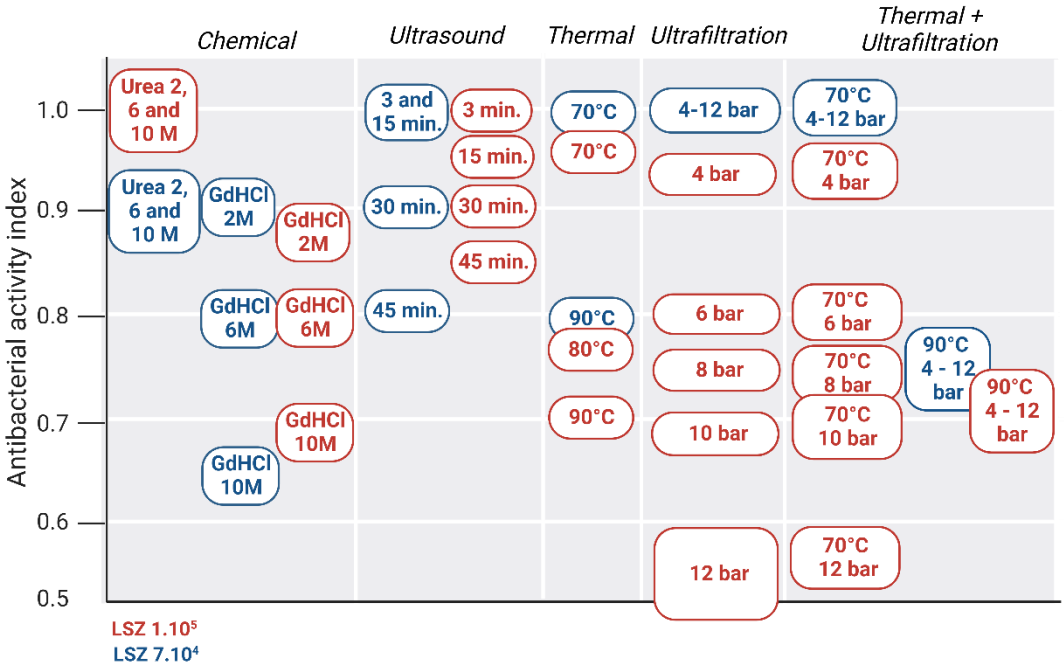

Figure III-18: Activity scale for LSZ 1.10^5 (red) and LSZ 7.10^4 (blue) after modification with different stress factors.

This comparative table can be also used to compare lysozymes. The one with bigger initial activity is presented in red and the other with smaller initial activity in blue. For the chemical and thermal treatments as already presented and discussed, for both LSZ a similar tendency was observed. The activity loss was proportional to the concentration and to the temperature, for chemical (GdHCl) and thermal treatments, respectively. No significate differences were observed for these two sources of protein. Both were thermally stable until 75°C and then, when treated at 90°C activity loss was observed, LSZ 1.10^5 lost approximately 30% of its activity while LSZ 7.10^4 lost 20%. For the chemical denaturants, urea induces only a limited change of activity in the range of concentration used. Higher losses of activity were observed for GdHCl (35% at 10M). On the other hand, guanidinium hydrochloride induced an activity decrease proportional to the applied concentration.

Difference between lysozymes was found during mechanical treatments. First, LSZ 7.10^4 was stable in terms of activity until 15 minutes of ultrasonic treatment while LSZ 1.10^5 started to loss its antibacterial action since this same treatment time. Besides that, HPLC could detect that soluble aggregate formation was higher for LSZ 7.10^4 than for LSZ 1.10^5 after 45 minutes of ultrasonic treatment. The formation of soluble aggregate was linear with time for

both lysozymes but the same behavior was not observed for insoluble aggregates. For these last ones, a two-step formation could be elucidated where on the beginning the amount of insoluble aggregates was the same and then it increased with time. These results together could suggest that for a small treatment period (until 15 minutes) LSZ 7.10^4 was more stable than LSZ 1.10^5, because it did not loss its initial antibacterial activity even with soluble and insoluble aggregates formation.

The second mechanical process studied was the ultrafiltration and it was the one that presented the higher activity loss in the permeate solutions. While LSZ 1.10^5 presented an activity decrease dependent on transmembrane pressure, LSZ 7.10^4 was stable and presented the same antibacterial activity after filtration. The first suggestion was that the purification step (dialysis) used only for LSZ 1.10^5 could be responsible for changing the behavior of lysozyme during pore passage. To study this hypothesis, LSZ 7.10^4 was dialyzed. However, LSZ 7.10^4 continued to show high stability in terms of biological activity after filtration. With this observation it can be stated that lysozymes have a different response to forced passage through the pores of the membrane.

This suggestion can be supported by the observed differences in the SEC-HPLC chromatograms, that show the reduction of hydrodynamic radius only for the LSZ 1.10^5 permeate. Taking into account this reduction in size with decrease in antibacterial activity it can be suggested that the ultrafiltration applied at high transmembrane pressures induces the unfolding of lysozyme native structure.

Different behaviors with both lysozymes were observed when ultrafiltration or ultrasonic treatment were applied. The results suggest that these two operations modify differently (in terms of energy and irreversibility) the protein conformation than thermal and chemical treatments. The table III-5 shows the energies involved for each treatment.

Table III-5. Energy variation for the studied treatments.

Treatment	Operating conditions	Energy variation
Ultrafiltration	12 bar	1.2 J/g
Ultrasound	-	0.9 J/g/min
Chemical	10 M	50 J/g
Thermal	90°C	270 J/g

The energy variations during ultrafiltration and ultrasound (application time < 15 minutes) are relatively low. That could result in a low energetic and slightly irreversible transformations. In these conditions, the stability of the protein would be the main parameter during these treatments (for example, via the presence stabilizing molecules). On the other hand, chemical and thermal treatments are very energetic and lead to strongly irreversible transformations, independently of the Lysozyme initial state.

Bibliography

(1) Housmans, J. A. J.; Wu, G.; Schymkowitz, J.; Rousseau, F. A Guide to Studying Protein Aggregation. *FEBS J.* **2021**, 1–30. https://doi.org/10.1111/febs.16312.

(2) Ecroyd, H.; Carver, J. A. Unraveling the Mysteries of Protein Folding and Misfolding. *IUBMB Life* **2008**, *60* (12), 769–774. https://doi.org/10.1002/iub.117.

(3) Mahler, H. C.; Friess, W.; Grauschopf, U.; Kiese, S. Protein Aggregation: Pathways, Induction Factors and Analysis. *J. Pharm. Sci.* **2009**, *98* (9), 2909–2934. https://doi.org/10.1002/jps.21566.

(4) Buell, A. K.; Dobson, C. M.; Knowles, T. P. J. The Physical Chemistry of the Amyloid Phenomenon: Thermodynamics and Kinetics of Filamentous Protein Aggregation. *Essays Biochem.* **2014**, *56* (1), 11–39. https://doi.org/10.1042/BSE0560011.

(5) Hédoux, A.; Krenzlin, S.; Paccou, L.; Guinet, Y.; Flament, M. P.; Siepmann, J. Influence of Urea and Guanidine Hydrochloride on Lysozyme Stability and Thermal Denaturation; A Correlation between Activity, Protein Dynamics and Conformational Changes. *Phys. Chem. Chem. Phys.* **2010**, *12* (40), 13189–13196. https://doi.org/10.1039/c0cp00602e.

(6) Siddaramaiah, M.; Satyamoorthy, K.; Rao, B. S. S.; Roy, S.; Chandra, S.; Mahato, K. K. Identification of Protein Secondary Structures by Laser Induced Autofluorescence: A Study of Urea and GnHCl Induced Protein Denaturation. *Spectrochim. Acta - Part A Mol. Biomol. Spectrosc.* **2017**, *174*, 44–53.

(7) Xing, L.; Lin, K.; Zhou, X.; Liu, S.; Luo, Y. Multistate Mechanism of Lysozyme Denaturation through Synchronous Analysis of Raman Spectra. *J. Phys. Chem. B* **2016**, *120* (41), 10660–10667. https://doi.org/10.1021/acs.jpcb.6b07900.

(8) Carrillo, W.; García-Ruiz, A.; Recio, I.; Moreno-Arribas, M. V. Antibacterial Activity of Hen Egg White Lysozyme Modified by Heat and Enzymatic Treatments against Oenological Lactic Acid Bacteria and Acetic Acid Bacteria. *J. Food Prot.* **2014**, *77* (10), 1732–1739. https://doi.org/10.4315/0362-028X.JFP-14-009.

(9) Mañas, P.; Muñoz, B.; Sanz, D.; Condón, S. Inactivation of Lysozyme by Ultrasonic Waves under Pressure at Different Temperatures. *Enzyme Microb. Technol.* **2006**, *39* (6), 1177–1182. https://doi.org/10.1016/j.enzmictec.2005.11.053.

(10) Vilcacundo, R.; Méndez, P.; Reyes, W.; Romero, H.; Pinto, A.; Carrillo, W. Antibacterial Activity of Hen Egg White Lysozyme Denatured by Thermal and Chemical Treatments. *Sci. Pharm.* **2018**, *86* (4), 1–17. https://doi.org/10.3390/scipharm86040048.

(11) Noritomi, H.; Minamisawa, K.; Kamiya, R.; Kato, S. Thermal Stability of Proteins in the Presence of Aprotic Ionic Liquids. *J. Biomed. Sci. Eng.* **2011**, *04* (02), 94–99. https://doi.org/10.4236/jbise.2011.42013.

(12) Zhao, W.; Yang, R. Comparative Study of Inactivation and Conformational Change of Lysozyme Induced by Pulsed Electric Fields and Heat. *Eur. Food Res. Technol.* **2008**, *228* (1), 47–54. https://doi.org/10.1007/s00217-008-0905-z.

(13) Krishnamurthy, R.; Lumpkin, J. A.; Sridhar, R. Inactivation of Lysozyme by Sonication under Conditions Relevant to Microencapsulation. *Int. J. Pharm.* **2000**, *205* (1–2), 23–34. https://doi.org/10.1016/S0378-5173(00)00473-7.

(14) Marchioni, C.; Riccardi, E.; Spinelli, S.; Dell'Unto, F.; Grimaldi, P.; Bedini, A.;

Giliberti, C.; Giuliani, L.; Palomba, R.; Congiu Castellano, A. Structural Changes Induced in Proteins by Therapeutic Ultrasounds. *Ultrasonics* **2009**, *49* (6–7), 569–576. https://doi.org/10.1016/j.ultras.2009.02.003.

(15) Frydenberg, R. P.; Hammershøj, M.; Andersen, U.; Greve, M. T.; Wiking, L. Protein Denaturation of Whey Protein Isolates (WPIs) Induced by High Intensity Ultrasound during Heat Gelation. *Food Chemistry*. 2016, pp 415–423. https://doi.org/10.1016/j.foodchem.2015.07.037.

(16) Gharbi, N.; Labbafi, M. Effect of Processing on Aggregation Mechanism of Egg White Proteins. *Food Chem.* **2018**, *252* (August 2017), 126–133. https://doi.org/10.1016/j.foodchem.2018.01.088.

(17) Miron, S. M.; de Espindola, A.; Dutournié, P.; Ponche, A. Study of the Relationship between Applied Transmembrane Pressure and Antimicrobial Activity of Lysozyme. *Sci. Rep.* **2021**, *11* (1), 1–8. https://doi.org/10.1038/s41598-021-91564-x.

(18) De Espindola, A.; Miron, S. M.; Dutournié, P.; Ponche, A. Ultrafiltration Operational Conditions Influence in the Antibacterial Activity of Native and Thermally Treated Lysozyme. *Comptes Rendus Chim.* **2023**, In Press.

(19) de Espindola, A.; Dutournié, P.; Ponche, A. Impact of Industrial Stress Factors on Lysozyme Enzyme: Role of Denaturation Processes and Initial Protein Activity. *Sustain. Chem. Pharm.* **2023**, *31* (December 2022), 100964. https://doi.org/10.1016/j.scp.2022.100964.

(20) Miron, S. M.; Dutournié, P.; Thabet, K.; Ponche, A. Filtration of Protein-Based Solutions with Ceramic Ultrafiltration Membrane. Study of Selectivity, Adsorption, and Protein Denaturation. *Comptes Rendus Chim.* **2019**, *22* (2–3), 198–205. https://doi.org/10.1016/j.crci.2018.09.011.

Chapter IV – Influence of surface chemistry on lysozyme adsorption

Résumé Chapitre IV.

Influence de la chimie de surface sur l'adsorption du lysozyme

Ce chapitre présente l'étude des interactions entre le lysozyme et différentes surfaces à hydrophilicité contrôlée. Ces essais ont été réalisés sur des surfaces planes immergées dans solution de protéine. Deux matériaux références ont été préalablement étudiés ; le PDMS, très hydrophobe et le verre très hydrophile. Par la suite, cinq surfaces à hydrophilicité contrôlée ont été réalisées (monocouches auto-assemblées sur verre - SAMs), caractérisés et utilisées pour étudier les interactions avec le lysozyme.

1- Cinétique d'adsorption sur le verre et le PDMS

Les surfaces étudiées sont prélevées à des temps donnés et caractérisées par FTIR. La quantité de lysozyme adsorbée, proportionnelle au pic d'amide I, est étudiée en fonction du temps de contact. Les courbes peuvent être décomposée en trois partie, une première partie au temps courts (premières heures), suivi par un palier pendant lequel la quantité adsorbée est constante. Enfin, la dernière partie qualifiée de second évènement se caractérise après plusieurs jours de contact par une augmentation de la quantité adsorbée suivie d'une diminution. La comparaison des résultats entre le verre et le PDMS montre que ce dernier évènement est plus important en intensité et plus tôt pour le matériau hydrophobe. Cet évènement est également caractérisé par une forte diminution des structures secondaires de type feiullet beta intermoleculaire.
Aux temps courts, les cinétiques d'adsorption du lysozyme sur le verre présentent un phénomène appelé « overshoot ». Ce phénomène, conduit à une sursaturation de lysozyme, puis pour minimiser les énergies du système, la protéine augmente sa surface de contact, ce qui a pour conséquence de réduire la quantité adsorbée à la surface. En parallèle, l'étude de la structure secondaire des protéines adsorbées montre une diminution du pourcentage d'hélice alpha et des non ordonnés associés à une augmentation des feuillets β inter et intramoléculaires Ce phénomène n'est pas observé sur le PDMS.

2- Synthèse et caractérisation de monocouches auto-assemblées sur verre – SAMs

Afin d'étudier l'importance de l'hydrophilicité sur les interactions protéines – surface, des monocouches auto-assemblées sur verre ont été réalisées afin de disposer de surfaces à hydrophilicité variable (méthodologie et synthèse décrites dans le chapitre matériels et méthodes) mais de rugosité constante. La caractérisation de ces surfaces montre un angle de contact à l'eau pure qui diminue en fonction du pourcentage de NH_2 et ce entre les valeurs des surfaces étudiées précédemment (PDMS et verre). L'observation de la rugosité de la surface par microscopie de force atomique (AFM) montre une surface à rugosité uniforme de 0.14 nm de moyenne contre 0,80 nm pour le verre avant le traitement.

3- Cinétiques d'adsorption sur les monocouches auto-assemblées

Les courbes de cinétiques d'adsorption obtenues sur ces surfaces présentent les trois mêmes parties ; un premier évènement aux temps cours pouvant être attribué à un phénomène de sursaturation, un palier pendant lequel la quantité adsorbée sur les matériaux est constante et un dernier évènement aux temps longs. De manière identique aux résultats obtenus avec le verre et le PDMS, le premier évènement se caractérise par une baisse des hélices alpha et une augmentation des feuillets bêta. Le deuxième évènement est quant à lui caractérisé par un minimum de pourcentage de feuillets bêta intermoléculaires, caractéristique des mécanismes agrégatifs.

Surface contact can induce protein denaturation and aggregation. Chapter IV presents the influence of the surface properties (chemistry and wettability) and solution concentration on lysozyme adsorption.

Infrared spectroscopy (FTIR-ATR) was used to analyze kinetics and conformational changes of adsorbed lysozyme. The amide I band area is used to estimate the amount of protein absorbed on the surface, and the peak fitting gives an estimation of the secondary structure quantification. Kinetic curves are constructed by plotting the area of the amide I band versus the time of the protein/surface contact.

1. Adsorption kinetic curves on model surfaces

1.1 Influence of surface wettability

Figure IV-I presents the lysozyme adsorption kinetic curve on glass (red) and PDMS (black) surfaces. The two curves are obtained after contact with a LSZ solution at a concentration of 0.36 mg.mL^{-1}. Each point is the average of Amide I area of three different locations on the same surface.

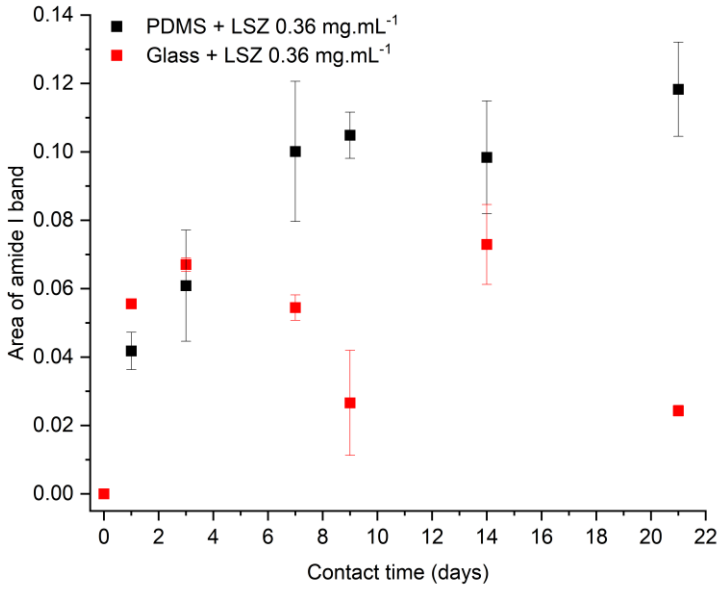

Figure IV-1: Adsorption kinetic curves on glass and PDMS surfaces in contact with lysozyme solution (C_{LSZ}= 0.36 mg.mL^{-1}, n=3).

For both curves (from 1 to 21 days), there is an increase in protein amount at the beginning until it reaches a plateau. On glass, the maximum amount of lysozyme adsorbed is obtained after 3 days (area = 0.065), while on PDMS, the saturation period starts after 7 days (area = 0.10).

The maximum of adsorption is reached faster on glass when compared with PDMS. As presented in figure IV-2A, lysozyme in solution has hydrophilic groups exposed on its surface, while the hydrophobic groups are on the core. This suggests that the interaction with glass is facilitated by the LSZ structure.

Hydrogen bonds are formed between the polar amino acid residues of the protein and the polar groups of the glass. In addition to hydrogen bonding, electrostatic interactions can occur. The test was performed in water, so the pH was approximately 6.4 and was below the pI of lysozyme (11.1). At this pH, lysozyme has a net positive charge, while the SiO groups on the glass are negative. Attractive electrostatic interactions may occur at the same time as hydrogen bonding.

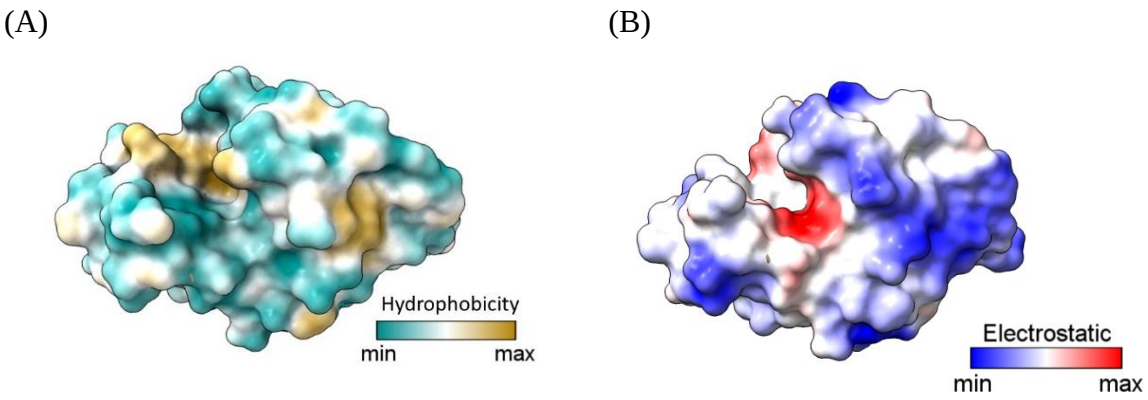

Figure IV-2: Lysozyme 3D structure with (A) hydrophobicity and (B) electrostatic scales. Figures created using ChimeraX.

The value of the plateau is more important for hydrophobic surface: 0.10 absorbance unit for PDMS whereas it is limited to 0.065 for glass surfaces. Lysozyme can expose its hydrophobic core to PDMS surface after conformational changes, which means that this

increase in adsorbed quantity may be due to structural changes in the protein and an increase in protein/surface interactions.

To confirm that the increase in lysozyme adsorption on PDMS was related to conformational changes, the secondary structure was analyzed. Figure IV-3 presents the quantification of secondary structure (expressed in percentage of the total area of amide I peak) obtained by peak fitting of the Amide I band.

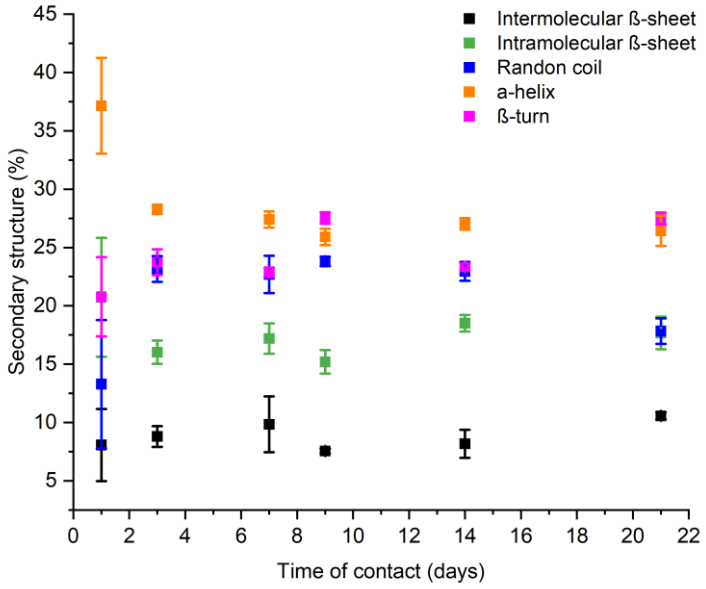

Figure IV-3: Evolution of secondary structure of adsorbed lysozyme on PDMS substrate (C_{LSZ} = 0.36 mg.mL^{-1}, n=3).

The secondary structure of lysozyme changed with adsorption time on PDMS, as observed in figure IV-3. The value of the α-helical structure was approximately 37% on the beginning (after 1 day of contact). Over time, a decrease in α-helices with an increase in random coils was observed. We suggest that this result is due to protein unfolding, which facilitates interactions between the hydrophobic core and surface. Consequently, the protein amount increased after the unfolding process (after 3 days). It is worth noted that, in the meantime, intramolecular and intermolecular β-sheets stay constant.

The same graph of the secondary structure evolution was obtained after adsorption on glass substrate, and is shown in Figure IV-4.

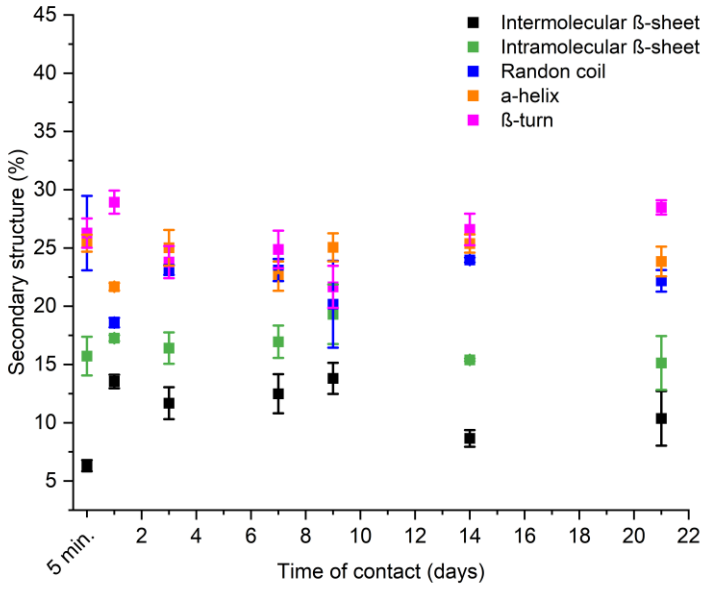

Figure IV-4: Evolution of secondary structure of adsorbed lysozyme on glass substrate (C_{LSZ} = 0.36 mg.mL^{-1}, n=3)

If we consider the percentages after different times of contact and the measurement errors, no significant difference in the LSZ secondary structure was observed. After 1 day of adsorption, the α-helix content was approximately 25% on glass. This proportion is different from the value of 37% obtained after 1 day on PDMS. The value of 25% of α-helices is obtained only after 7 days on PDMS. The hypothesis is that electrostatic interactions cause lysozyme to change its conformation immediately after being in contact with the surface. The contact between LSZ and glass begins with attractive forces between positive charges on LSZ and negative charges on the surface. There are also negative charges on the LSZ molecule and repulsive forces can occur simultaneously. This repulsion between negative part of the LSZ molecule and the surface results in conformational changes to minimize Gibbs free energy of the system.

The obtained results demonstrated the importance of the type of surface in the adsorption of proteins. The amount adsorbed, as well as the conformational change, can differ according to the hydrophilicity of the material.

Highlights:

- The adsorption plateau is reached faster on glass than on PDMS.
- The maximum amount of LSZ adsorbed on PDMS is higher and related to a decrease of the α-helix content over the first 7 days of the adsorption.
- Adsorption kinetics and structural modifications depend on the surface hydrophilicity.

1.2 Influence of lysozyme concentration

Lysozyme solution concentration was modified during adsorption tests to understand its impact on kinetic curves and/or protein adsorption amount. Kinetic curves in this topic were divided in two main periods. One from 0.5 until 24 hours and a second one from 1 to 21 days. These assays were conducted on glass and PDMS surface, varying LSZ concentration at 0.36, 1.00 and 2.00 $mg.mL^{-1}$.

1.2.1 Adsorption on PDMS

The adsorption kinetic curves between PDMS and lysozyme are shown in figure IV-5. Before 24h and at the lower concentration of 0.36 $mg.mL^{-1}$, no exploitable data was obtained by the ATR-FTIR analysis of PDMS.

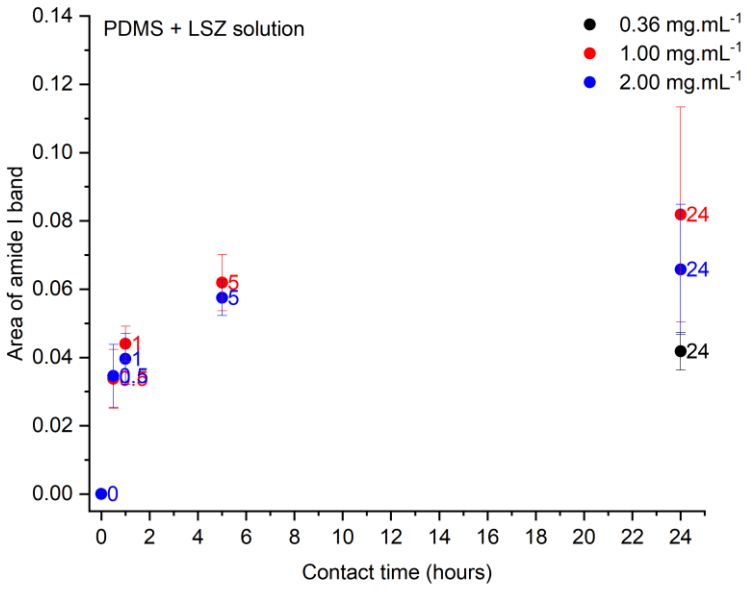

Figure IV-5: Adsorption kinetic curve for lysozyme in contact with PDMS varying protein concentration. First adsorption period (from 0.5 to 24 hours).

Similar results were obtained for the three concentrations. For the initial adsorption period, concentration (from 1.00 to 2.00 $mg.mL^{-1}$) did not interfere with the adsorption kinetics and protein amount for the initial adsorption period. For the solution of 0.36 $mg.mL^{-1}$, a smaller amount of protein can be detected after 24h of contact. For lower times of contact at a concentration of 0.36 $mg.mL^{-1}$, the amount of proteins adsorbed seems to be below the detection limit of the ATR-FTIR technique (estimated to be 0.033 absorbance unit).

As presented in figure IV-3, the increase in lysozyme amount on PDMS is related to a conformational change. According to Rabe *et al.* 2011, two simple kinetic models take into account conformational changes (see figure IV-6).

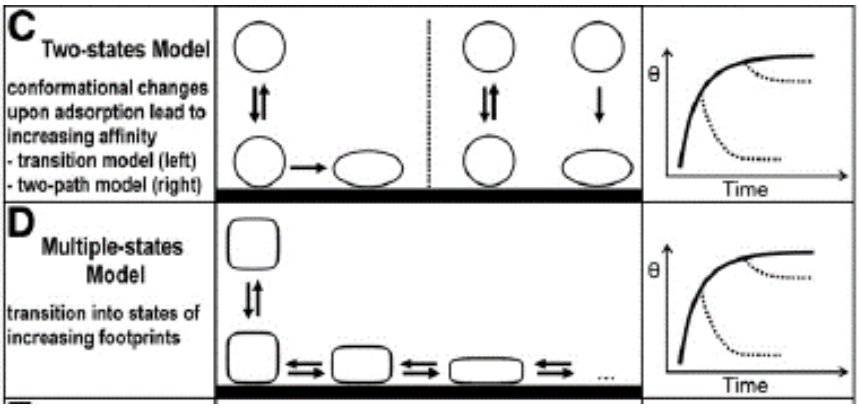

Figure IV-6: Kinetic models that could describe lysozyme adsorption on PDMS[1].

Models C and D were proposed by *McGuire et al.* 1995[2] and *Szöllősi et al. 2004*[3], respectively. The first explains that proteins can adsorb on the surface in two ways: reversible and irreversible. It means that weak adsorption (reversible) does not present many interactions, and strong adsorption (irreversible) is favored due to increased interactions with the surface. Model C considers only two different states of the protein, while model D states that the protein can evolve to different conformations increasing its footprint on the surface and, consequently, reach the irreversible state. Whatever the model, the kinetic curve is similar and an increase in the protein amount is observed due to conformational changes that favor protein/surface interactions. This increase is followed by a saturation state in which all adsorbed proteins are on their irreversible state. Thus, our kinetic curves obtained for PDMS are in agreement with one of the two models.

To understand if these kinetic models can be supported during a long period of adsorption, the test was done up to 21 days. The results are shown in figure IV-7.

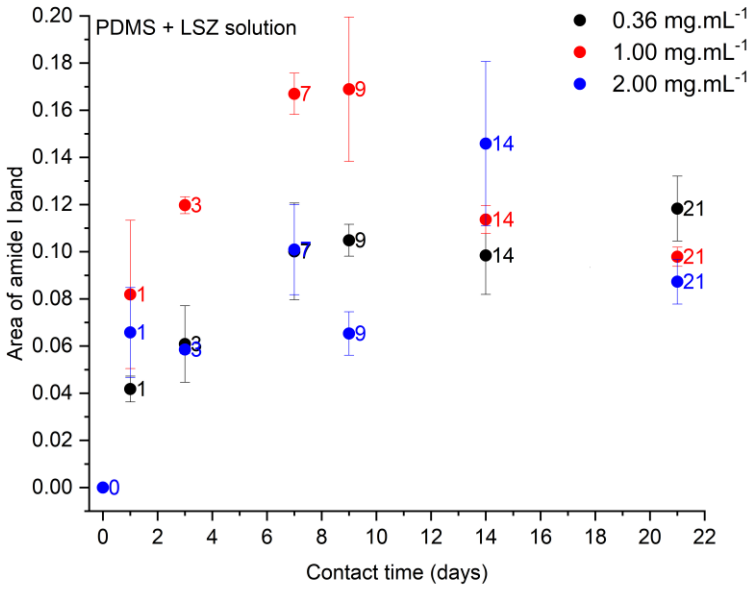

Figure IV-7: Adsorption kinetics curve for lysozyme in contact with PDMS varying protein concentration. Second adsorption period (from 1 to 21 days).

The kinetic curves show a gradual increase of the amount of adsorbed protein with time. The increase was followed by a plateau after 7 days for concentrations of 0.36 and 2.00 mg.mL^{-1}. Concentration of 1.00 mg.mL^{-1} shows a greater protein adsorption between 3 and 9 days, when compared to the others. After 9 days, the amount of LSZ on the surface decreased to similar values close to the other concentrations. This difference between 9 and 14 days, for 1.00 mg.mL^{-1}, could be explained by the formation of aggregates followed by the release in solution. The same was observed for 2.00 mg.mL^{-1} with a smaller difference between 14 and 21 days. We suggest that aggregates are formed on the surface and are progressively released in solution.

DLS measurements were conducted on the final test solutions (after 21 days of contact) to confirm this hypothesis. The results are shown in Table IV-1.

Table IV-1. DLS results of lysozyme solutions after 21 days of contact with PDMS.

Solution	***Hydrodynamic diameter (nm)***
LSZ native solution 1.00 mg.mL^{-1}	3.9 ± 0.2
LSZ 0.36 mg.mL^{-1} + PDMS	3.7 ± 0.3
LSZ 1.00 mg.mL^{-1} + PDMS	11.9 ± 3.0
LSZ 2.00 mg.mL^{-1} + PDMS	28.2 ± 2.5

An increase in the hydrodynamic diameter in solution was observed with lysozyme concentration. These results supported our hypothesis that the variability of amide I area in the kinetic curve are associated with aggregate formation. For LSZ solution at concentration 1.00 mg.mL^{-1} smaller aggregates were formed when compared to 2.00 mg.mL^{-1}. This difference between the concentrations can be explained by the amount of lysozyme molecules available in the solution. The higher the amount of protein in the solution, the larger the aggregates formed.

Highlights:

- Lysozyme adsorbs on PDMS following the multiple-states model.
- The plateau of adsorption on PDMS was reached after 7 days for 0.36 mg.mL^{-1}.
- A variability is observed for higher concentrations (1.00 and 2.00 mg.mL^{-1}) and is associated with aggregates formation (detected by DLS)

1.2.2 Adsorption on glass

The concentration influence on lysozyme adsorption was also studied on glass. The results of the beginning of adsorption (from 0.5 to 24 hours) are presented in figure IV-8.

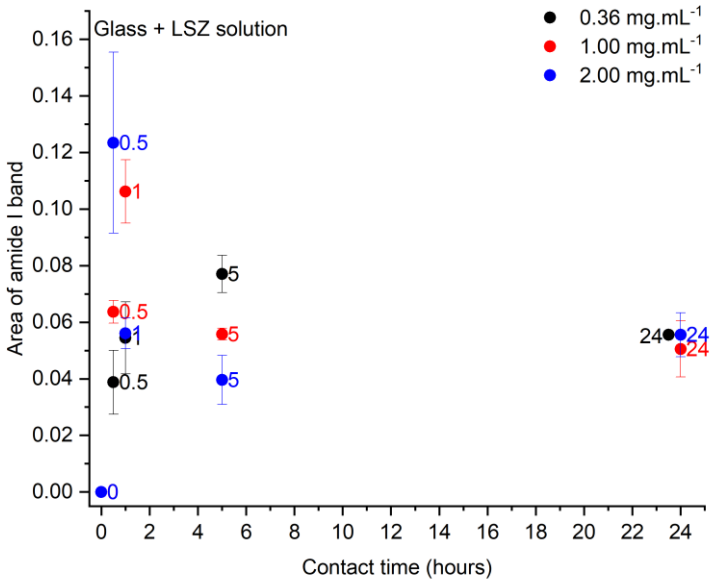

Figure IV-8: Adsorption kinetic curve for lysozyme in contact with glass varying protein concentration. First adsorption period (from 0.5 to 24 hours).

For all the concentrations, a higher value of amide I area is observed at the beginning of adsorption. This effect is known as “overshoot” and occurs when the protein is rapidly adsorbed on the surface in a reversible manner, reaching a state of oversaturation. However, when the proteins in the neighborhood start to increase their footprint by changing conformation to increase protein/surface interactions, the neighboring molecules that are not strongly adsorbed are released from the surface. The phenomenon is schematically presented in figure IV-9.

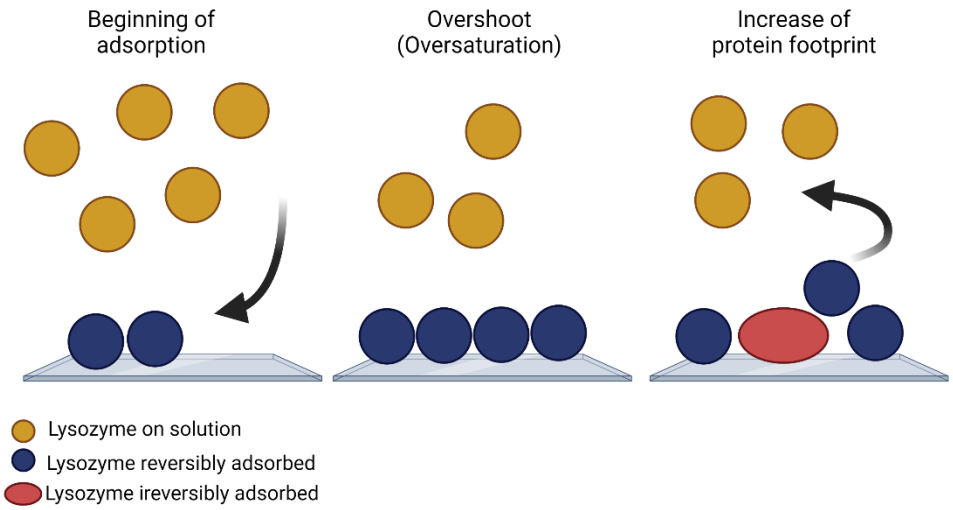

Figure IV-9: Scheme of overshoot for lysozyme on glass. Created with BioRender.com.

The overshoot time differed according to the concentration of lysozyme used. The higher the concentration, the faster the oversaturation state is reached. For concentrations of 0.36, 1.00 and 2.00 $mg.mL^{-1}$, overshoot was observed at 5, 1 and 0.5 hour, respectively. The overshoot phenomenon assumes that the surface is saturated, and it happens faster when the concentration increases.

The plateau, according to our data, appears to be after 24h when the Amide I areas for the three concentrations are the same. After 24h, it is not possible to be sure that adsorption is at equilibrium. Experiments were conducted over a period of 21 days to check if the amount adsorbed on each surfaces is still evolving. Figure IV-10 shows the adsorption curves during this test period.

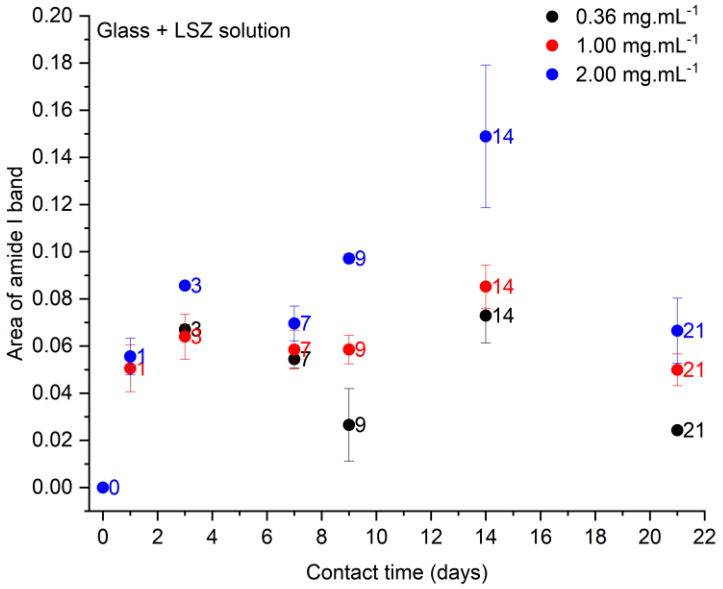

Figure IV-10: Adsorption kinetic curve for lysozyme in contact with glass varying protein concentration. Second adsorption period (from 1 to 21 days).

The amount of adsorbed lysozyme is similar for the three concentrations up to 7 days. The intensity of amide I peak after 9 days is not stable. Difference could be explained by accumulation of proteins in the coating and sudden release of aggregates. DLS measures were done to understand if this difference could be associated to aggregates as observed for PDMS. Results are presented in table IV-2.

Table IV-2. DLS results of lysozyme solutions after 21 days of contact with glass.

Solution	***Hydrodynamic diameter (nm)***
LSZ native solution 1.00 mg.mL^{-1}	3.9 ± 0.2
LSZ 0.36 mg.mL^{-1} + Glass	4.3 ± 0.9
LSZ 1.00 mg.mL^{-1} + Glass	3.9 ± 0.7
LSZ 2.00 mg.mL^{-1} + Glass	3.7 ± 0.7

The DLS results did not show significant differences between the hydrodynamic diameters for the studied concentrations. In this case, differences cannot be associated with

aggregate formation and release from the surface to the solution. The reason for the increase in the amount of lysozyme adsorbed on the glass after 14 days should be further investigated with other techniques such as ellipsometry or QCM.

From the previous results, the LSZ concentration used for the adsorption tests on SAMs prepared in glass is 1.00 $mg.mL^{-1}$. This concentration was chosen because no variability was observed on the LSZ adsorption kinetics curve. Besides that, we want to guarantee the adsorption of LSZ on SAMs and the highest concentration tested without variability was 1.00 $mg.mL^{-1}$.

Highlights:

- Kinetic curves for lysozyme adsorption on glass surfaces showed an overshoot feature.
- The overshoot happened at different times according to LSZ concentration. The higher the concentration, the faster the overshoot is detected.
- Variability on kinetic curve for 2.00 $mg.mL^{-1}$ were observed during second adsorption period (1 to 21 days). The reasons should be further investigated.

The results obtained on the first part of this chapter suggest that the adsorption kinetics as well as the amount of adsorbed protein depend on the surface chemistry. We have currently worked with one hydrophobic (PDMS) and one hydrophilic surface (glass) but the chemistry and physical characteristics of these two substrates are truly different. We propose in the next part to manufacture surfaces with controlled chemistry and morphology to study the influence of continuous hydrophilicity variation on lysozyme adsorption. Self-assembled monolayers (SAMs) are good candidates as they present high control of surface chemistry, layer structure and molecular organization. The advantage of comparing SAMs is that the chemistry of surface can be modified (and so wettability) by keeping similar roughness. Mixed SAMs were prepared on borosilicate glass with varied ratio between NH_2 and CH_3 on the surface. Preparation was explained in Part II item 1.2 of Materials and Methods chapter and the characterization are presented in the following item.

2. Self-assembled monolayer characterization

Self-assembled monolayer surfaces were characterized by contact angle experiments, X-ray Photoelectron Spectroscopy (XPS) and Atomic Force Microscopy (AFM). With the wettability results, information on hydrophobicity and surface energy can be obtained. XPS indicates the chemical composition of the monolayer as well as allows the calculation of the ratio between NH_2 and CH_3. AFM images are used to analyze the homogeneity of the monolayer and to evaluate its roughness with the Ra and Sa parameters. Analysis of these results can indicate whether the monolayer was successfully formed on borosilicate surfaces.

2.1 Wettability and surface energy

The water contact angle was measured on 3 points of 2 different surfaces (6 independent measures). Figure IV-11 presents the average value and the standard deviation for all samples (from 0 to 100% of NH_2). Theoretical values of NH_2 were used in X-axis (figure IV-11), the experimental one will be determined in paragraph 2.3 (XPS) of this chapter.

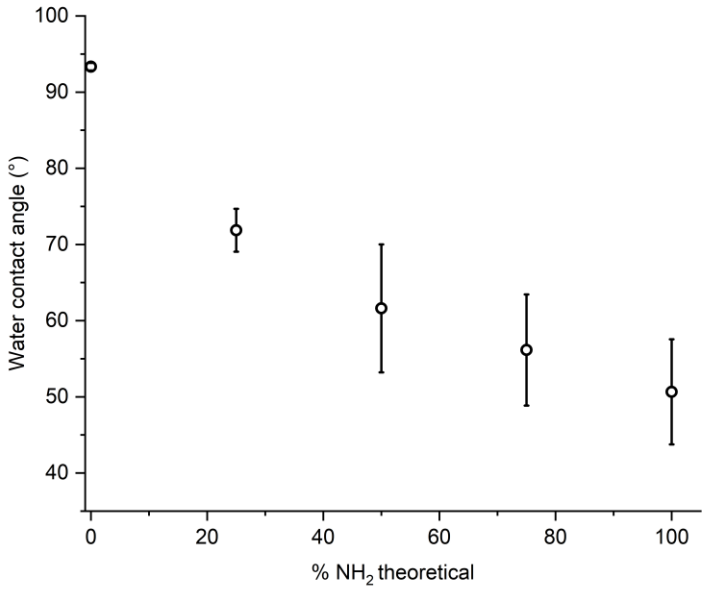

Figure IV-11: Water contact angle for prepared SAMs surfaces.

Decrease of contact angle was obtained with the increase of number of amino groups on the surface. It indicates the surface change with hydrophilicity increase due to the terminal groups (NH_2). The most hydrophobic surface was Glass 0%NH_2, with contact angle value around 95°. This surface corresponds to a monolayer with all molecules terminated by CH_3 groups. This value is in the same range as reported in the literature, indicating that the silane is densely packed on the surface[4,5]. As expected, the most hydrophilic surface was the Glass 100%NH_2 (contact angle around 50°). This surface is composed of 100% of silane with amine terminal groups and the value of water contact angle obtained is consistent with the literature[4].

Mixed SAMs on borosilicate glass were prepared with variable hydrophilicity. These surfaces present intermediate wettability between the others studied, the PDMS with a contact angle of 111° and the borosilicate of 36°. This large variation in wettability is interesting to understand its influence on protein adsorption.

Surface energy was calculated as explained in materials and method part (item 3.5) by using equation 1.

$$\Delta G = -A_{LS}(1+\cos\theta)\gamma = -2A_{LS}\left(\sqrt{\gamma_S^{LW}\gamma_L^{LW}} + \sqrt{\gamma_S^{+}\gamma_L^{-}} + \sqrt{\gamma_S^{-}\gamma_L^{+}}\right) \quad \text{Equation 1}$$

Where A_{LS} is the contact area between the liquid and the surface, γ_S and γ_L are the apparent surface tension on the interface solid/gas and liquid/gas, respectively. LW is the apolar van der Waals interactions and the polar contribution is divided on two components γ^+ (electron acceptor) and γ^- (electron donor).

By measuring the contact angle θ with three liquids (knowing the values of γ_L^{LW}, γ_L^- and γ_L^+), it is possible to estimate the polar and apolar surface tension components of the surface. The contact angles with water, diiodomethane, and ethylene glycol were measured, as shown in Table IV-3.

Table IV-3. Contact angle between the surface and water, diiodomethane and ethylene glycol.

	Contact angle (°)		
Surface	*Water*	*Diiodomethane*	*Ethylene glycol*
Polydimethylsiloxane (PDMS)	111.1 ± 1.0	90.6 ± 4.4	99.1 ± 2.9
Glass 0%NH_2	93.2 ± 0.5	62.8 ± 0.9	81.8 ± 1.1
Glass 25%NH_2	71.9 ± 2.8	44.0 ± 3.5	24.4 ± 2.8
Glass 50%NH_2	61.6 ± 8.4	48.7 ± 5.7	39.8 ± 13.1
Glass 75%NH_2	56.2 ± 7.3	44.3 ± 1.0	20.7 ± 1.9
Glass 100%NH_2	50.7 ± 7.0	38.5 ± 0.5	19.0 ± 1.7
Glass	35.9 ± 0.8	64.4 ± 2.2	31.1 ± 1.9

The surface tension components are calculated for each surfaces and the results are presented in Table IV-4.

Table IV-4. Estimation of the surface tension components (polar and apolar) of the studied surfaces.

Surface	γ_S^{LW} (mN.m^{-1})	γ_S^+ (mN.m^{-1})	γ_S^- (mN.m^{-1})
Polydimethylsiloxane (PDMS)	12.3	0.0	2.3
Glass 0%NH_2	27.0	0.4	6.9
Glass 25%NH_2	37.0	1.8	6.0
Glass 50%NH_2	35.0	0.3	21.2
Glass 75%NH_2	37.4	1.0	20.8
Glass 100%NH_2	40.4	0.5	26.8
Glass	26.0	0.9	54.3

For PDMS, the major contribution of the surface energy is the apolar component (12.3 mN.m^{-1}). The surface energy for glass presented a major contribution from the polar components (54.3 mN.m^{-1}) and an apolar contribution (26.0 mN.m^{-1}). Comparing the monolayers with the glass substrate, a small increase in the apolar component was observed. This increase was due to the inclusion of silane alkyl chains on the surface (monolayer formation). It exposes CH_2 and CH_3 groups on the surface.

An increase in polar components was observed from Glass 0% NH_2 to 100%. It is in agreement with the results of hydrophilicity observed in figure IV-11. There was an increase mainly in the polar component related to electron donor groups. This result indicates the presence of terminal amine groups, since the electron donor character comes from the free electron pairs of nitrogen. The bigger the amount of amino groups (100%), the higher the value of surface tension polar component.

Highlights:

- The water contact angle decreased with increasing amounts of amine groups, indicating a surface modification.
- Apolar component of surface tension increased comparing SAMs with glass due to addition of silane.
- Polar component (electron donor) was higher for Glass 100%NH_2 when compared to the other SAMs, due to the higher amount of free electron pairs of nitrogen.

2.2 Surface homogeneity and roughness calculation

The images obtained with atomic force microscopy (AFM) are shown in figure IV-12. The images were obtained in two different modes: Z-axis and phase. Three dimensional images were created using the Z-axis mode and Gwyddion Software 2.62.

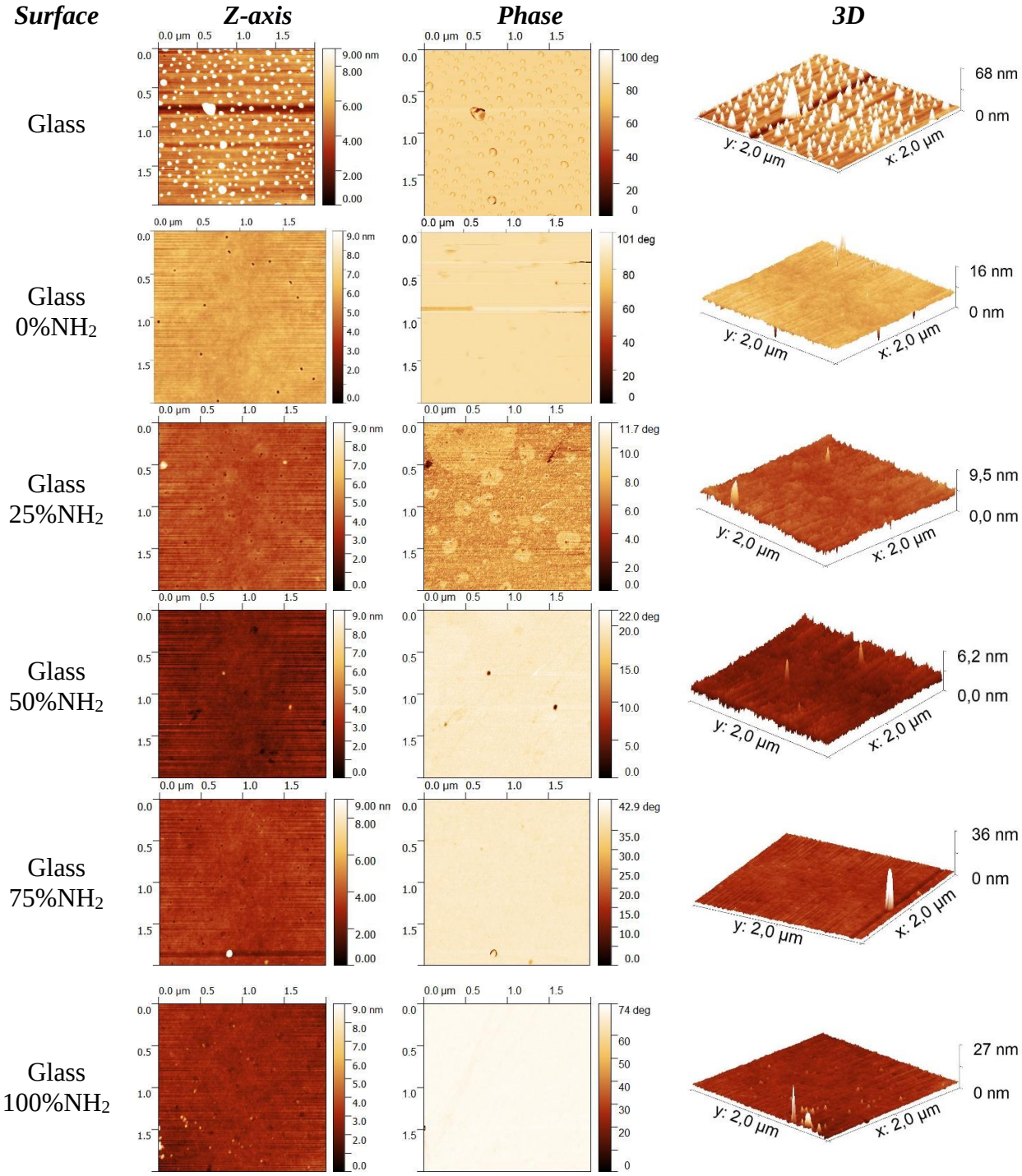

Figure IV-12: AFM images for mixed Self-Assembled Monolayers prepared on glass.

The surface of coverslip in borosilicate (glass) is not completely smooth. There are repetitions of grains across the surface, with average heights of 3 nm. Grained surfaces for the borosilicate were observed by other authors in the literature[6–11]. They explain that liquid-liquid immiscibility can be observed during glass forming melts, resulting in phase separation. The coverslips used were from the same manufacturer and as consequence, all bare samples, even after cleaning step, presented the grained surface.

Comparing the SAMs with the bare glass it is possible to see that the monolayers were homogeneously formed and presented a smoother surface. It indicates that monolayers covered some of the initial glass grains. The defaults present in images from Glass 25%NH_2 to Glass 100%NH_2 can be related to the initial glass surface or some impurity.

Roughness parameters (R_a and S_a) were determined using the AFM images and Gwyddion Software 2.62. The R_a is the average of surface heights along a measurement line, while S_a is the average roughness over an area. R_a was obtained as the average of 10 lines chosen without the defaults/impurities. S_a values were determined considering the whole area (4 μm^2) of AFM images. The results are shown in Table IV-5.

Table IV-5. Roughness parameters obtained with AFM images

Surface	***R_a (nm)***	***S_a (nm)***
Glass	0.80 ± 0.10	1.8
Glass 0%NH_2	0.15 ± 0.03	0.3
Glass 25%NH_2	0.13 ± 0.02	0.4
Glass 50%NH_2	0.14 ± 0.02	0.3
Glass 75%NH_2	0.14 ± 0.02	0.5
Glass 100%NH_2	0.12 ± 0.02	0.5

The roughness values of S_a are bigger than R_a because of defaults/impurities on the surface that were considered in the S_a calculation. R_a parameter was used to compare the glass surfaces and it was observed a bigger roughness to the bare glass. Roughness of SAMs surfaces were smaller, around 0.15 nm, it means that a layer was formed covering the glass initial defaults. The SAMs presented similar roughness and different hydrophobicity as presented in the topic above (item 2.1) according to the goal of this work.

Highlights:

- AFM images showed the homogeneity of prepared SAMs.
- Similar roughness was obtained for monolayers (around 0.15 nm).

2.3 Chemical composition of SAMs by XPS

The surface chemical composition of coverslip was determined by X-ray Photoelectron Spectroscopy (XPS). Survey spectrum of borosilicate glass is shown in Figure IV-13.

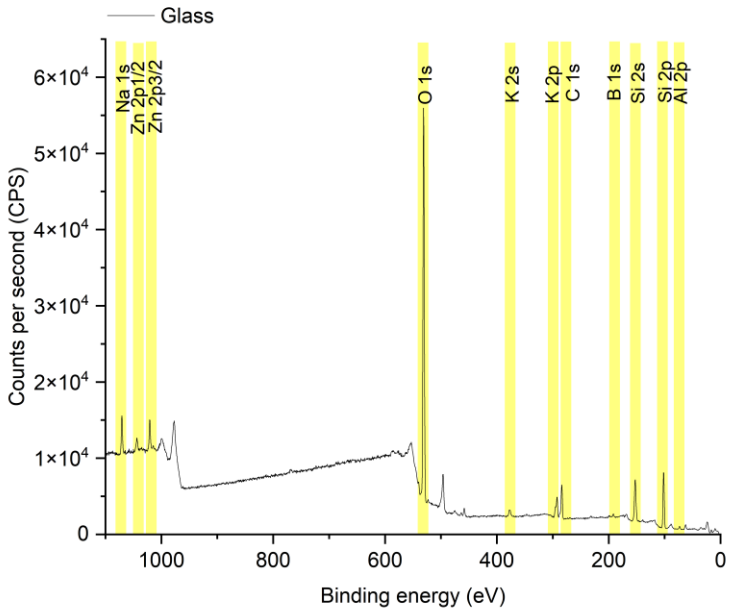

Figure IV-13: XPS survey spectrum of borosilicate glass.

All expected elements were detected according to the theoretical borosilicate composition. Borosilicate is composed of substantial amounts of SiO_2 (70-80 wt%), containing boron oxide – B_2O_3 (7-13 wt%), sodium and/or potassium oxide – Na_2O, K_2O (4-8 wt%) and alumina – Al_2O_3 (2-8 wt%)[12]. The presence of carbon and zinc are due to impurities on the surface. Experimental amounts of each component were determined with the area of XPS peak. The results are presented in Table IV-6.

Table IV-6: Elementary composition of glass surface determined by XPS.

Al 2p	*B 1s*	*C 1s*	*K 2p*	*Na 1s*	*O 1s*	*Si 2p*	*Zn 2p3/2*
1.5%	4.9%	13.9%	2.3%	2.6%	53.8%	20.2%	0.8%

The composition determined for the glass is close to the theoretical one with approximately 63% of SiO_2 and 5% of B_2O_3.

Survey spectra were obtained for the SAMs. Figure IV-14 presents the survey spectrum for self-assembled monolayer 100%NH_2.

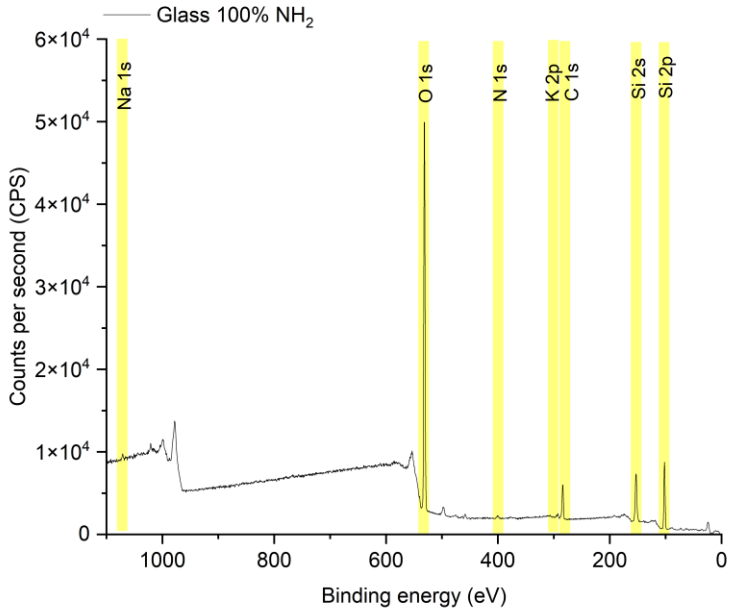

Figure IV-14: XPS survey spectrum of Glass 100% NH_2.

Some elements of glass (Si, Na and K) are still detected with a lower intensity. In addition to borosilicate composition, nitrogen is present confirming the successful monolayer preparation. The bromine atom which is present on the first step of SAM preparation, was not detected, showing that the conversion of the bromine terminal groups into amine was complete. Elementary composition was calculated and the result for Glass 100%NH_2 are presented in Table IV-7.

Table IV-7: Elementary composition of Glass 100% NH_2 determined by XPS.

C 1s	***K 2p***	***Na 1s***	***O 1s***	***Si 2p***	***N 1s***
15.4%	0.5%	0.3%	56.8%	26.0%	1.0%

The ratio between oxygen (O) and silicon (Si) for the glass and Glass 100%NH_2 was calculated to understand if the monolayer is homogeneously deposited on glass. If the values are close, it means that in the survey spectrum, silica coming from the glass was seen even after monolayer formation. The values obtained for glass and Glass 100%NH_2 were 2.7 and 2.2, respectively. This small difference can be due to addition of silicon atoms coming from the silane used to prepare the SAM.

XPS high-resolution spectra were obtained for carbon and nitrogen. Figure IV-15 show the nitrogen high-resolution spectra for SAMs from 0 to 100% of NH_2. The area of N1s peak is also shown in the figure.

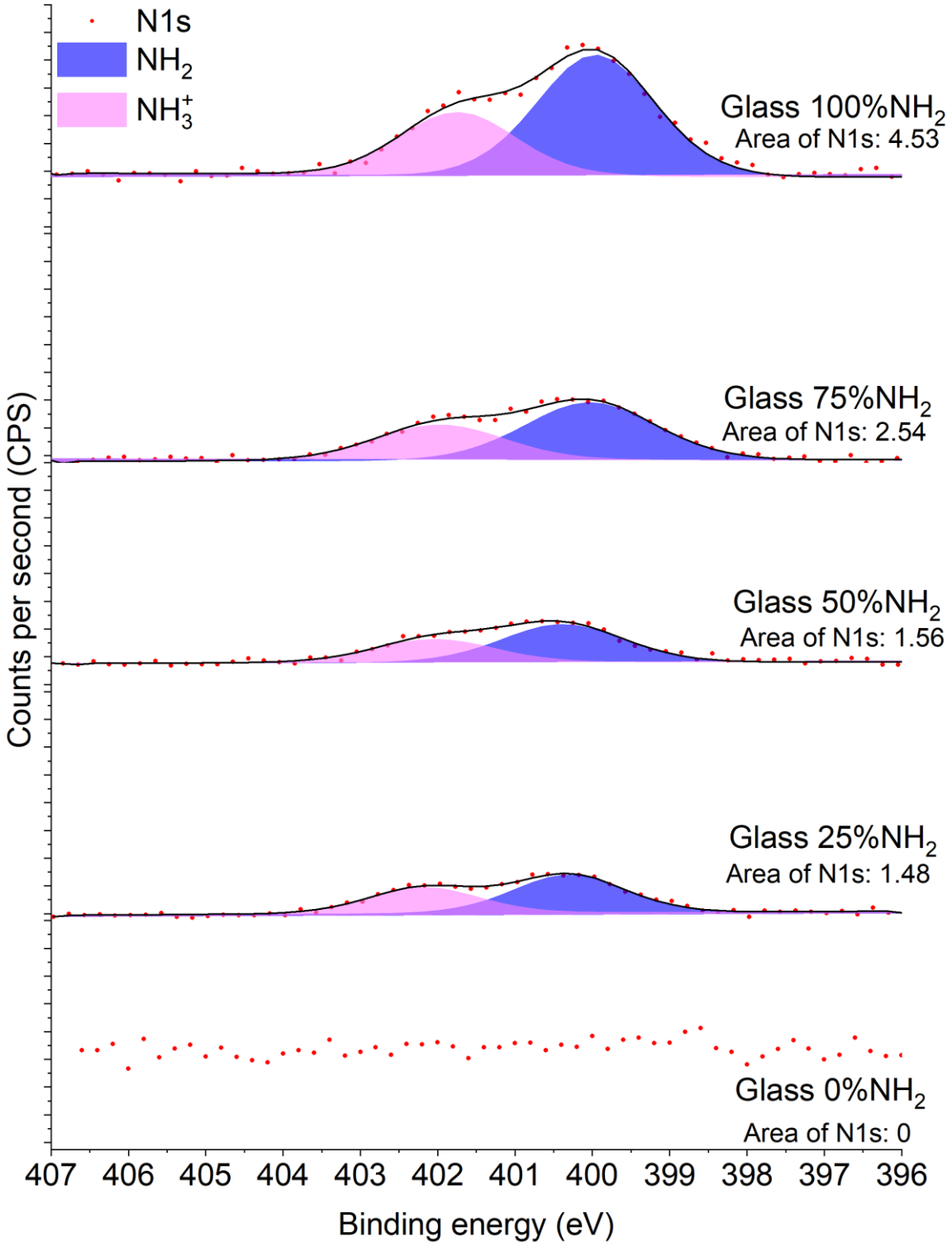

Figure IV-15: XPS N1s high resolution spectra of SAMs from 0 to 100% of NH_2.

The presence of nitrogen was observed on the surfaces, except for Glass 0%NH_2 as expected. NH_2 and NH_3^+ components were identified after SAMs preparation at a binding energy of respectively 400.2eV and 402.0eV. The area of N1s increases with the theoretical amount of nitrogen on the surface, proving the varied amount of amino groups on the surface as observed by contact angle and surface energy measures.

C1s high-resolution spectra are presented in Figure IV-16.

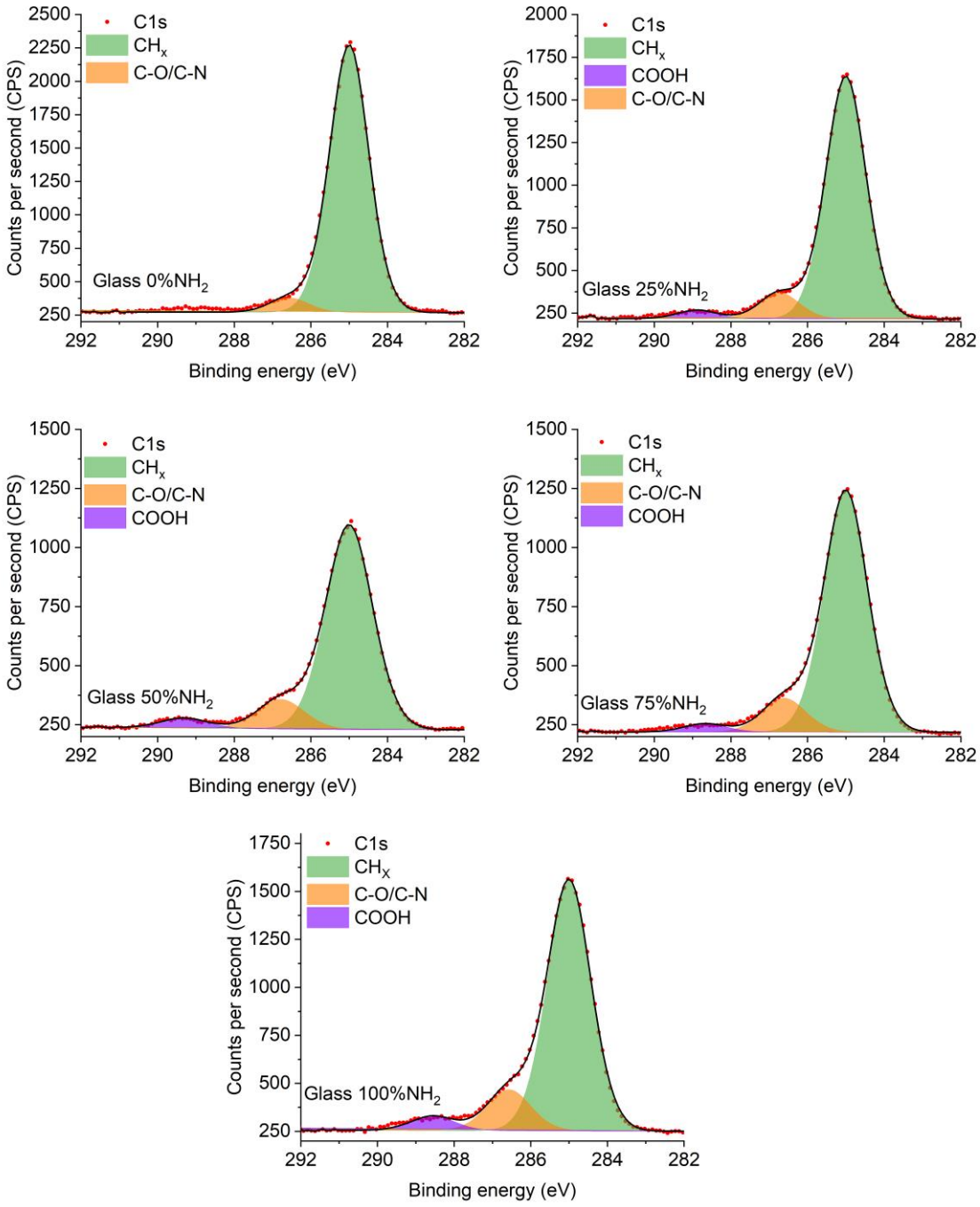

Figure IV-16: XPS high resolution spectra of carbon for SAMs from 0-100% of NH_2.

Carbon CH_x and C-O/C-N groups were observed for all surfaces at 285 and 286.6 eV, respectively. The C-N peak area increased with percentage of NH_2 groups. This result is in agreement with what was observed for the high-resolution N1s. An extra peak attributed to

COOH (288.5 eV) was observed on SAMs containing the amino groups on the monolayers. The CH_x groups can be attributed to the monolayer silane and also to impurities. Other peaks appearing as a result of contamination are the C-O and COOH. As C-O and C-N have the same binding energy (around 287 eV), only the COOH could be separated and avoided to the estimation of experimental N/C.

The peak areas of N1s and C1s were obtained to calculate the experimental ratio between N and C. The theoretical value of N/C considers eleven carbons of silane chain and the terminal amino groups (figure IV-17). For example, for the sample called Glass 25%NH_2, one molecule of aminosilane is present for 3 molecules of alkylsilane and the N/C expected is 1/44 = 0.023 as showed in the figure below.

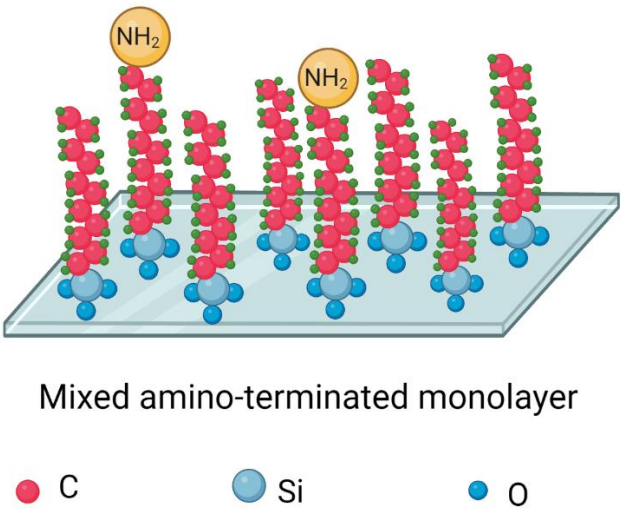

Figure IV-17: Scheme of Glass 25% NH_2 surface. Created with BioRender.com.

The Table IV-8 presents the corrected area of N1s and C1s peaks that were used to obtain the experimental N/C ratio. For the carbon area, the COOH peak was not considerate as it is attributed to contamination and not to the monolayer.

Table IV-8: XPS peak areas of N1s and C1s and result of experimental N/C.

Sample	*Area of N1s*	*Area of C1s*	*Experimental N/C*
Glass 0%NH_2	0.00	79.33	0.00
Glass 25%NH_2	1.48	63.85	0.023
Glass 50%NH_2	1.56	38.53	0.040
Glass 75%NH_2	2.54	51.38	0.049
Glass 100%NH_2	4.53	67.53	0.067

Experimental values of N/C were compared with the theoretical ones and the results are shown in figure IV-18.

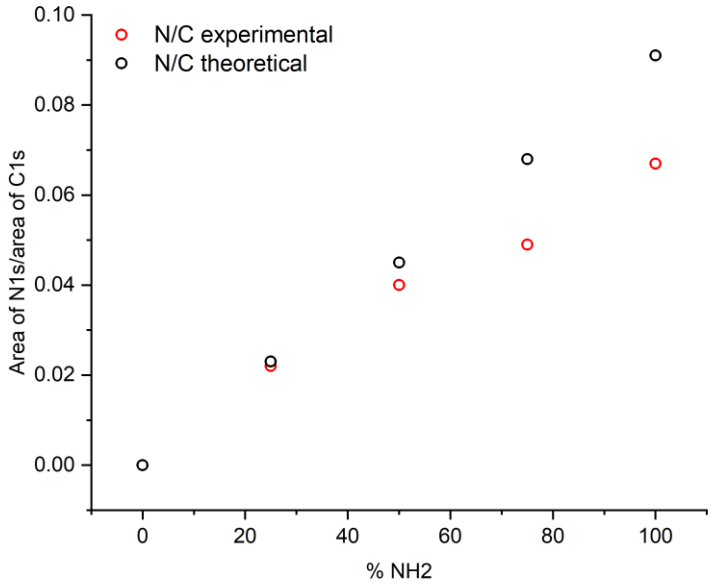

Figure IV-18: Experimental N/C values obtained with XPS measure versus theoretical N/C.

An increase of N/C was observed with the percentage of amino groups. For 50% to 100% NH2 substrates, a deviation is observed between experimental and theoretical values. This difference is due to the consideration of carbon groups that comes not only from the added silane but also from surface contamination (atmosphere). Hydrophilic substrates being more prone to atmosphere contamination and adsorption of polar species on the hydration layer. Even

with deviation from theoretical values, XPS, AFM and contact angle measures proved together that self-assembled monolayers with different amounts of NH_2 groups were formed. As consequence, surfaces with variable wettability were obtained with the same roughness. These surfaces will allow the study of protein adsorption by varying only the surface chemistry and wettability and maintaining constant characteristics such as roughness and surface hardness.

Highlights:

- The complete conversion of bromide groups into amino groups was observed.
- Experimental N/C ratio increases and allow to determine the experimental amount of NH2 on the surface.

3. Lysozyme adsorption on SAMs surfaces

3.1 Surface influence on adsorption kinetic curve

The adsorption kinetic curves were obtained for lysozyme on the Glass 0-100% NH_2 surfaces. The results are presented in Figure IV-19. For these graphs, the logarithm of time (from 0.5 to 504 hours) was used to better visualize the results. Owing to the complexity and time of the experiment (surface preparation, characterization, and 21 days of adsorption), the complete assay was performed only once for each type of surface. The standard deviation was obtained from measurements at three different points on the same surface.

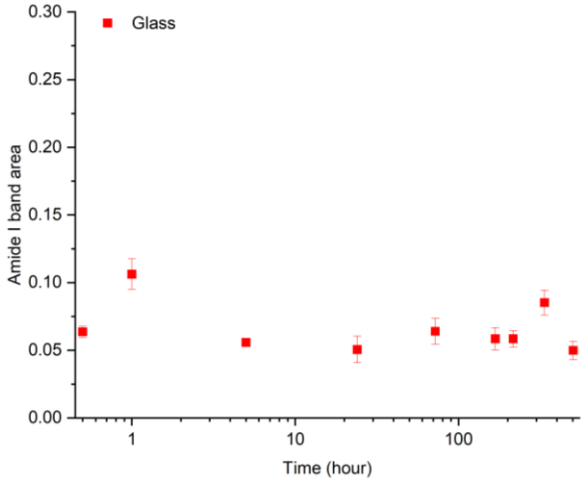
Glass
Amide I band area
Time (hour)

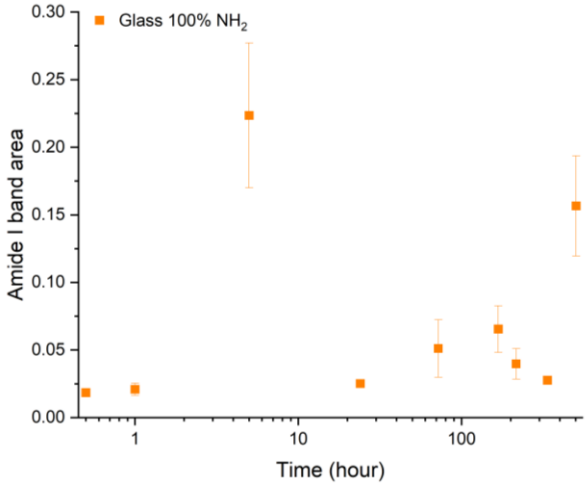
Glass 100% NH2
Amide I band area
Time (hour)

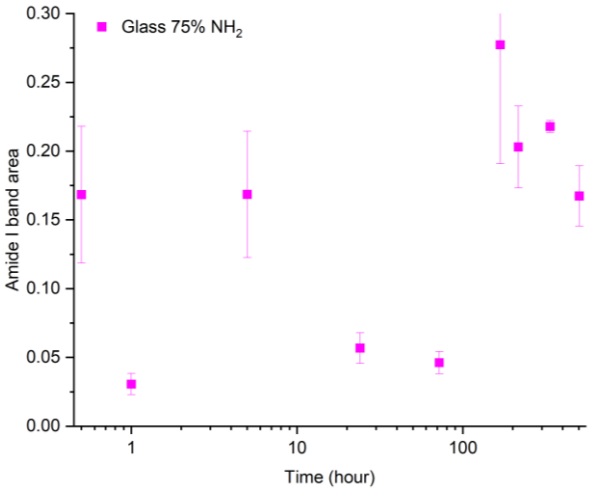
Glass 75% NH2
Amide I band area
Time (hour)

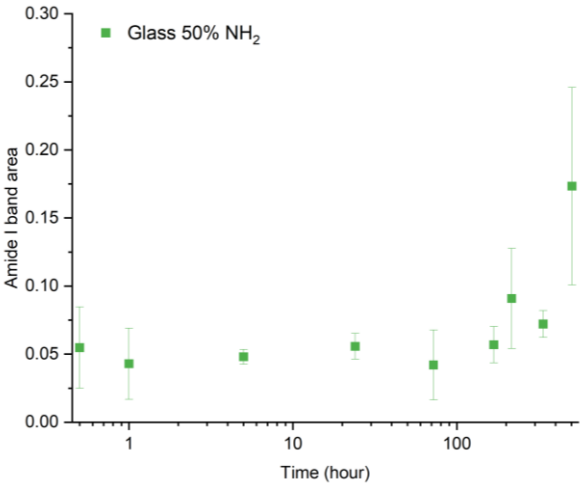
Glass 50% NH2
Amide I band area
Time (hour)

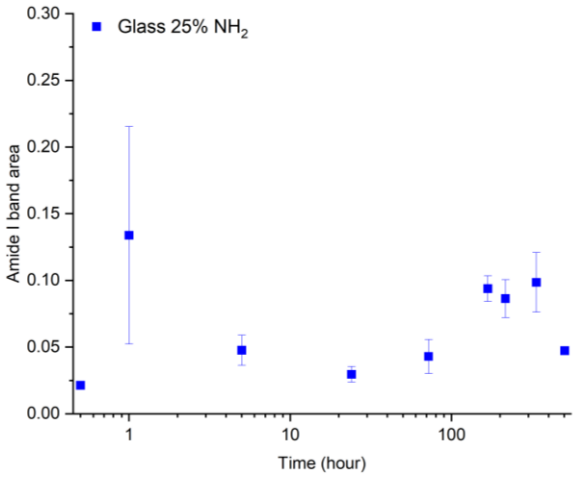
Glass 25% NH2
Amide I band area
Time (hour)

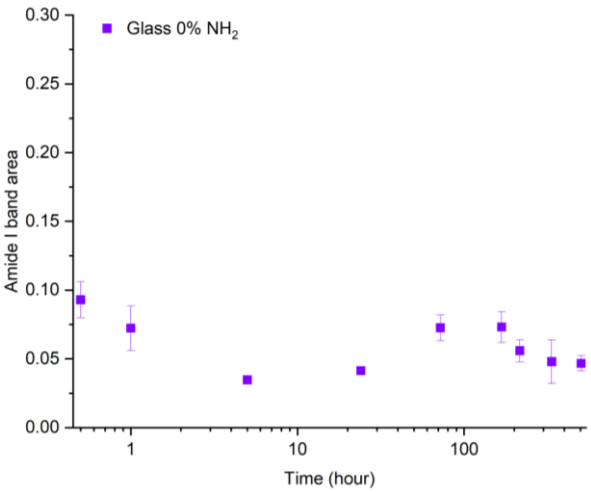
Glass 0% NH2
Amide I band area
Time (hour)

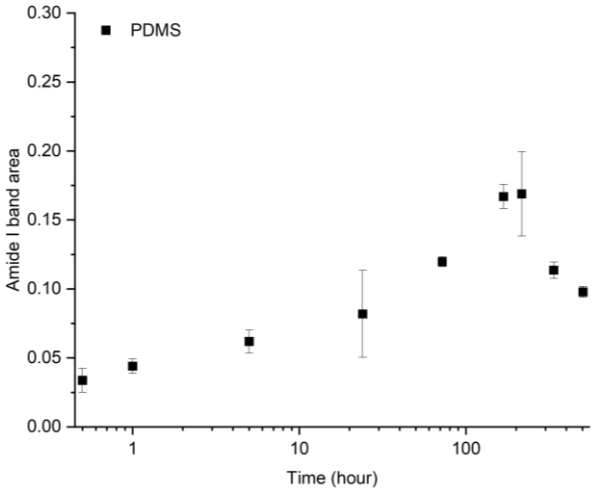

Figure IV-19: Adsorption kinetic curves for Glass, PDMS and SAMs surfaces

(C_{LSZ} = 1.00 mg.mL^{-1}, n=3).

Kinetics curves show the evolution of amide I area as a function of contact time from 0.5 to 504 hours. For Glass and SAMs, except for Glass 50% NH_2, it was observed two events of area increase followed by a decrease. We have already described the overshoot for lower time of adsorption. A second increase can be detected at longer period of contact (called "2nd event"). The time of each event was determined on the kinetic curves, and the results are shown in Table IV-9.

Table IV-9. Time of adsorption events on SAMs.

Surface	***Overshoot time (hour)***	***2nd event (hours)***
Glass	1	216-504 (9-21 days)
Glass 100% NH_2	5	336-504 (14-21 days)
Glass 75% NH_2	0.5	168-504 (7-21 days)
Glass 50% NH_2	-	216-504 (9-21 days)
Glass 25% NH_2	1	72-504 (3-21 days)
Glass 0% NH_2	0.5	24-216 (1-9 days)
PDMS	-	72-336 (3-14 days)

The SAMs showed characteristics closer to glass than to PDMS. Most of them, except 50%, present the event at the beginning of the curve, and suggest an overshoot. The second event was present for all surfaces. The two events will be investigated below.

1st event investigation

As previously discussed, the overshoot is the event of surface oversaturation. It means that the amount of protein adsorbed is bigger than at the equilibrium. Over time, proteins increase interaction with the surface and expel neighboring proteins that are weakly adsorbed. Thus, saturation is reached. Therefore, it is expected that the secondary structure during overshoot is different from the structure out of this period. To confirm if the first event can be associated to an overshoot, the secondary structure on the initial adsorption (from 0.5 to 24h) was analyzed. The results are presented in Figure IV-20.

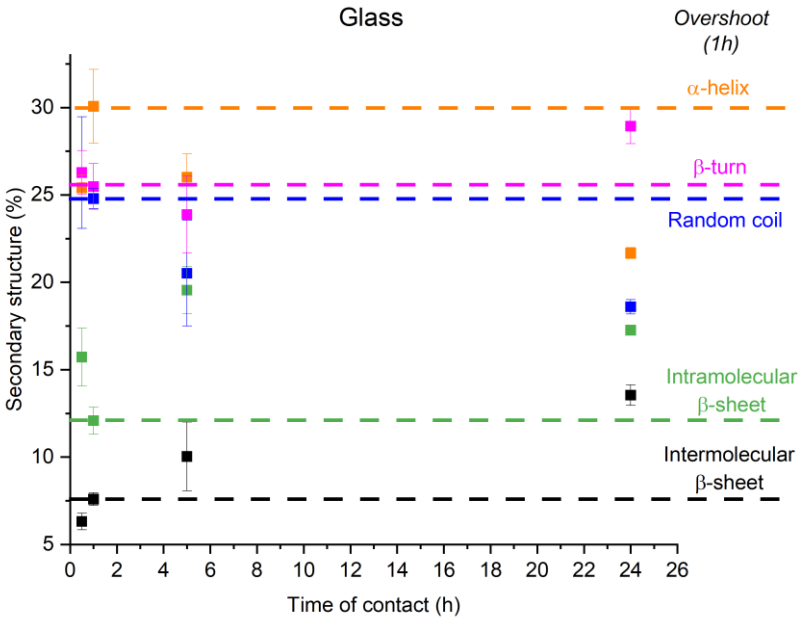

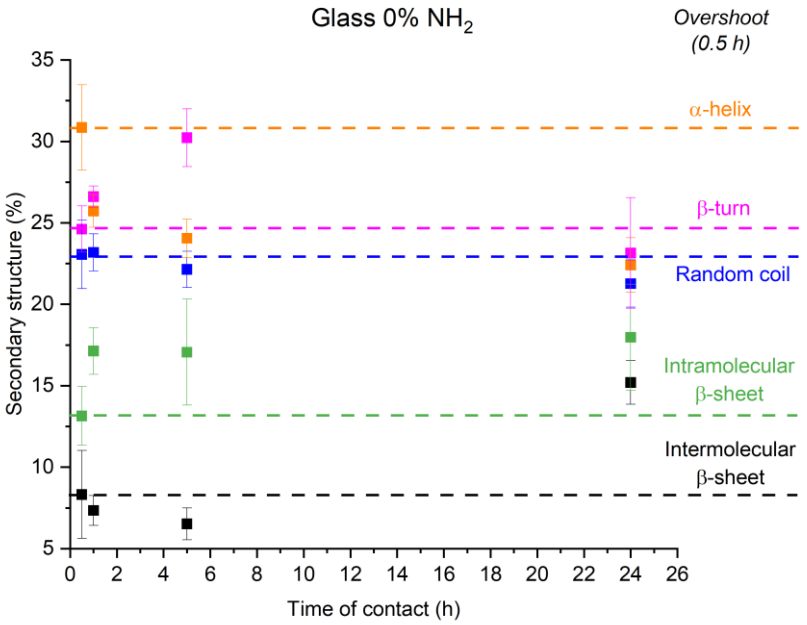
Glass 0% NH2
Overshoot
(0.5 h)
α-helix
β-turn
Random coil
Intramolecular
β-sheet
Intermolecular
β-sheet
Secondary structure (%)
Time of contact (h)

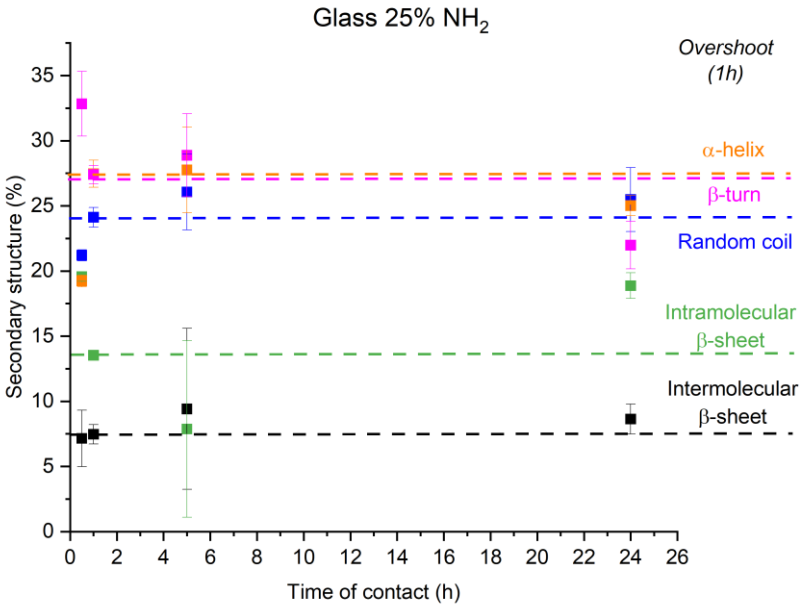
Glass 25% NH2
Overshoot
(1h)
α-helix
β-turn
Random coil
Intramolecular
β-sheet
Intermolecular
β-sheet
Secondary structure (%)
Time of contact (h)

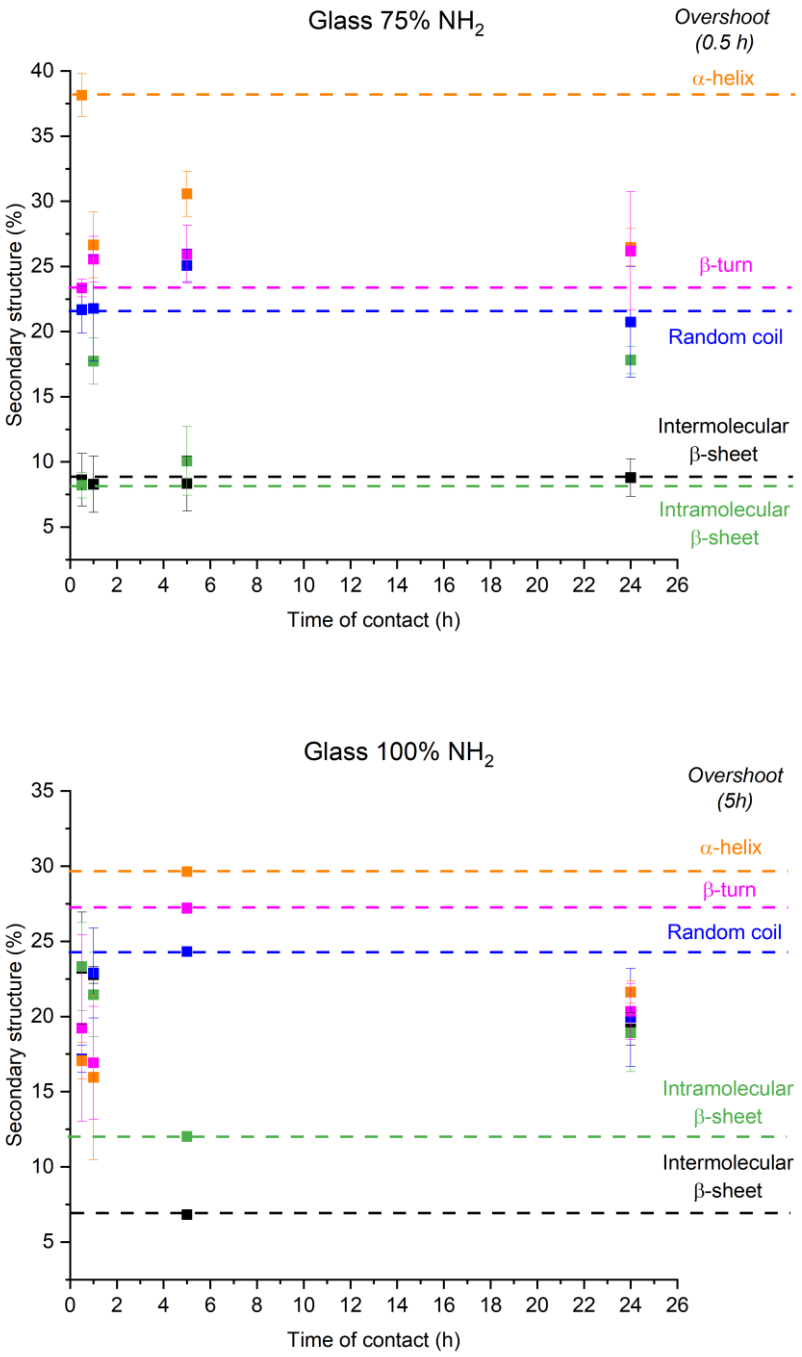

Figure IV-20: Secondary structure from the first adsorption period on Glass, Glass 0%NH_2, Glass 25%NH_2, Glass 75%NH_2 and Glass 100%NH_2.

Analyzing the secondary structures in the figure above and comparing the overshoot with the other points on the graph, it is possible to observe a difference. When the overshoot occurred, the alpha helix values were higher and the beta-sheet percentages lower. After the overshoot period, the α-helix decreased with the increase of β-sheet, showing a conformational

evolution. All surfaces presented this secondary structure evolution except the glass 25% NH_2. The area difference in the amide I band for this sample must be within experimental error and does not correspond to the overshoot.

2nd event investigation

The second event was also studied in terms of secondary structure. Between 1 and 21 days, at the time of second event (increase of area), a percentage reduction in the intermolecular β-sheet was observed. The graphs showing the relationship between this increase in area and the decrease in the β-sheet structure are shown in figure IV-21.

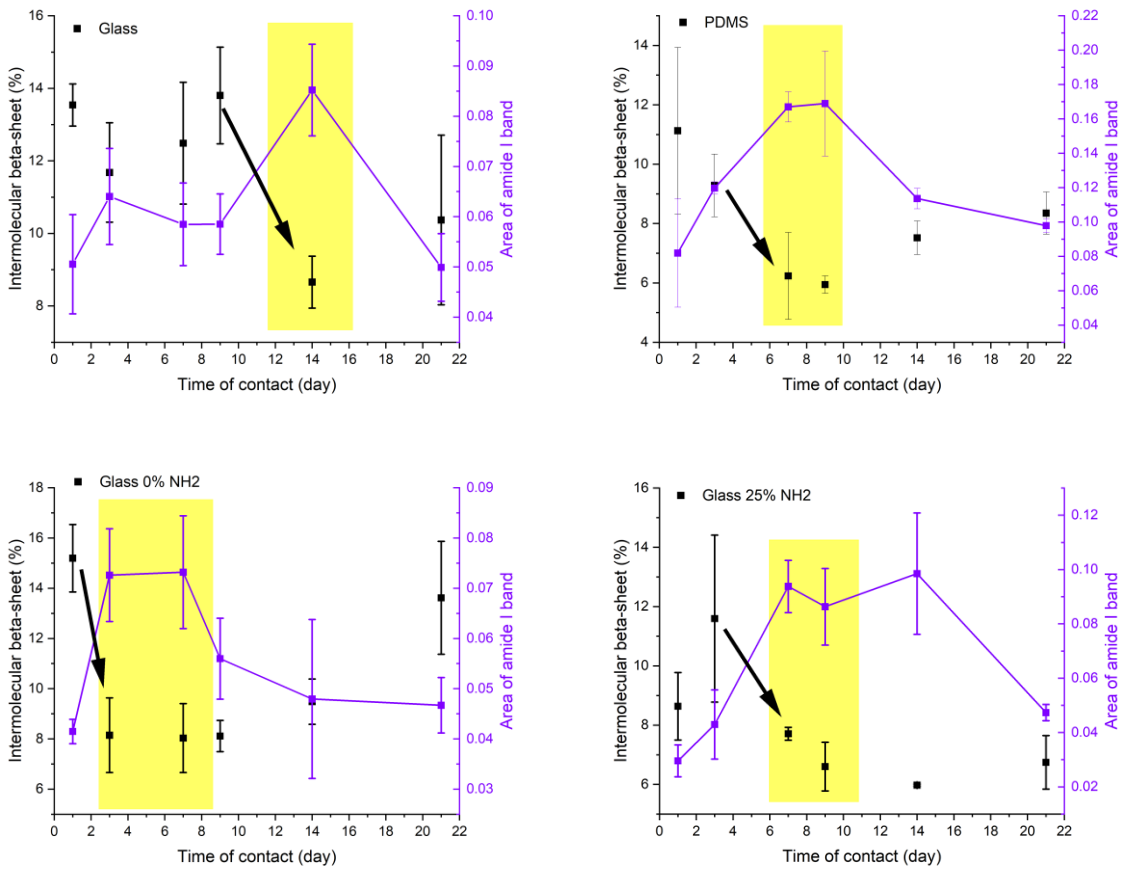

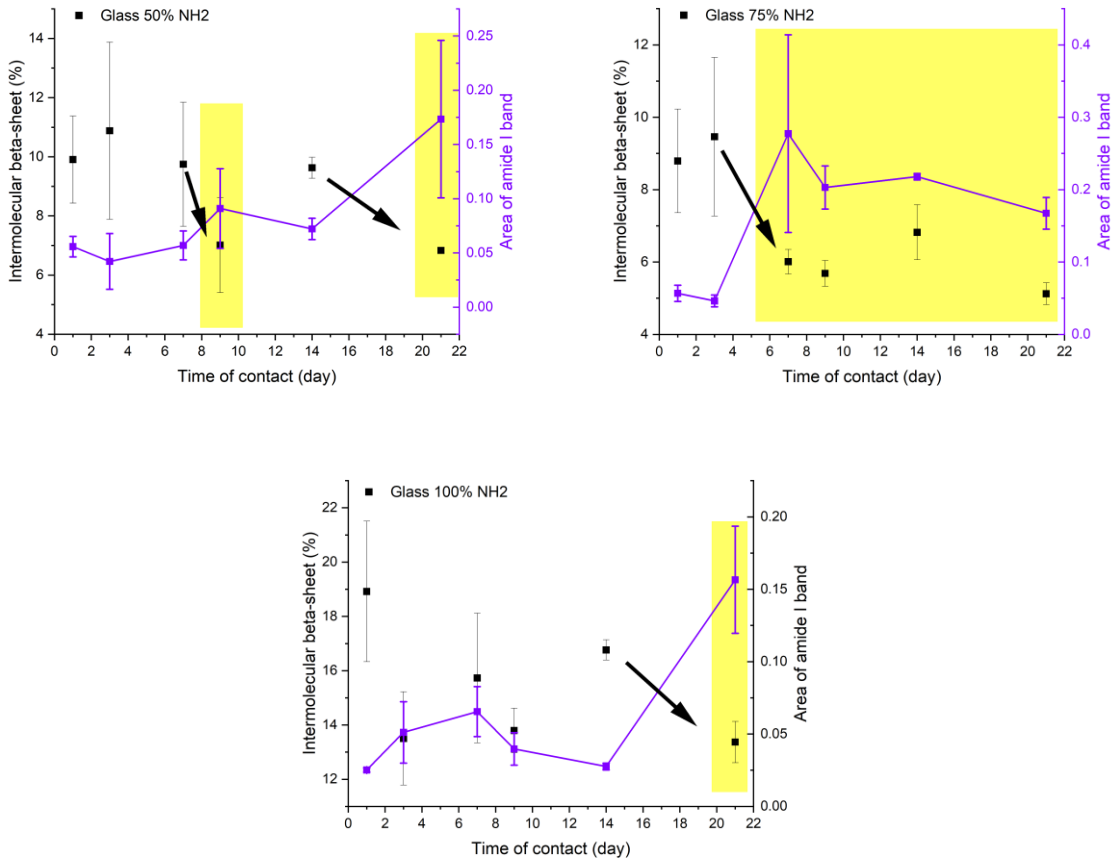

Figure IV-21: Relationship between β-sheet decrease and the second event of adsorption.

At the beginning of adsorption, between 0 and 24h (Figure IV-20), for most of the surfaces, an intermolecular β-sheet increase was observed. This is associated with the formation of aggregates on the surface. A posterior decrease in β-sheet may be due to aggregates leaving the surface. With the removal of aggregates, a part of the surface became available for other proteins to be adsorbed, which could explain the increase in the area of amide I. So, the second event could be associated with the release of aggregates from the surface and the adsorption of new proteins. This second event, like the overshoot, presents a bigger area value that after decreases with time but the evolution of the secondary structure are different: modification of α-helix content for the first event (early phase of adsorption) and evolution of β-sheet for the second (longer time of contact with solution)

An unexpected autocorrelation was observed between area increase and percentage of beta-sheets decrease. We could think that the relationship between the area increase and beta sheet decrease is due to curve fitting errors. In this case, a higher peak intensity could influence

the results of the peaks at the extreme of the curve. In the developed model, the intermolecular β-sheet component was centered at 1622 and β-turn at 1688 cm^{-1}. The β-turn structure is the other extreme of the curve and does not decrease with increasing area. So, the mathematical error can be discarded. Another fact that eliminates this mathematical error is that in the overshoot, which is the largest area of amide I found, a decrease in the beta sheet is not always found, as observed in figure IV-20.

To reinforce the suggestion about the second event, the presence of aggregates in solution was studied using the DLS technique. If the aggregates have come out of the surface at some point, they must be found in the solution. At the end of adsorption (21 days), solutions were analyzed by DLS and the results are shown in Table IV-10.

Table IV-10. DLS results for LSZ solutions after adsorption onto glass, PDMS and SAMs surfaces (21 days of contact).

Solution	***Hydrodynamic diameter (nm)***
LSZ 1.00 $mg.mL^{-1}$ + Glass	3.9 ± 0.7
LSZ 1.00 $mg.mL^{-1}$ + Glass 100% NH_2	6.0 ± 1.2
LSZ 1.00 $mg.mL^{-1}$ + Glass 75% NH_2	6.5 ± 0.3
LSZ 1.00 $mg.mL^{-1}$ + Glass 50% NH_2	13.6 ± 2.1
LSZ 1.00 $mg.mL^{-1}$ + Glass 25% NH_2	11.2 ± 2.7
LSZ 1.00 $mg.mL^{-1}$ + Glass 0% NH_2	10.8 ± 0.8
LSZ 1.00 $mg.mL^{-1}$ + PDMS	11.9 ± 3.0

Aggregates were identified in all solutions, except the one in contact with glass substrate. When in contact with the SAMs and PDMS, the LSZ had aggregates formed in solution with different sizes. There was no proportional relationship between aggregate size and surface characteristics as hydrophobicity or surface energy but higher hydrodynamic diameters are found for hydrophobic monolayers (%NH_2 >50%).

In this study, we identified two events in lysozyme adsorption kinetics on chemically modified surfaces (SAMs). The first event was characterized by an overshoot and was present for all surfaces, except for PDMS. The second event occurred for all the surfaces studied. It was explained by the formation and release of aggregates from the surface, that let an available

space for new protein molecules adsorption. The presence of aggregates on solution after 21 days of test could reinforce the hypotheses that aggregation occurs on the surface and that aggregates are released from the surface in the solution where they probably grow. The results presented here are preliminary and new studies must be conducted to better characterize this second event, as for the glass no aggregates on solution were found.

Highlights:

- The kinetic curves of lysozyme adsorption on SAMs were closer to the curve on glass, independent of hydrophobicity.
- The overshoot effect was observed for all surfaces, except for the PDMS.
- Overshoot was confirmed by the change in secondary structure.
- A second event (amide I area increase) was observed and it was associated to the formation and release of aggregates in solution.
- Soluble aggregates were formed in different sizes after contact with the modified surfaces.

4. Conclusion

Influence of surface chemistry on lysozyme adsorption was investigated in the present chapter. This initial study was done on static mode, without flow rate. The next chapter will try to reproduce these measurements with shear stress. The effect of different flow regimes on Lysozyme-surface interactions will be studied and the results presented in chapter 5.

Bibliography

(1) Rabe, M.; Verdes, D.; Seeger, S. Understanding Protein Adsorption Phenomena at Solid Surfaces. *Adv. Colloid Interface Sci.* **2011**, *162* (1–2), 87–106. https://doi.org/10.1016/j.cis.2010.12.007.

(2) McGuire, J.; Wahlgren, M. C.; Arnebrant, T. Structural Stability Effects on the Adsorption and Dodecyltrimethylammonium Bromide-Mediated Elutability of Bacteriophage T4 Lysozyme at Silica Surfaces. *J. Colloid Interface Sci.* **1995**, *170* (1), 182–192.

(3) Szöllősi, G. J.; Derényi, I.; Vörös, J. Reversible Mesoscopic Model of Protein Adsorption: From Equilibrium to Dynamics. *Physica A* **2004**, *343*, 359–375.

(4) Böhmler, J.; Ponche, A.; Anselme, K.; Ploux, L. Self-Assembled Molecular Platforms for Bacteria/Material Biointerface Studies: Importance to Control Functional Group Accessibility. *ACS Appl. Mater. Interfaces* **2013**, *5* (21), 10478–10488. https://doi.org/10.1021/am401976g.

(5) Tomasovic, L.; Fioux, P.; Gilbert, F.; Jacquet, D.; Verchère, D.; Bally-Le Gall, F.; Ponche, A. Self-Assembled Monolayers with a Controlled Density of Hydroxyl Groups: A Relevant Model to Investigate the Adhesion Properties of Epoxy Adhesives. *J. Phys. Chem. C* **2022**, *126* (6), 3227–3234. https://doi.org/10.1021/acs.jpcc.1c10432.

(6) Frischat, G. H.; Poggemann, J. F.; Heide, G. Nanostructure and Atomic Structure of Glass Seen by Atomic Force Microscopy. *J. Non. Cryst. Solids* **2004**, *345–346*, 197–202. https://doi.org/10.1016/j.jnoncrysol.2004.08.022.

(7) Dalmas, D.; Lelarge, A.; Vandembroucq, D. Quantitative AFM Analysis of Phase Separated Borosilicate Glass Surfaces. *J. Non. Cryst. Solids* **2007**, *353* (52–54), 4672–4680. https://doi.org/10.1016/j.jnoncrysol.2007.07.005.

(8) Tan, K. C.; Lee, Y. S.; Yap, S. L.; Kok, S. Y.; Nee, C. H.; Siew, W. O.; Tou, T. Y.; Yap, S. S. Pulsed Laser Deposition of Al-Doped ZnO Films on Glass and Polycarbonate. *J. Nanophotonics* **2014**, *8* (1), 084091. https://doi.org/10.1117/1.jnp.8.084091.

(9) Wang, T. S.; Du, X.; Yuan, W.; Duan, B. H.; D. Zhang, J.; Chen, L.; Peng, H. B.; Yang, D.; Zhang, G. F.; Zhu, Z. H. Morphological Study of Borosilicate Glass Surface Irradiated by Heavy Ions. *Surf. Coatings Technol.* **2016**, *306*, 245–250. https://doi.org/10.1016/j.surfcoat.2016.06.018.

(10) Wheaton, B. R.; Clare, A. G. Evaluation of Phase Separation in Glasses with the Use of Atomic Force Microscopy. *J. Non. Cryst. Solids* **2007**, *353* (52–54), 4767–4778. https://doi.org/10.1016/j.jnoncrysol.2007.06.073.

(11) Chada, N.; Sigdel, K. P.; Sanganna Gari, R. R.; Matin, T. R.; Randall, L. L.; King, G. M. Glass Is a Viable Substrate for Precision Force Microscopy of Membrane Proteins. *Sci. Rep.* **2015**, *5*, 1–8. https://doi.org/10.1038/srep12550.

(12) Bauccio, M. L. *Engineered Materials Reference Book*, Second ed.; ASM International, 1994.

Chapter V: Influence of shear stress on protein-surface interaction

Résumé Chapitre V.

Influence du cisaillement sur les interactions protéine-surface

Ce chapitre présente l'étude des interactions entre le lysozyme et différentes surfaces en présence d'un écoulement (laminaire ou turbulent). Ces essais ont été réalisés sur des surfaces planes de grande dimension positionnées dans des cellules fluidiques. Les deux matériaux choisis ont été préalablement étudiés ; le PDMS, très hydrophobe et le verre très hydrophile. Plusieurs types d'écoulement ont été étudiés, laminaire, turbulent ou diphasique turbulent (air – eau). Les mesures sont effectuées sur 25 points répartis le long du parcours fluide.

1- Ecoulement turbulent sur le verre et le PDMS après un écoulement laminaire

Il a été décidé dans un premier temps de réaliser les essais en écoulement turbulent (5 heures à Re > 9000) après un écoulement laminaire (Re = 153) appliqué durant plusieurs jours (durée correspondante à l'obtention du plateau d'adsorption – référence chapitre précédent), soit 9 jours pour le PDMS et 3 jours pour le verre. Les quantités de protéine adsorbée sont dans tous les cas étudiés assez fluctuantes en fonction du point de mesure et cela d'autant plus avec le PDMS. Il apparait en moyenne que les quantités adsorbées en mode laminaire ou en mode laminaire + turbulent sont les mêmes que celles adsorbées en mode statique lorsque le plateau est atteint.

Si la quantité adsorbée est approximativement la même, l'analyse de la structure secondaire montre une augmentation des feuillets β inter et intramoléculaires sur les deux matériaux ainsi qu'une diminution des coudes β et des structures non-ordonnées sur le matériau hydrophobe (PDMS) et une diminution des hélices α avec le verre.

Ces résultats montrent que la structure secondaire des protéines adsorbées est différente suite à un cisaillement fluide et cela de manière différente, dépendant de la nature de la surface.

2- Ecoulement turbulent avec ou sans air sur le verre et le PDMS

Ces essais ont été réalisés directement après la mise en place des surfaces dans la cellule fluidique (écoulement turbulent pendant 5 heures). Il apparait que la quantité de protéines adsorbées en surface est indépendante de la présence ou non d'air dans le système. Pour le

PDMS, cette quantité adsorbée est intermédiaire entre celle obtenue en mode statique après 5h et celle obtenue au palier (9 jours).

Pour le verre, la quantité adsorbée après 5 heures d'écoulement turbulent est supérieur aux résultats obtenus en statique après 5 heures et au palier (3 jours).

Ces résultats montrent également que le cisaillement fluide augmente la quantité de protéines adsorbées à la surface et la cinétique initiale d'adsorption. L'étude de la structure secondaire des protéines adsorbées présente des différences avec les essais en statique mais aucune différence due à la présence d'air en solution. Par rapport aux essais en statique avec le PDMS, la proportion de coudes β et des non-ordonnées augmentent quand la proportion des feuillets β intramoléculaires et des hélices α diminuent. Avec le verre, la proportion des feuillets β intermoléculaires augmente et les coudes β et hélices α diminuent, liés à la présence d'agrégats en surface du matériau.

De plus, si l'on compare les résultats obtenus après application directe de l'écoulement turbulent et après un écoulement laminaire, les structures secondaires diffèrent considérablement.

Ces résultats montrent qu'à paramètres hydrodynamiques identiques, les interactions protéines / surface dépendent de la nature de la surface et qu'à surface identique, le mode d'application du facteur de stress modifie également la nature des interactions.

Quant à la présence de l'air, les modifications sont seulement visibles dans la solution via la formation d'agrégats sur le PDMS et une augmentation de la taille de ces agrégats (en solution) avec le verre.

The chapter 5 presents the results of shear stress influence on lysozyme adsorption. PDMS and glass were used in the flow cell described in the Materials and Methods chapter (part II, item 2.2). These surfaces were chosen because of their different wettability. PDMS is a hydrophobic surface with a water contact angle of 111° and glass is hydrophilic with a contact angle of 36°. Lysozyme (LSZ 1.10^5) adsorption was studied by varying the surface characteristics in the static mode (chapter 4). It was observed that LSZ adsorbed in a higher amount on PDMS surface when compared to glass. However, the adsorption plateau was reached faster on glass. In this section, influence of fluid dynamic is investigated. Three test configurations were used on these surfaces (PDMS and glass):

1- Laminar flow 3 or 9 days + turbulent flow 5h: The surface was in contact with LSZ solution for a time corresponding to the plateau in the static mode (i.e. 3 and 9 days for glass and PDMS, respectively). To have a homogeneous and constant concentration of lysozyme in the cellule, the fluid is flowing at low velocity (laminar flow, 50.6 $mL.min^{-1}$, Re (channel) = 76). After this period, the flow rate was increased to 3.0 $L.min^{-1}$ (turbulent flow, Re (channel) = 9000) for 5h.
2- Turbulent flow 5h: the same experiments were performed with immediately contact with the lysozyme solution (turbulent flow, 3.0 $L.min^{-1}$ for 5h)
3- Air/liquid turbulent flow 5h: Same experiments performed with a diphasic flow (air/liquid interface, turbulent flow, 3.0 $L.min^{-1}$ for 5h). The outlet tube is removed in the feed tank to promote air bubbles into the solution.

The scheme on Figure V-I shows how the tests were carried out in dynamic mode.

(a)

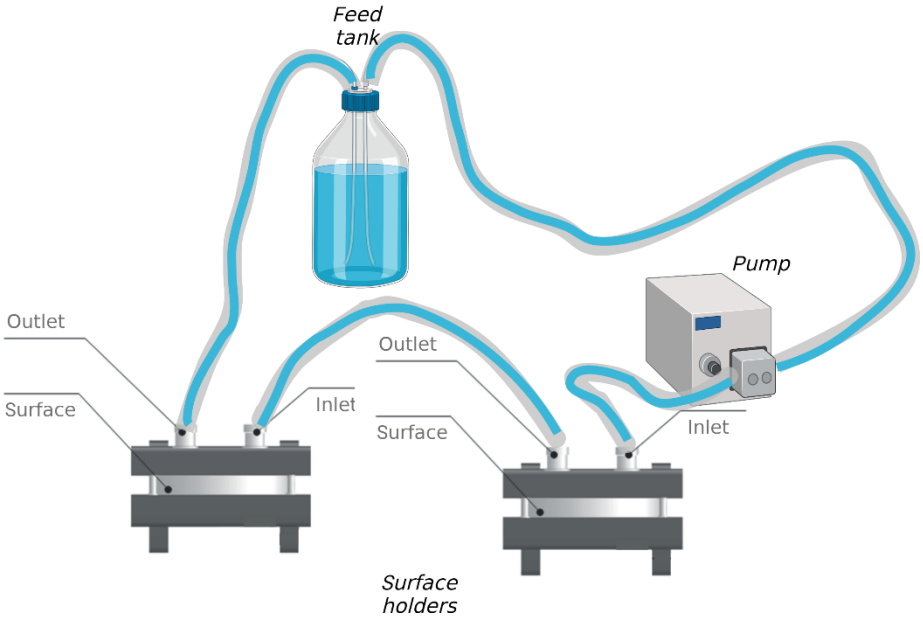
Feed tank
Pump
Outlet
Surface
Inlet
Outlet
Surface
Inlet
Surface holders

(b)

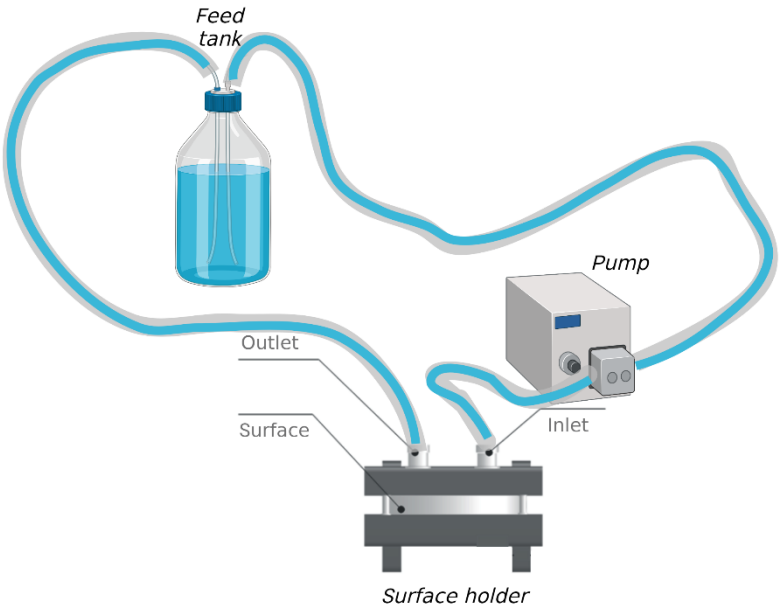
Feed tank
Pump
Outlet
Surface
Inlet
Surface holder

(c)

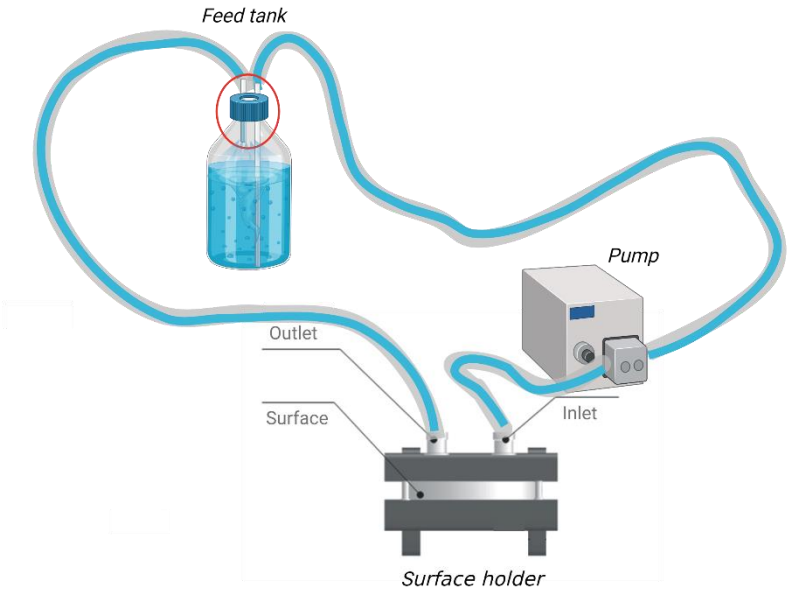

Figure V-1: Scheme to study the combination of surface contact and shear stress on protein adsorption. (a) configuration 1: laminar + turbulent, (b) configuration 2: turbulent flow and (c) configuration 3: turbulent diphasic flow. (Created with BioRender.com).

For the configuration 1 (laminar flow 3 or 9 days + turbulent flow 5h), two surfaces were placed in series, as shown in the figure V-1a. The solution passed on the surfaces at a flow rate of 50.6 $mL.min^{-1}$ during 3 or 9 days. After this period, one surface was removed from the carter (for further analysis) and the other was let in the pilot and submitted to a turbulent flow (5h at 3.0 $L.min^{-1}$) with the same solution.

Test configurations 2 and 3 were performed in the same flow cell with only one surface (figures V-1 b and c, respectively). Contact between the surface and protein was done directly at a flow rate of 3.0 $L.min^{-1}$. In configuration 2, the outlet tube goes directly into the liquid, avoiding air bubbles formation in the solution. To create the air/liquid flow and perform the test in configuration 3, this tube was removed and the outlet was placed higher than the solution. The force with which the liquid enters creates small air bubbles and they go through the pilot into the protein solution. The difference between configurations 2 and 3 is shown with real pictures in Figure V-2.

Feed tank during experiments done with configuration 2

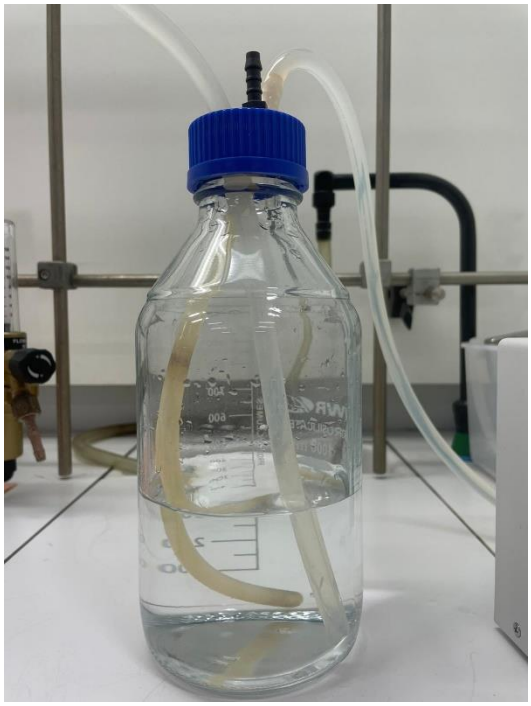

Feed tank during experiments done with configuration 3

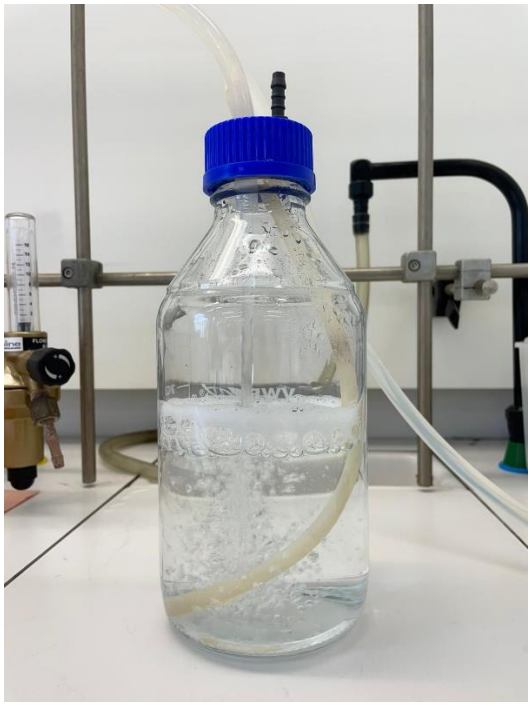

Figure V-2: Photographs of feed tank during test configurations 2 (left) and 3 (right)

After the tests performed (configurations 1, 2 and 3), the surfaces were rinsed with deionized water and dried under air flow before FTIR-ATR analysis. The amide I band was measured on 25 points following the flow in the cell by FTIR-ATR spectroscopy as presented in Figure V-3. Final solutions were analyzed by Dynamic Light Scattering (DLS) to evaluate aggregate formation.

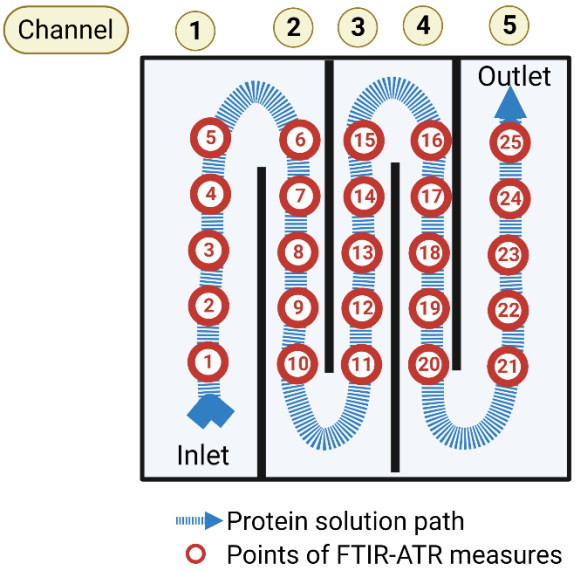

Figure V-3: Scheme of measurement points in FTIR-ATR after tests in dynamic mode. Created with BioRender.com.

1. Lysozyme adsorption on PDMS in dynamic mode

1.1 PDMS - Laminar flow 9 days + turbulent flow 5h (configuration 1)

The graph of amide I band area for the 25 measuring points is shown in figure V-4.

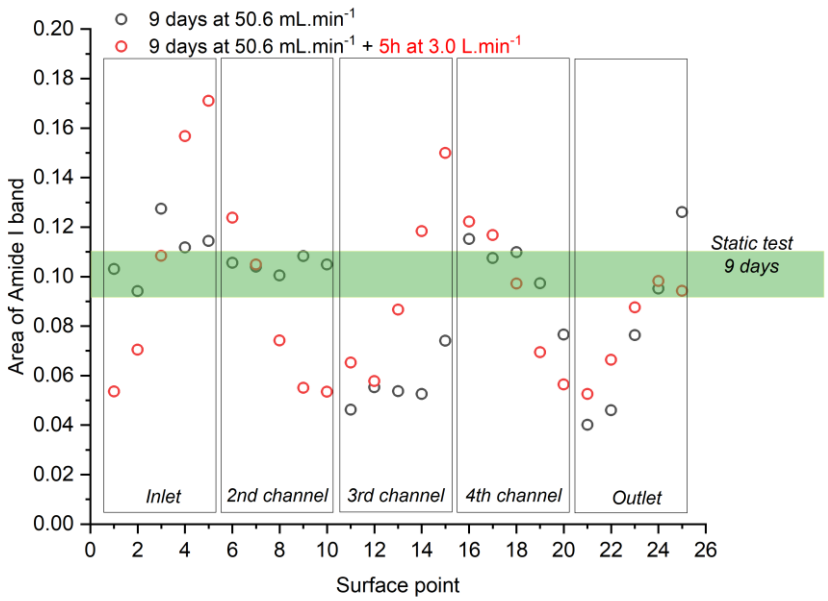

Figure V-4: Amount of Lysozyme adsorbed on PDMS after laminar flow and laminar + turbulent flow (C_{LSZ} = 0.36 mg.mL^{-1}).

The area obtained after 9 days of static test is presented in green for comparison. Dynamic test, both in laminar and turbulent modes, exhibits different amount of adsorbed protein (variability) according to the surface location. Results obtained after 9 days without flow (area = 0.10) are included in the range of areas obtained during the dynamic test (between 0.04 and 0.17). This variability cannot be due to experimental error and consequently, needs to be further studied. So far, there are no apparent reason to explain these observations.

Amide I bands were fitted to obtain the percentage of secondary structures. The results are presented in figure V-5.

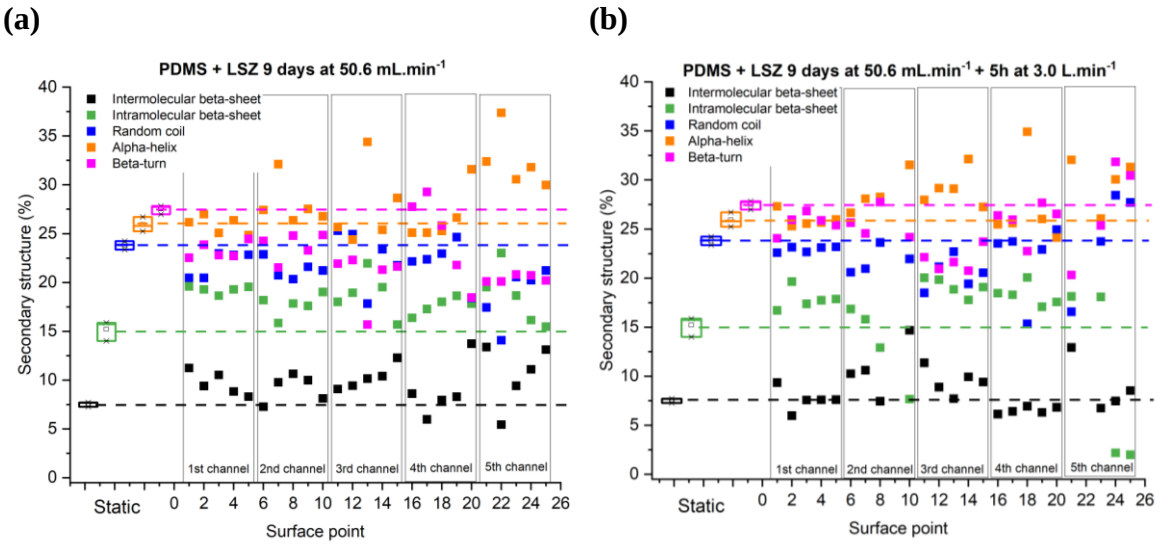

Figure V-5: Secondary structure evaluation for the 25 measuring points after 9 days of LSZ adsorption on PDMS at 50.6 mL.min^{-1} (a) and 9 days at 50.6 mL.min^{-1} + 5h at 3.0 L.min^{-1} (b) (C_{LSZ} = 0.36 mg.mL^{-1})

The secondary structure of LSZ on PDMS surface could be compared in three different situations. For the dynamic test, laminar (fig V.5.a) and laminar with turbulent flow (fig V.5.b) presented the same results. It indicates that turbulent flow rate of 3.0 L.min^{-1} did not cause modifications on the already adsorbed lysozyme. However, comparing these results with static assay (box plot), a slight increase of intramolecular β-sheet and α-helix was observed. It seems that lysozyme is adsorbed with a different structure or that the conformation changed because of shear. This change may be occurring because in dynamic mode there is a constant renewal of protein solution that is not occurring in static mode.

The time of protein renewal in solution was calculated to compare static with laminar flow (50.6 mL.min^{-1}). Protein diffusion on static mode was obtained using Stokes-Einstein relation (equation 1).

$$D = \frac{kT}{6\pi r\mu} \qquad \text{Equation 1}$$

Where D is the diffusion coefficient, k is the Boltzmann constant, T is the temperature, r is the protein radius and μ is dynamic viscosity. Applying this equation, using a temperature of 25°C and protein radius (Stokes radius) of 2 nm, the diffusion coefficient obtained was $1.1x10^{-10}$ m^2s^{-1}. Considering a protein diffusion over a length of 5mm to attain the surface, the time for the protein to diffuse will be around 3 days in the static mode test.

On the laminar flow, the velocity is approximately 0.015 $m.s^{-1}$. The flow path on the surface carter is about 30 cm in length. Taking these values, the time to change completely the solution that is in contact with the surface is 20 seconds. It means that during dynamic mode, the renewal of protein in solution is almost 13000 times faster than in static mode. We suggest that this faster solution renewal (dynamic mode), modifies protein/protein and protein/surface equilibria, resulting in a different final structure.

Lysozyme solution was analyzed by DLS after the experimental tests. The results are shown in Table V-I.

Table V-1. DLS of lysozyme solution after contact with PDMS surface (configuration 1).

Solution	***Hydrodynamic diameter (nm)***
LSZ after 21 days of contact (static mode)	3.9 ± 0.2
LSZ after 9 days of laminar flow	3.9 ± 0.9
LSZ after 9 days of laminar + 5h of turbulent flow	8.3 ± 0.7

Similar hydrodynamic diameters were obtained for the LSZ solution after static assay (shear rate = 0) and laminar flow during 9 days. LSZ with a bigger hydrodynamic size was observed after turbulent flow. The turbulent flow performed after 9 days of laminar flow did not significantly modify the amount of adsorbed protein and the protein conformation. However, it increased the lysozyme size on solution that can be associated to soluble aggregate formation.

Highlights:

- The amount of adsorbed protein after dynamic mode tests (configuration 1) is different and depends on the location of the measuring point along the flow.
- Laminar + turbulent flow test resulted in a different lysozyme secondary structure when compared to static test.
- Turbulent regime applied after 9 days of laminar flow induced soluble aggregate formation.

1.2 PDMS - Turbulent flow 5h (configuration 2) and air/liquid turbulent flow 5h (configuration 3)

The influence of shear rate was studied by applying turbulent flow for 5 hours on pristine substrate. The test was also realized in the presence of air in liquid. The presence of air in solution is a parameter that sometimes is responsible for protein denaturation. It can be present in industrial steps such as filling that combines turbulent flow, surface/liquid and air/liquid interfaces. The results are presented in Figure V-6.

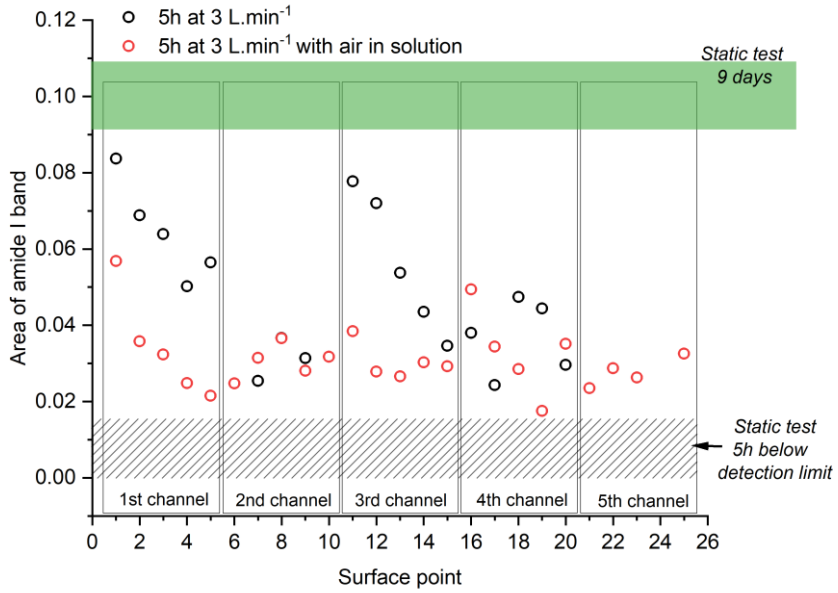

Figure V-6: Amount of Lysozyme adsorbed on PDMS after 5h of turbulent flow with and without air in the solution. (C_{LSZ} = 0.36 mg.mL^{-1})

At these operating conditions (time = 5h, C = 0.36 mg.mL^{-1}), it was not possible to have an exploitable FTIR spectrum in static mode test to use as reference. We suggest that the amount of protein adsorbed is lower than the detection limit (it was previously estimated at 0.032 for static tests in chapter 4, but seems to be lower than 0.02 after adsorption under flow). In this case, results from dynamic mode using turbulent flow were compared with area < 0.016 at 5h and area after 9 days of static tests.

The turbulent flow increased the amount of adsorbed protein compared with static test. This indicates that shear stress accelerates lysozyme adsorption on PDMS. A difference of amount of adsorbed protein was observed when air-liquid mix was used (especially for channels 1, 3 and 5). The two tests accelerated the adsorption, reaching area values lower than the static mode after 9 days of contact (corresponding to the adsorption plateau). As previously showed, a significant difference of absorbed amount (variability) was observed at different locations. The secondary structure of LSZ on PDMS was studied and the results are shown in figure V-7. The results obtained in static mode are represented with box plot for a repetition of 5 measures to give a reference. Secondary structures were determined from an additional test performed for 5h with a higher LSZ concentration (1.00 mg.mL^{-1}) to avoid the problem of detection limit.

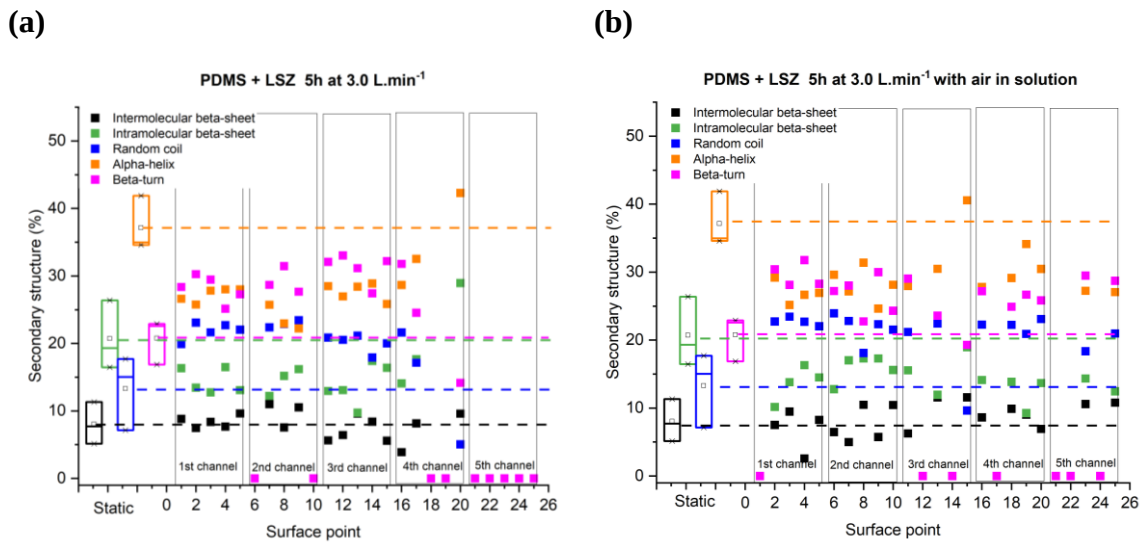

Figure V-7: Secondary structure estimation by surface point for LSZ adsorption on PDMS 5 hours at 3.0 L.min^{-1} (a – configuration 2) and 5 hours at 3.0 L.min^{-1} with air in solution (b - configuration 3). (C_{LSZ} = 0.36 mg.mL^{-1})

Comparing static results with dynamic ones, the secondary structure of the adsorbed LSZ is different. For the same operating time, it was observed a decrease in α-helix and an increase in random coil. This result was consistent with or without air in the solution. It means that air-liquid diphasic flow did not significantly change the lysozyme conformation on PDMS surface. After 5h of adsorption in turbulent flow on every point measured along the flow, the content of α-helix is similar to the one obtained after 3 days in static mode on every point measured along the flow. It can be notice that the secondary structure did not show the same variability regarding the position than the amide I area. As presented in the chapter 4, during static mode test, LSZ on PDMS changed its conformation according to the time of adsorption by increasing the random coil and decreasing the alpha-helix structures (results summarized in Table V-2).

Table V-2: Secondary structure estimation to LSZ adsorbed on PDMS during static mode test.

Contact time	***Intermolecular β-sheet***	***Intramolecular β-sheet***	***Random coil***	***α-helix***	***β-turn***
5 min.	8.5%	14.3%	11.2%	44.8%	21.3%
5 h	9.1%	18.7%	14.6%	36.3%	21.3%
1 day	8.1%	20.7%	13.3%	37.1%	20.8%
3 days	8.8%	16.0%	23.2%	28.3%	23.7%
7 days	9.8%	17.2%	22.7%	27.4%	22.9%
9 days	7.6%	15.2%	23.8%	25.9%	27.5%
14 days	8.2%	18.5%	23.0%	27.0%	23.3%
21 days	10.6%	17.7%	17.8%	26.4%	27.5%

In static mode, the amount of adsorbed protein rises rapidly during the three first days with a significant change in secondary structure. The structure found after 5h in turbulent flow (configurations 2 and 3) is quite different than the structure after 5h in static mode. It was closer to that obtained after 3 days in static mode. Turbulent flow accelerates LSZ adsorption on PDMS and its conformational change. The quantification of secondary structure by FTIR in the flow cell after 5h turbulent flow is very close from the values obtained at the plateau after several days without flow.

Hydrodynamic diameter was measured after each test by DLS. The results are presented in Table V-3.

Table V-3. DLS of lysozyme solution after contact with PDMS surface (configurations 2 and 3).

Solution	***Hydrodynamic diameter (nm)***
LSZ after 21 days of contact (static mode)	3.9 ± 0.2
LSZ after 5 h of turbulent flow (configuration 2)	3.7 ± 0.3
LSZ after 5 h of turbulent flow with air in solution (configuration 3)	10.7 ± 0.1

DLS results show that turbulent flow didn't change the hydrodynamic radius of LSZ in solution. However, for air/liquid turbulent flow 5h (configuration 3) soluble aggregates were formed.

Highlights:

- Turbulent flow accelerates the lysozyme adsorption on PDMS.
- Secondary structure after 5h of turbulent flow is similar to the structure after several days without flow.
- Conformation of adsorbed protein were similar with or without air in liquid
- Air/liquid turbulent flow caused soluble aggregate formation.

2. Lysozyme adsorption on Glass in dynamic mode

2.1 Glass - Laminar flow 3 days + turbulent flow 5h (configuration 1)

The amount of adsorbed LSZ on glass after laminar flow and laminar + turbulent flow was obtained and the results are presented in Figure V-8.

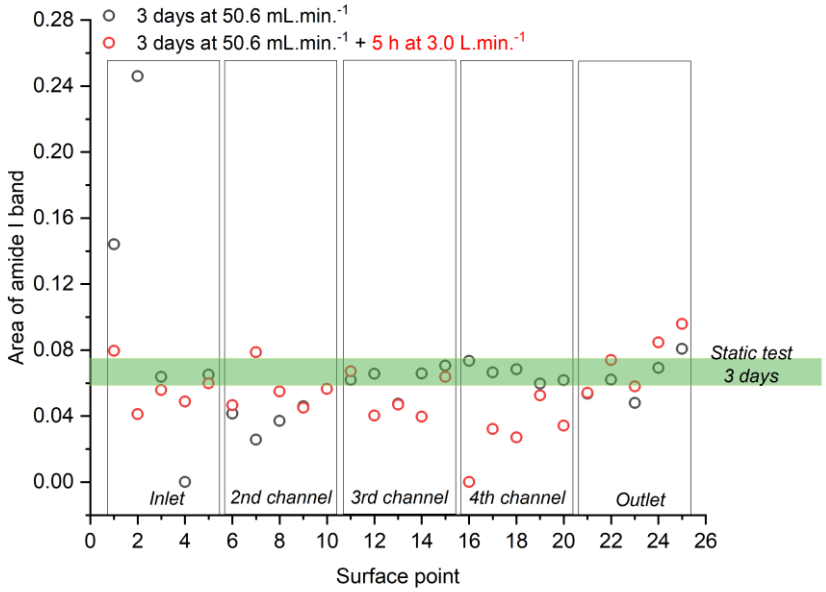

Figure V-8: Amount of Lysozyme adsorbed on glass after laminar flow 3 days and laminar 3 days + turbulent flow 5h. (C_{LSZ} = 1.00 mg.mL^{-1})

The areas obtained by FTIR after the dynamic test were very close from the values obtained after 3 days of static adsorption, with a limited variability. This indicates that the shear rate had no influence on the amount of adsorbed protein when combined with previous laminar flow. Secondary structure was estimated and the results are shown in figure V-9 for each point.

(a) **(b)**

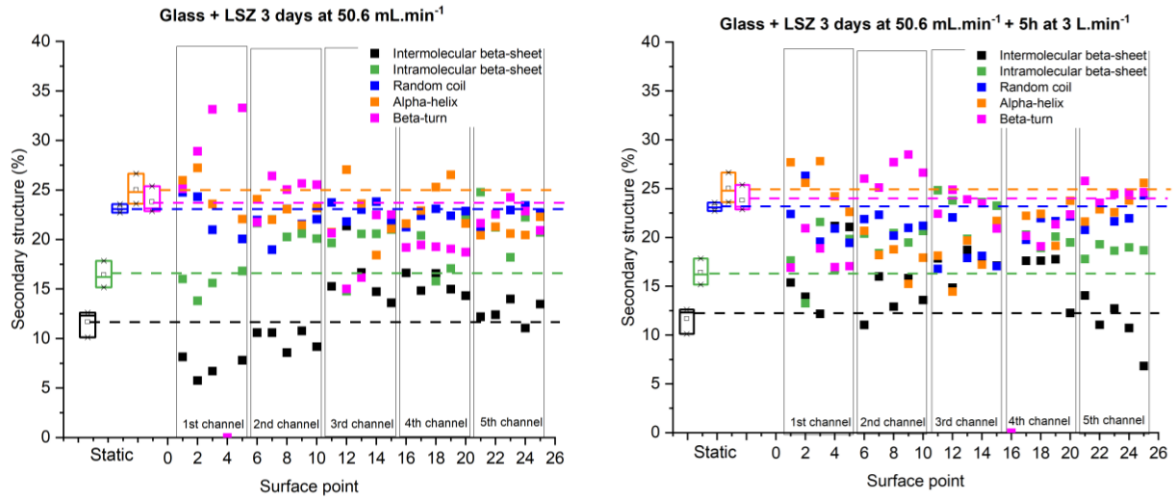

Figure V-9: Secondary structure estimation by surface point for LSZ adsorption on glass 3 days at 50.6 mL.min^{-1} (a) and 3 days at 50.6 mL.min^{-1} + 5h at 3.0 L.min^{-1} (b). (C_{LSZ} = 1.00 mg.mL^{-1})

With this choice of graph and data distributed by surface point, the analysis of structure evolution is not evident (Figure V-9). The data can be presented as a box plot of the 25 points along the flow (Figure V-10). This representation allows a better analysis of the flow effect on secondary structure of adsorbed lysozyme.

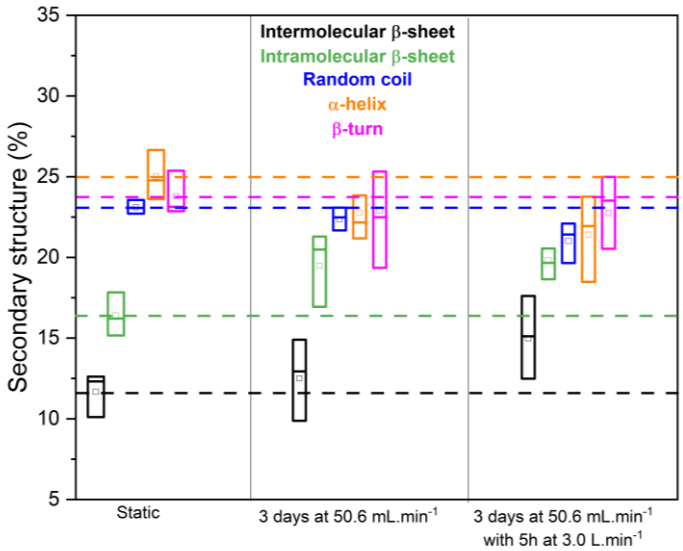

Figure V-10: Box plot of secondary structure for LSZ adsorption on glass during static and dynamic mode tests. (C_{LSZ} = 1.00 mg.mL^{-1}).

When lysozyme adsorbs on glass under laminar flow, the secondary structure is modified. Content of alpha helixes and random coils are systematically reduced and intramolecular beta sheet increases. Adding a turbulent flow during 5h has a major effect on the content of intermolecular beta sheets. The increase of beta sheet is associated with aggregate formation and can be confirmed by DLS experiment (cf. Table V-4) where the hydrodynamic diameter is estimated to 8.2 nm.

Table V-4. DLS of lysozyme solution after contact with glass surface (configuration 1).

Solution	***Hydrodynamic diameter (nm)***
LSZ after 21 days of contact (static mode)	3.9 ± 0.7
LSZ after 3 days of laminar flow	5.3 ± 0.4
LSZ after 3 days of laminar + 5h of turbulent flow	8.5 ± 0.7

An increase of hydrodynamic diameter was observed with bigger values after turbulent flow. It seems that soluble aggregates are formed when flow rates are applied, but no modification can be detected after static adsorption on glass.

Highlights:

- The amount of LSZ adsorbed on glass seems to be independent of the flow type.
- Laminar + turbulent flow test resulted in a different lysozyme secondary structure when compared to static test.
- Turbulent regime done after laminar flow induced soluble aggregate formation in the solution.

2.2 Glass - Turbulent flow 1h or 5h (configuration 2) and air/liquid turbulent flow 5h (configuration 3)

After 1h adsorption in static mode an event called overshoot was observed on glass surface. At this timepoint, there was a higher amount of protein adsorbed on the surface when compared to the plateau (after 3 days). The influence of the turbulent regime on the overshoot was also investigated. For this, a flow rate of 3.0 L.min^{-1} was applied for 1h and the results obtained for amide area I are shown in figure V-11. Reference values for the amount of protein adsorbed at 3 days of static test and at overshoot time (1 hour) are shown in green and yellow, respectively.

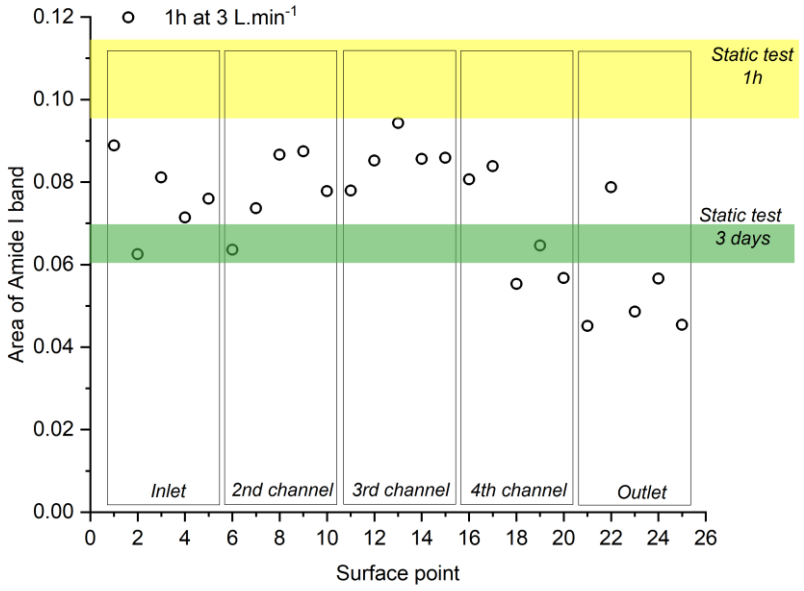

Figure V-11: Amount of Lysozyme adsorbed on glass after turbulent flow (1 hour).

(C_{LSZ} = 1.00 mg.mL^{-1})

Comparing the area values at the overshoot time (static test) with results in dynamic mode, a smaller amount of adsorbed protein was observed when turbulent flow was used. There are three possible explanations:

- the occurrence time of the overshoot decreases due to turbulent flow. In this case, the results come from the post-overshoot period;
- there was a delay for the overshoot to occur and this time has not yet been reached;

- the turbulent flow completely modifies the adsorption mechanism.

To analyze these three hypotheses, the secondary structure was estimated and compared with those obtained after1h and 3 days of adsorption without flow. The results are presented in Figure V-12.

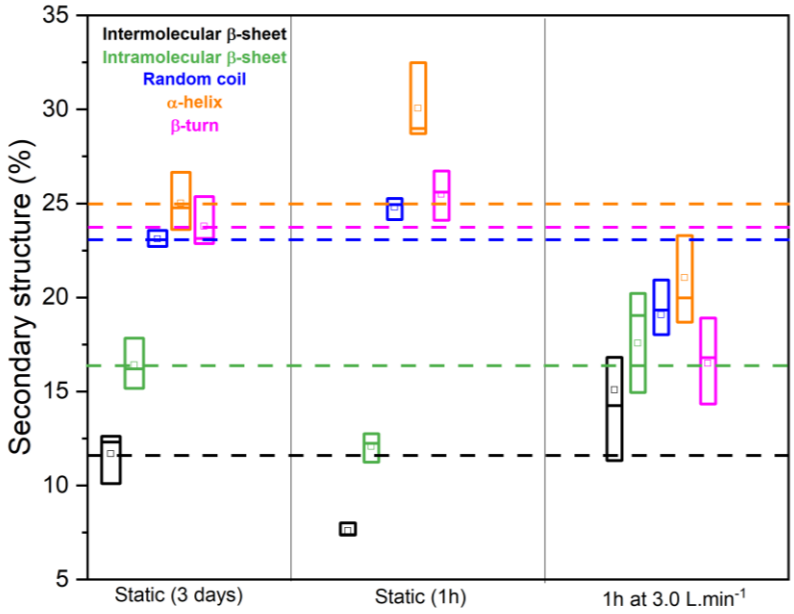

Figure V-12: Secondary structure estimation by surface point for LSZ adsorption on glass 1 hour at 3.0 L.min^{-1}. (C_{LSZ} = 1.00 mg.mL^{-1})

After the application of high shear stress, a completely different structural profile was observed for the adsorbed protein (1h). Turbulent flow during this period induced a change in lysozyme conformation, with a decrease in alpha-helix, beta-turn, and random coil. An increase in beta-sheet percentage was also observed. This structure is even different to that found after three days of contact with glass (static mode). With this result, the third hypothesis is the most adequate, since the conformation of lysozyme is completely different when compared to the static test after 1h and 3 days of adsorption. Furthermore, the areas obtained in the dynamic mode were between those obtained in the overshoot and 3 days of the static test. Thus, shear stress altered the adsorption kinetic curve.

Figure V-13 presents the experimental results for configurations 2 (turbulent flow for 5h) and 3 (air/liquid turbulent flow for 5h).

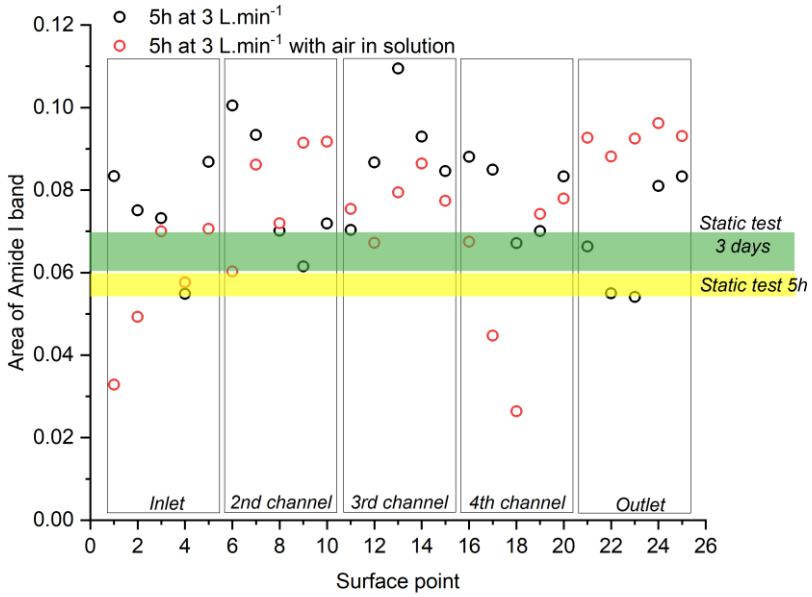

Figure V-13: Amount of Lysozyme adsorbed on glass after 5h of turbulent flow with and without air in solution. (C_{LSZ} = 1.00 mg.mL^{-1})

The area obtained for configurations 2 and 3 after 5 h of turbulent flow showed higher amount of absorbed protein than obtained in static tests (during 5h or 3 days). The presence or absence of air in solution did not significantly affect this result. It shows that the turbulent mode accelerates protein adsorption on glass. Secondary structure percentages are shown in figure V-14.

(a) **(b)**

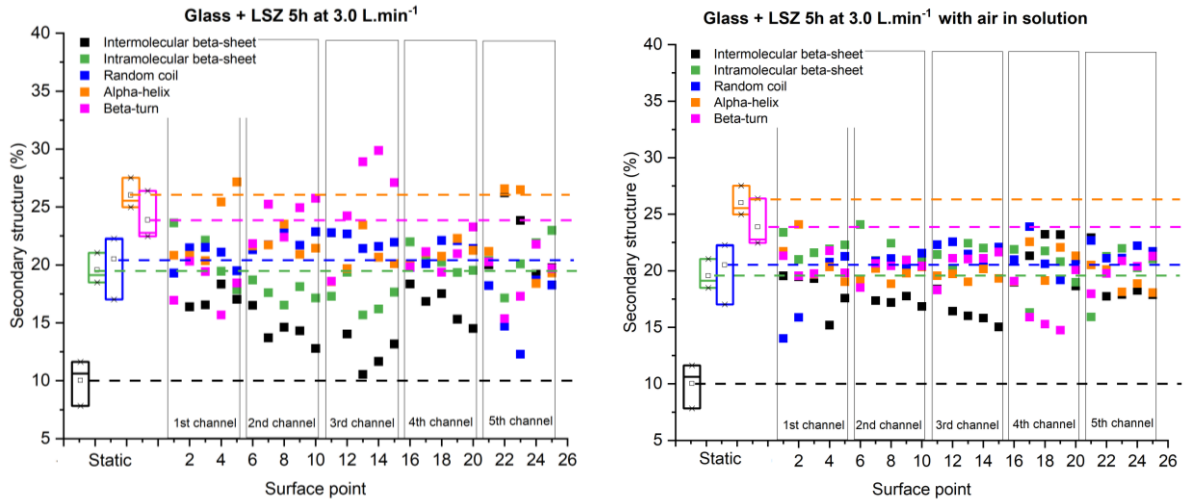

Figure V-14: Secondary structure estimation by surface point for LSZ adsorption on glass 5 hours at 3.0 L.min^{-1} (a – configuration 2) and 5 hours at 3.0 L.min^{-1} with air in solution (b - configuration 3). (C_{LSZ} = 1.00 mg.mL^{-1}).

For both cases, with or without air in liquid, LSZ conformation changed when we compare static to dynamic mode tests. A decrease in alpha-helix and an increase in intermolecular beta-sheet are observed. It can be due to the high flow rate that forces the protein to change its conformation to stay adsorbed on the surface. The increase of intermolecular beta-sheet means that more protein-protein interactions are happening and can also indicate the presence of aggregates on the surface.

The influence of turbulent flow on the solution was analyzed by DLS measures and the results are presented on Table V-5.

Table V-5. DLS of lysozyme solution after contact with glass surface (configurations 2 and 3).

Solution	***Hydrodynamic diameter (nm)***
LSZ after 21 days of contact (static mode)	3.9 ± 0.7
LSZ after 1 h of turbulent flow (configuration 2)	6.8 ± 0.9
LSZ after 5 h of turbulent flow (configuration 2)	14.9 ± 1.4
LSZ after 5 h of turbulent flow with air in solution (configuration 3)	11.2 ± 1.4 and 27.8 ± 0.4

Soluble aggregates were formed in the solution after testing under turbulent flow. The longer the solution circulation time, the larger the aggregate diameter. When air was introduced in liquid, two aggregate populations were obtained. This indicates that even if the presence of air does not affect the amount of adsorbed proteins on the surface, larger aggregates are formed in the solution.

Highlights:

- Turbulent flow modifies the adsorption mechanisms on glass.
- Secondary structures after dynamic tests were different from static results.
- High shear stress accelerates LSZ adsorption on glass.
- Turbulent regime induces soluble aggregate formation with or without air in solution and aggregate size depends on the flow duration.

3. General discussion

The dynamic test performed on PDMS with configuration 1 (laminar flow 9 days + turbulent flow 5h) showed that the amount of LSZ adsorbed varies according to the surface point location. However, the amide I area for the static test plateau (Area = 0.10 after 9 days) was in the same range of the area values after laminar + turbulent flow. Despite the variability of values between the 25 measurement points, the flow in configuration 1 did not significantly modify the LSZ amount adsorbed on PDMS. On the contrary, the secondary structure after the dynamic test (configuration 1) was different than in the static mode. The difference in structure

between the test done without flow rate and the test with laminar flow 9 days + turbulent flow 5 h, can be explained by the continuous renewal of protein in the solution.

For the glass, the amount of LSZ adsorbed after test conducted with configuration 1 (laminar flow 3 days + turbulent flow 5h) seems to be independent of the flow type. Even if a small variability was also observed depending on the surface location, close values to the static test (3 days) were obtained. Secondary structure after laminar + turbulent flow tests was different than on static test 3 days. Alpha helixes and random coils reduced with intramolecular beta sheet increases after laminar flow. Adding a turbulent flow during 5h, intermolecular beta sheets increased. This increase was due to aggregate formation in the surface that was confirmed by DLS measures.

Similar results (no influence of laminar + turbulent flow test in the adsorbed protein amount) were obtained for PDMS and glass after dynamic mode test performed with configuration 1. However, the variation of the amount of lysozyme adsorbed for the 25 measuring point was greater for PDMS than for glass (Figures V-4 and V-8, respectively). This observation can be explained by a difference in the flow at specific points, for example in the center of the channel and at the turn. Furthermore, PDMS is a soft and deformable surface. When placing this surface in the flow cell, due to tightening, the liquid passage section, which was previously rectangular, changes according to the deformation of PDMS (Figure V-15a). Consequently, the amount of protein in each measurement point can vary, since the contact area between the surface and liquid is not the same. In addition, the tightening can be done differently at the 4 corners of the surface resulting in deformation differences. With the glass surfaces (figure V-15b) this deformation cannot occur because the surface is rigid and fragile. In this operating conditions, differential tightening can result in a surface breakage. Consequently, the test would not be conducted due to leaks.

Figure V-15: Longitudinal cross-section of a canal with a) PDMS and b) Glass.

The direct application of turbulent flow was also investigated with and without air in solution (configurations 2 and 3, respectively). For PDMS, the direct application of turbulent flow for 5 h without air in solution (configuration 2) increased the amount of adsorbed lysozyme. The secondary structure obtained after 5h of turbulent flow was comparable to the structure obtained after several days of static test. The characterization of the adsorbed films on PDMS surface (conformation and adsorption quantity) were similar with air in solution. The difference between configurations 2 and 3 was observed only in solution. Turbulent flow 5h with air in solution induced the formation of soluble aggregates (hydrodynamic diameter of 8 nm) that were not observed for turbulent flow alone.

The configurations 2 and 3 also changed the adsorption balances on glass. It was observed that direct application of turbulent flow with or without air increased the adsorption kinetics and quantity of protein on the surface. For the glass, even the turbulent flow without air in the solution induced soluble aggregate formation. The aggregate size increased according to the applied time of turbulent flow. Aggregates of 7 nm were obtained after 1h and of 15 nm after 5h. The biggest ones (between 11 and 30 nm) were observed after 5 h of diphasic turbulent flow.

Our results are in agreement with the literature. *Grigolato and Arosio 2019*[1] used two immunoglobulins, IgG1 and IgG2 and they showed that the synergistic effect of flow and surface contact happened when glass syringe was used. For this surface, aggregate size increased with the applied flow rate (1, 5, 10 and 20 $mL.min^{-1}$). *Duerkop et al. 2018*[2] studied the effect of high shear stress (with and without cavitation) on human serum albumin (HSA) aggregation. They showed that shear stress combined with gas in liquid intensifies the formation of soluble aggregates. *Frachon et al. 2016*[3] developed a setup in which the insulin can move back and forth over the surface and, as consequence, the triple surface solid-air-liquid can be continuously displaced. They demonstrated insulin aggregation on the triple interface and not in the regions submitted to only hydrodynamic shear stress. Once again, the literature shows that the influence of shear stress must be evaluated by combining parameters such as the surface and the presence of the air/liquid interface.

The lack of studies in the literature that considers the influence of shear stress on lysozyme, highlights the importance of the results obtained in the present work. The influence of shear stress was analyzed at two levels: on the surface (amount of adsorbed protein and conformation) and in solution (soluble aggregates). The results suggest that diphasic turbulent flow significantly affects proteins into the solution (aggregates formation) but no change was

observed at the surface. In contrast, shear stress changes substantially the adsorption kinetics, the amount and the conformation of adsorbed protein. All results obtained show that parameters such as choice of surface, flow rate and presence of air in the solution can interfere with the final stability of the protein. Also, it shed light that the evolution of the protein in solution must be interpreted in regard of the surface of contact and the presence of air. For the same flow, results can be different according to the type of surface.

Bibliography

(1) Grigolato, F.; Arosio, P. Synergistic Effects of Flow and Interfaces on Antibody Aggregation. *Biotechnol. Bioeng.* **2020**, *117* (2), 417–428. https://doi.org/10.1002/bit.27212.

(2) Duerkop, M.; Berger, E.; Dürauer, A.; Jungbauer, A. Influence of Cavitation and High Shear Stress on HSA Aggregation Behavior. *Eng. Life Sci.* **2018**, *18* (3), 169–178. https://doi.org/10.1002/elsc.201700079.

(3) Frachon, T.; Bruckert, F.; Le Masne, Q.; Monnin, E.; Weidenhaupt, M. Insulin Aggregation at a Dynamic Solid−Liquid−Air Triple Interface. *Langmuir* **2016**, *32*, 13009–13019.

Chapter VI – Conclusions and perspectives

1. Conclusions

The first part of this study was devoted to optimize a test to measure the antibacterial activity of lysozyme. The antibacterial assay against Gram-positive bacteria presented satisfactory results. The initial lysozyme activity obtained was similar to that reported by the manufacturer. This test combined with quantification of soluble and insoluble aggregates was used to follow the effect of different stresses encountered in manufacturing line of pharmaceutical products.

Whatever the treatment used and their stress factors, a total loss of antibacterial activity of lysozyme has never been observed. For all treatments, increasing stress factors (i.e. concentration of denaturants, temperature, treatment time) caused an increase of the amount of insoluble aggregates. The presence of soluble aggregates was observed only after ultrasound treatment and was proportional to the time of application.

Some treatments, for example urea 6 and 10M induced a high percentage of insoluble aggregates formation. It means that urea can strongly modify the LSZ structure. However, the antibacterial activity decrease (around 10%) of the LSZ treated with urea was independent of the concentration. The opposite is also true: ultrafiltration did not show soluble or insoluble aggregates while the lysozyme activity reduced of about 40% depending on the transmembrane pressure and the membrane used. In general, protein aggregation and loss of antibacterial activity are not correlated. It indicates that each stress factor leads to different denaturation mechanisms. So, the change in conformation may not necessarily result in a decline of biological activity.

During ultrafiltration, adsorption of lysozyme in pore is associated with increased selectivity and reduced hydraulic performance of the membrane. After successive lysozyme filtrations (approximately 3), the loss of activity in the permeate is dependent on the transmembrane pressure. The activity loss, as previously reported by the group, is more pronounced if the real membrane cut-off is small. This loss of activity has also been shown to be dependent on the lysozyme source used. A loss of activity for a lysozyme with the highest initial activity is observed, while the other maintained its antibacterial activity after several filtrations in the same conditions. Despite being produced from the same animal specie,, the purification processes of the two sources are different, and this purification step may alter or

prevent the interaction between the protein and the membrane pore. According to the manufacturer, the difference between the two lysozymes is a dialysis step. Similar changes of hydraulic and selectivity properties of the membrane are measured during ultrafiltration of dialyzed LSZ 7.10^4 and LSZ 1.10^5. In the permeate, activity of LSZ 1.10^5 is dependent of the pressure whereas dialyzed LSZ 7.10^4 maintained its antibacterial activity for all transmembrane pressures.

Differences observed for the two sources during ultrafiltration was confirmed by combining this mechanical stress with the thermal one. When treated at 70°C, both lysozymes showed the same behavior as the non-thermally treated. It means that only LSZ 1.10^5 gradually loses a part of its activity with increasing pressure. Ultrafiltration of LSZ solutions treated at 90°C showed that filtration process was not capable of adding a loss of biological activity to a previously thermally denatured protein.

A small difference between the two sources of lysozyme was also observed during ultrasonic treatment. While LSZ 7.10^4 maintained its biological activity up to 15 minutes of treatment, LSZ 1.10^5 began to lose its activity after 3 minutes. For the other treatments (chemical and thermal), no significant difference was observed between lysozymes. We suggest that the slight difference between these lysozymes (stabilization) can only be detected during operations with low energy. The chemical and thermal modification are very energetic and lead to strongly irreversible transformations, independently of the lysozyme initial state.

Adsorption kinetics were studied with a static mode test (flow rate = 0) on two “model” surfaces: PDMS and glass. The results show that lysozyme adsorbs faster on glass, but in greater quantity on PDMS. In addition, during adsorption on glass, an overshoot was observed, which occurs when an oversaturation is achieved, followed by the release of weakly adsorbed proteins. The effect of lysozyme concentration on adsorption kinetics was studied and it was shown that for adsorption on glass, the higher the concentration, the faster the overshoot effect. For PDMS, the increase in concentration of the protein solution promoted the formation of aggregates, which did not occur during adsorption on glass (static mode).

The results obtained for PDMS and glass suggest that the adsorption kinetics as well as the amount of adsorbed protein depend on the surface chemistry. To study the relationship between the hydrophilicity of the surface and the adsorption of proteins, materials with controlled hydrophilicity and similar roughness were prepared. Mixed self-assembled monolayers with different wettability were successfully prepared on borosilicate glass

(coverslips) and characterize with atomic force microscopy, contact angle measurement and X-Ray Photoelectron Spectroscopy. No direct relationship between the SAMs hydrophilicities and adsorption kinetics was observed. Regardless of the amount of NH_2 groups on the surface, LSZ in contact with the SAMs has a behavior closer to the glass than to the PDMS. Two events were observed for adsorption on SAMs: the overshoot (short time) and a second effect (after several days). The second is assumed to be related to the release of soluble aggregates in the solution. Aggregate formation was confirmed using dynamic light scattering (DLS).

The influence of surface chemistry on lysozyme adsorption was also analyzed in different conditions of flow. When turbulent flow is directly applied, the adsorption kinetics and the amount of adsorbed proteins increase. A change in the secondary structure of the protein adsorbed on the surface was observed for both laminar and turbulent flows, probably due to the constant renewal of protein solution in the laboratory set-up.

Aggregates in solution were observed for PDMS after laminar flow 9 days + turbulent flow 5h. On the other hand, the direct application of the turbulent flow for 5h without previous laminar regime, did not form aggregates in solution. For glass, aggregates were formed after applying turbulent flow in both cases. The addition of air in the solution increased the formation of soluble aggregates, but did not interfere with the results obtained on the surface. Thus, shear stress seems to significantly modify adsorption balances on the surface, while the presence of air in the solution induces the formation of soluble aggregates whatever the surface in contact.

The results presented here show the importance of industrial operating conditions on the stability and efficiency of proteins. For each stress factor, there are limits to the application, such as temperature below 70°C, ultrasound for 3 minutes and ultrafiltration at 4 bar. In addition, it is important to know the protein and its environment. We showed that the same protein, with different purification processes, could behave differently when submitted to mechanical stress. Our results also show that glass has the least influence on the formation of aggregates in solution. However, under turbulent flow with air in the solution, large aggregates were formed. This indicates that air/liquid mixture should be avoided in industrial protein processes.

2. Perspectives

Interesting results were obtained from this study. To improve the understanding of the observed phenomena, other tests can be conducted. With bactericidal activity in solution, differences between lysozymes from hen egg white were observed after mechanical treatments. Through mass spectroscopy, the presence or absence of stabilizing molecules in LSZ 7.10^4 could be detected and identified. Dialysis was performed in water, however, different buffers should be tested. Even if the elimination of small molecules was observed by SEC-HPLC, other stabilizers can be strongly interacting with the protein and continue after dialysis using water. However, a buffer compatible with the ultrafiltration process must be used.

To understand which treatment causes the greatest structural change in LSZ, it would be interesting to study the reversibility. For example, remove chemical denaturants after treatment (by dialysis) and perform the aggregation and antibacterial tests.

The adsorption kinetics on SAMs presented two events and, to better characterize them, techniques such as QCM-D and ellipsometry should be performed to study in situ the mass adsorbed on the surface and the thickness of the protein layer, respectively. The adsorption on the SAMs could also be performed by changing the flow regime. In this study we showed that it was possible to prepare SAMs on borosilicate surfaces and this method could be used for the preparation of larger glass surfaces (8x8 cm).

Tests in dynamic mode showed a change not only in the adsorbed protein film but also in the solution. When diphasic flow was used, the protein undergoes aggregation. It would be interesting to recover part of this solution and perform antibacterial tests according to the optimized method. For this, it would be necessary to define where to collect the solution from. If it is recovered at the end of the test, all contact surfaces must be considered (feed tank glass, cell surface and hoses) and not just the influence of the turbulent mode and the diphasic flow.

The surface contact tests used and adapted for lysozyme in this work can be extended to the use of other proteins. It would be interesting to obtain the results for proteins softer (that are easily denatured) than lysozyme. For example, immunoglobulins as the IgG1 that is a soft protein with molecular weight of 150 kDa. It is already used as a therapeutic protein for infectious diseases, immunodeficiency, and immunomodulation. It is a high-cost protein that is mainly commercialized in the liquid form. The impact of the surface contact with IgG1 is important to avoid loss of protein by adsorption and/or aggregate formation.

List of Scientific Valorization

Publications:

- Miron, S.M ; De Espindola, A. ; Dutournié, P. ; Ponche, A. Study of the relationship between applied transmembrane pressure and antimicrobial activity of lysozyme. *Scientific Reports*, **2021**, 11:12086, https://doi.org/10.1038/s41598-021-91564-x.

- De Espindola, A. ; Miron, S.M. ; Dutournié, P. ; Ponche, A. Ultrafiltration operational conditions influence in the antibacterial activity of native and thermally treated lysozyme. *Comptes Rendus Chimie*, **2023**, 1-8, https://doi.org/10.5802/crchim.217.

- De Espindola, A. ; Dutournié, P. ; Ponche, A. Impact of industrial stress factors on lysozyme enzyme: Role of denaturation processes and initial protein activity. *Sustainable Chemistry and Pharmacy*, **2023**, 100964, https://doi.org/10.1016/j.scp.2022.100964.

Conference participations:

Oral presentations (international)

- A. de Espindola, P. Dutournié, A. Ponche, *Impact of ultrafiltration process in the lysozyme antibacterial activity*, 9th International Conference on Sustainable Solid Waste Management June 2022, Corfu, Greece.
- A. de Espindola, P. Dutournié, A. Ponche ; *Relationship between ultrafiltration hydrodynamic properties and antibacterial activity of lysozyme*, Curiosity – A French-German Young Chemists Conference, June 2022, Mulhouse, France.
- A. de Espindola, P. Dutournié, A. Ponche, *Impact of processing stresses on enzymatic activity of lysozyme*, Chania 2023, June 2023, Chania, Greece.
- A. de Espindola, P. Dutournié, A. Ponche, *Relation between enzymatic activity and denaturation of lysozyme under different stress factors*, ECCE & ECAB 2023, September 2023, Berlin, Germany. (accepted)

Oral presentations (national)

- A. de Espindola, P. Dutournié, A. Ponche, *Impact of ultrafiltration process in the lysozyme antibacterial activity,* 4th edition of the Young Scientists Day – IS2M, March 2022, Mulhouse, France.
- A. de Espindola, P. Dutournié, A. Ponche, *Relationship between antibacterial activity and modification of lysozyme under different stress factors,* 5th edition of the Young Scientists Day – IS2M, March 2023, Mulhouse, France.

Poster presentation

- A. de Espindola, P. Dutournié, A. Ponche, *Ultrafiltration impact in the enzymatic activity of lysozyme*, 32nd Annual Conference of the European Society for Biomaterials, septembre 2022, Bordeaux, France.